TARTU ÜLIKOOLI
TOIMETISED

УЧЕНЫЕ ЗАПИСКИ ТАРТУСКОГО УНИВЕРСИТЕТА

ACTA ET COMMENTATIONES UNIVERSITATIS TARTUENSIS

880

STUDIES ON AEROSOLS AND HIGH FREQUENCY DISCHARGES

IONIZATION, AEROSOLS, ELECTROMETRY

TARTU 1990

TARTU ÜLIKOOLI TOIMETISED
УЧЕНЫЕ ЗАПИСКИ ТАРТУСКОГО УНИВЕРСИТЕТА
ACTA ET COMMENTATIONES UNIVERSITATIS TARTUENSIS
Alustatud 1893.a. VIHIK 880 ВЫПУСК Основаны в 1893.г.

STUDIES ON AEROSOLS AND HIGH FREQUENCY DISCHARGES

IONIZATION, AEROSOLS, ELECTROMETRY

TARTU 1990

CONTENTS

СОДЕРЖАНИЕ

PROPAGATION OF THE POINT-ELECTRODE HF DISCHARGE IN THE AIR

M. Aints and K. Kudu

Introduction

If to apply 10-20 MHz HF voltage of about 5-10 kV to a point-electrode with a diameter of some millimeters in the ambient air, the discharge channels begin to propagate into the discharge gap with velocities $10\text{-}10^4$ m/s depending on conditions. These channels can bridge discharge gaps up to some tens of centimeters. A survey of numerous papers dealing with experimental investigation of propagation velocity of the HF discharge can be found in [9]. This research indicates that propagation velocity increases together with overvoltage and the frequency of applied voltage, and decreases approximately exponentially with the increase of distance from the point-electrode tip. If to apply an additional DC potential to the point-electrode, the velocity changes in complex dependence on the value of the DC potential [10-12]. The discrepancies between the results of different authors exceed measurement errors. In papers [10-12] the propagation velocity was determined from distance vs. time curves, where the distance was the shortest route from the point-electrode tip to the definite plane, perpendicular to the point-electrode axis. However, as can be seen from the photos in [1-4], the HF discharge in general propagates along complex trajectories. The appearance of new branches and the spatial structure of the channel system behave according to statistical laws and depend on the value of HF and additional DC potential, as well as on gap geometry. This may be one of the reasons of the complex dependence of the propagation velocity on the value of the DC potential, and it serves as a source of discrepancies between the results of different authors.

Another reason complicating the measurements is connected with a feature of the development mechanism of the point-electrode HF discharge. It is known [5,10,12] that streamers may propagate before the main channel of the HF discharge, in any case the propagation of streamers takes place at frequencies of 10 MHz and less. These streamers have a length up to some tens of millimeters depending on frequency and voltage. They radiate only during a very short time interval at every

positive half-cycle. These streamers may be not recorded with low-sensitivity channel length measurement systems. The latter circumstances have not been discussed in many of the previous studies.

We have also experimentally established a very strong influence of air humidity on the form of the discharge channels, a phenomenon not pointed out in earlier investigations.

To understand the physical mechanism of discharge development, it would be expedient to examine single channel propagation separately from the development of discharge burst as a whole, i.e. as a system of channels with a different orientation. The second task, namely the explanation of the spatial structure formation of the HF discharge burst channels, can be solved only after the elucidation of development regularities of a single channel, and the determination of its physical characteristics.

Velocity measurements

To produce straight single discharge channels propagating along the point-electrode axis the method given in [3,13] was used. The discharge was initiated by supplying square-shape radiopulses to the point-electrode. By varying the duration of the radiopulses discharge channels of different lengths were produced. The additional DC potential was varied in an interval of ± 20 kV. Conically tipped point-electrodes (tip-angle 30° -90°) of 2-6 mm diameter were used. At a frequency of 20 MHz straight single channels could be produced only when an additional DC potential was supplied to the point-electrode (some kV in the case of positive and 10 kV or more in the case of negative DC potential). At 10 MHz the probability of the generation of the straight channel was high enough without any DC potential. The velocity was determined by measuring the HF discharge channel length at a definite time moment without taking into account the streamers before the channel tip. The distance of the opposite grounded electrode from the point-electrode tip was changed from 12 to 40 cm and this did not cause any changes in the propagation velocity. The air humidity was maintained at a value of about 20 g/m^3 . The curves in Fig. 1 represent the propagation velocity of the single straight HF discharge channel tip depen-

ding on the distance for different values of the HF potential on the point-electrode. The measurements show that from the distance of some millimeters from the point-electrode tip the propagation velocity does not depend on the shape of the point-electrode. These parts of curves in Fig. 1 are represented by a continuous line.

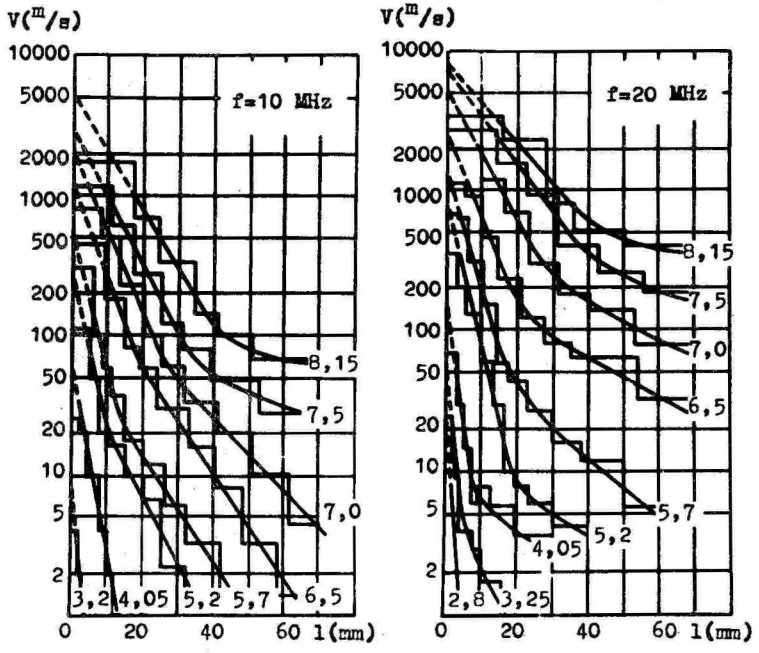

Fig.1. Propagation velocity of the HF discharge channel vs. distance. Parameter - HF potential amplitude in kV.

The propagation velocity depends weakly (less than 5%) on the value and the sign of the DC potential, if channel shape does not change. The change of the DC potential may cause more appreciable changes in velocity, but this is always connected with changes in channel shape. For example, the appearence of brush-shape broadening of the very tip of the channel slows down the velocity. Weak dependence of channel propagation velocity on the DC potential gives evidence of the independence of the physical processes in the HF point-

discharge channel from the DC potential mentioned in [6].

The velocities with which the channels start from the point-electrodes can be determined by prolonging the linear parts of the curves in Fig. 1 to the ordinate axis (dotted parts of the curves in Fig. 1). Thus the values of velocity v_0 were obtained for every value of the point-electrode potential. The corresponding curves are represented in Fig. 2. These curves could also be taken to represent the channel-tip velocity on the channel-tip potential. These curves make possible to determine the channel-tip potential by measuring the channel propagation velocity.

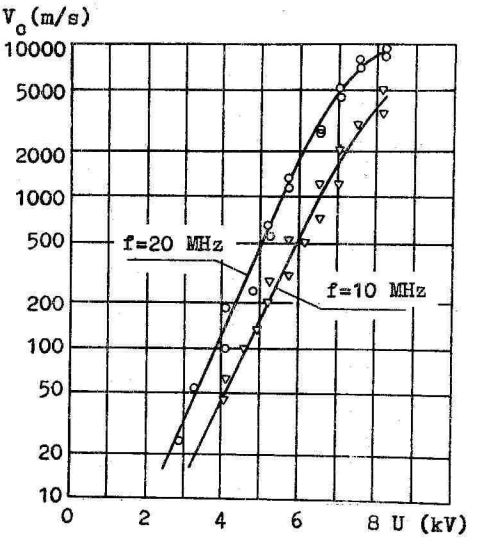

Fig. 2. The propagation velocity of the discharge channel as a function of the HF potential of the channel-tip.

Influence of humidity

It is well-known that at frequencies above 10 MHz if special precautions are not used, the point-discharge channels propagate along arc-shape trajectories. These trajectories are in the plane of the point-electrode axis and have a curvature radius of some centimeters. The direction of propagation varies up to 270° . After the propagation of the crooked channel stops and if the applied voltage is sufficiently

high, new branches arise from the curved sections of the channels. It was found that the distance from the point-electrode where the propagating direction diverges from the initial one, and the curvature radius of the trajectory are dependent on the air humidity.

The influence of humidity becomes especially apparent at a frequency of 20 MHz, if together with the HF potential the point-electrode has negative DC potential of about 15-20 kV. Photographs of discharge bursts taken in the case of different radiopulse durations τ at different humidities h are represented in Fig. 3. The discharge arises from the conical tip of a vertically disposed wire of a diameter of 2 mm. The

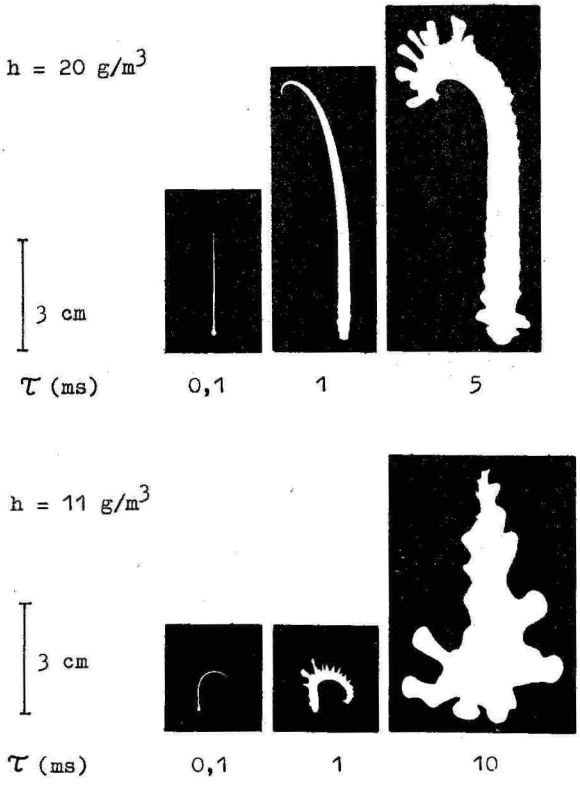

Fig. 3. Development of the HF discharge at different humidities.

HF voltage peak value is 6.5 kV, DC voltage is -20 kV and the frequency is 20 MHz. It can be seen that the time interval during which the discharge channel covers a certain distance in humid air can be more than an order of magnitude smaller than the respective time interval in dry air. Thus the effect of humidity should be taken into account in investigating the propagation velocity of the HF discharge bursts.

Discussion

Before explaining the effect of humidity on the shape of HF discharge bursts, the reason for the bending down of the discharge trajectory should be clarified. In [4,14] the propagation trajectory bending was considered to be a result of the HF potential phase change along the discharge channel. The channel length increases together the difference of phase of the HF potential at the channel tip and at the electrode. For example, the phase difference $\pi/2$ is reached at channel lengths of some centimeters [4,14]. The propagation direction diverges from the initial one, and the discharge propagates along a crooked trajectory in the direction of the channel part with an HF potential phase opposite to that on the channel tip. Phase change per unit length of the channel depends mainly on the channel conductivity.

The development of the HF discharge channel proceeds as follows. At first a greater part of the energy absorbed by the discharge is spent on the excitation of vibrational levels of the gas molecules. After that V-T relaxation occurs, i.e. the energy transmission from vibrational levels to rotational and translational levels. For example, the gas temperature in the HF discharge channel reaches a value of 1500-2000 K in about 100 μs while the vibrational temperature grows to about 5000 K in 50 μs [8]. In this respect the HF discharge channel development process is similar to that of a long spark. According to [7] the time constant of the V-T relaxation τ_{VT} has a value in an interval of 10^{-3} - 10^{-6} s, depending on the temperature and the air humidity. With an increase in both the temperature and the humidity, decreases. With an increase in temperature there is a considerable increase in the frequency of electron emission from negative ions [7]. The negative ions created earlier are decomposed and a sharp increase in the conductivity takes

place. The temperature interval 1500-2000 K is called critical because the ratio of the concentration of electrons and of negative ions exceeds unity in this interval [7]. Due to the dependence of τ_{VT} on humidity, the time required for the channel temperature growth is also dependent on humidity. The higher the humidity, the quicker the increase in the conductivity. As is demonstrated by calculations and experiments with a long spark [7], the time of temperature growth up to 1500-2000 K can change many times depending on humidity. Taking into account the above similarity, it can be supposed that the conductivity of the HF discharge channel increases more slowly in dry air and thus the phase difference of the HF potential at the channel tip and at the electrode is greater. The latter causes steeper bending of the channel propagation trajectory.

REFERENCES

1. Veimer V., Kudu K. Observation of HF point-to-plane discharge development phases // IX ICPIG, Contr. Papers.- Bucharest, 1969. - P. 285.
2. Veimer V., Kudu K. The development phases of HF point-to-plane corona // X ICPIG, Contr. Papers. - Oxford, 1971. - P. 165.
3. Aints M., Kudu K., Haljaste A. A single-channel HF point discharge in the atmospheric air // XV ICPIG, Contr. Papers. - Minsk, 1981. - P. 623-624.
4. Aints M., Kudu K. Formation of the spatial structure of HF point-discharge bursts in the air at atmospheric pressure // XVII ICPIG, Contr. Papers. - Budapest, 1985. - P. 540-542.
5. Aints M., Haljaste A., Kudu K. Investigation of HF point-discharge formation by electron-optical technique // XIII ICPIG, Contr. Papers. - Berlin, 1977. - P. 437-438.
6. Aints M., Kudu K., Haljaste A. Electrical parameters of a single-channel high-frequency discharge bursts // XVI ICPIG, Contr. Papers. - Düsseldorf, 1983. - P. 534-535.
7. Gallimberti G. The mechanism of the long spark formation // XIV ICPIG, Inv. Papers. - Grenoble, 1979. - P. 193-250.

8. Laan M., Susi J. Determination of N_2 $C^3\Pi_u \rightarrow B^3\Pi_g$ 0 → 0 band absorption in the propagating HF discharge channel // XVII ICPIG, Contr. Papers. - Budapest, 1985. - P. 1014-1016.

9. Куду К. О начальных стадиях одноэлектродного ВЧ разряда в атмосферном воздухе// Уч. зап. Тарт. ун-та. - 1973. - Вып. 320. - С. 287-307.

10. Бердышев А.В. Фотоэлектрические исследования формирования высокочастотных разрядов с острия в воздухе: Автореферат дис. канд. физ.-мат. наук. - Л., 1971.

11. Веймер В.А., Куду К.Ф. Изучение фаз развития униполярного ВЧ разряда в диапазоне 3-20 МГц // Уч. зап. Тарт. ун-та. - 1971. - Вып. 283. - С. 49-61.

12. Айнтс М. Х., Куду К.Ф., Халъясте А.Я. Пространственно-временное развитие одноэлектродного ВЧ разряда // Уч. зап. Тарт. ун-та. - 1977. - Вып. 409. - С. 28-58.

13. Айнтс М.Х., Куду К.Ф., Хальясте А.Я. Исследование развития одноэлектродного высокочастотного разряда в условиях смешанного напряжения // Уч. зап. Тарт. ун-та. - 1981. - Вып. 588. - С. 11-19.

14. Айнтс М.Х., Куду К.Ф. Формирование пространственной структуры одноэлектродных высокочастотных вспышек в воздухе атмосферного давления // Тезисы докладов Всесоюзного совещания ФЭПГ II. - Тарту, 1984. - С. 85-89.

РАСПРОСТРАНЕНИЕ ОДНОЭЛЕКТРОДНОГО ВЧ РАЗРЯДА В ВОЗДУХЕ

М.Х. Айнтс, К.Ф. Куду

Р е з ю м е

Обсуждаются вопросы методики определения скорости распространения ВЧ разряда с остриевых электродов на факельных частотах в атмосферном воздухе. Представлены экспериментальные кривые зависимости скорости распространения отдельного канала ВЧ разряда от расстояния проиденного разрядом, при разных значениях ВЧ напряжения. Обнаружено сильное влияние влажности воздуха на форму разрядных каналов, от чего время перекрытия промежутка может изменяться более чем на порядок величины. Дается качественное объяснение влияния влажности.

OPTICAL DETERMINATION OF ION CONCENTRATION IN HF NITROGEN PLASMA: ABSORPTION MEASUREMENTS

M. Laan, P. Paris and J. Susi

Introduction

The determination of charged particle concetration in HF discharges at atmospheric pressure is a complicated problem. In the experiment this main plasma parameter should be determined with maximum directness to ensure the accuracy of further theoretical analysis.

One of the methods for the determination of N_2^+ ion concentration in low temperature nitrogen plasma is the measurement of absorption of the nitrogen first negative (1^-) system radiation. This system of molecular bands corresponds to the transition between the electronic states $B^2\Sigma_u^+ \rightarrow X^2\Sigma_g^+$, the latter being the ground state of N_2^+. The population of the lower state can be determined from absorption measurements. For practical purposes this population can be considered equal to the total N_2^+ ion concetration as the concetration of N_2^+ in excited states is negligible in comparison with the population of the ground state.

Experiment

A non-stationary HF pulse-excited discharge in nitrogen at atmospheric pressure was the object of investigation. The point-to-plane discharge gap (the point electrode being a conically tipped 2mm tungsten wire) was placed into a vacuum chamber which was evacuated up to 4.10^{-6} Torr and then filled with pure nitrogen up to 760 Torr. 20 MHz 1 ms radiopulses were supplied to the point electrode at a repetition rate of 50 Hz. The pulses excited non-stationary discharge channels propagating from the point electrode along the gap axis. The total length of discharge channels at the end of a 1 ms radiopulse was about 4 cm, but the propagation velocity of channel tips was not constant. It was lower at initial states of propagation and increased towards the end of the radiopulse.

Fig.1 presents the experimental set-up for absorption measurements. A spherical mirror 1 is placed at a distance of

its curvature radius from the investigated part of the discharge channel (the part was 2mm high and 0.15 mm wide, situated at a height of 1 mm above the point tip). The investigated area and its reflected image were both projected onto the monochromator slit with an achromatic objective 3. As the signal detected by a PM was insufficient for averaged analog signal from PM output, 2000 signals were summed up by means of an NTA - 1024 amplitude analyzer operating in the digital oscilloscope mode.

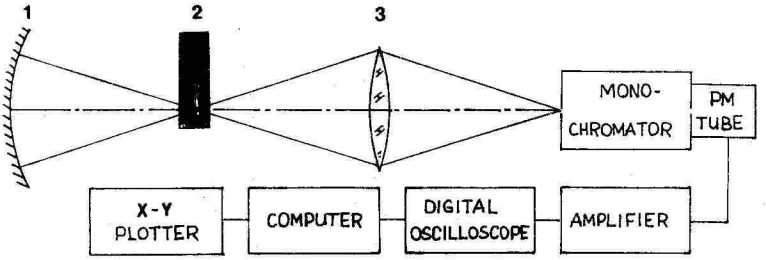

Fig.1. Experimental set-up for absorption measurements.

The 1 system $0 \rightarrow 0$ band (391.14 nm) was taken under observation. The mirror-method is especially valuable as at weak absorptions ($\varkappa_0 l < 1$) the contours of radiated and absorbed lines remain identical with sufficient accuracy. The $1^- \; 0 \rightarrow 0$ band satisfies this condition reasonably well.

The relative absorption A can be determined empirically and expressed as

$$A = \frac{(1+r)\,\frac{I'}{I}}{r}\,, \qquad (1)$$

where I is the measured intensity with covered mirror, I' is the intensity with uncovered mirror and r is the effective mirror reflectivity.

Here a problem is posed by correct measurement of the band intensity. The bandheads frequently overlap with the rotational structure of other bands which makes it necessary to take into account the background intensity. In the experiment the intensity of the $1^- \; 0 \rightarrow 0$ bands was detected with a 5 Å

spectral width of the monochromator output slit. The spectral plate (Fig. 2) shows an overlap at the head of the 1^- 0 → 0 band.

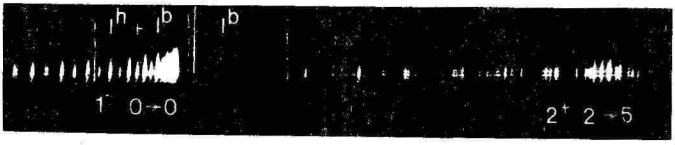

Fig. 2. The intensity of the bandhead and the background of the 1^- 0→0 band.

The background intensity is caused by the rotational structure of N_2 second positive (2^+) bands 0 → 3, 1 → 4 and 2 → 5. By locating the monochromator slit on the bandhead, it is possible to measure only $I^h + I^b$, where I^h is the bandhead intensity and I^b is the background intensity. The background intensity can be measured by locating the monochromator slit on the background at a minimal distance from the bandhead (Fig. 2). The background is to be considered quasi-continuous in the bandhead region and of constant intensity. The last assumption, however, is incorrect and causes an error in the results. In the computation of values of relative absorption intensities I^h are used in formula 1, whereas the background intensity is, in first approximation, not affected by absorption. Proceeding from the time dependence of the relative absorption A, and applying the dependence $A = f(\varkappa_0 l)$ [1] it is possible to obtain the time dependence of the optical density. Here $\varkappa_0$ is the absorption constant in the centre of a spectral line and l is the optical length.

In Fig. 3 the time dependence of the radiopulse envelope and the optical density $\varkappa_0 l$ for the 1^- 0 → 0 band are presented. The value of $\varkappa_0 l$ measured for the bandhead is extended to the whole band on the assumption that the main part of the band intensity is concentrated near the bandhead. Optical length l is here equal to the effective diameter of the discharge channel. The time dependence of the effective channel diameter was obtained from microdensitometric measurements of the discharge photos. The criterion for effective

channel diameter was the decay of radial intensity in e ≈2.7 times as compared with the intensity in the centre of the channel.

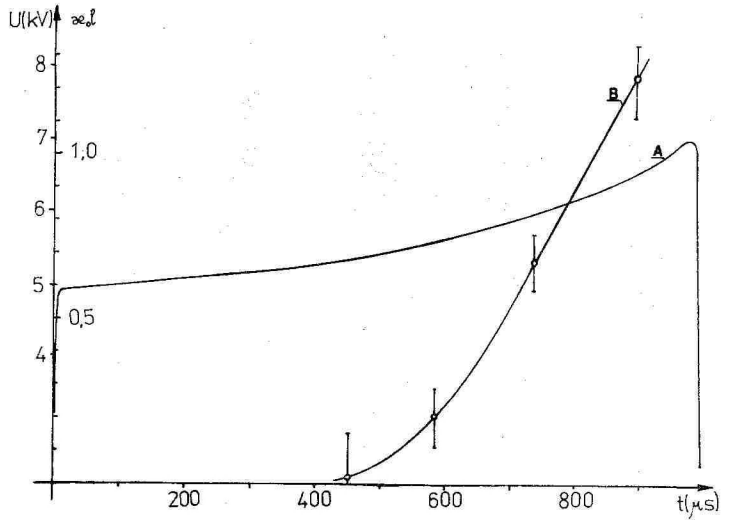

Fig. 3. Envelope of the radiopulse (A) and optical density $\varkappa_0 l$ for the $1^- 0 \to 0$ bandhead.

Results and discussion

In the determination of concentration from absorption measurements it is necessary to known the type of widening and half-widths of spectral lines. Under the conditions of the present discharge the half-widths of Doppler and Lorenz contours are practically equal. They were both calculated using well-known formulae [1]. The Doppler-case formula for population determination can be taken as a point of departure, because the central part of a widened spectral line is approximately described by the Doppler contour and the absorption constant $\varkappa_0$ is used (see the definition of $\varkappa_0$ above). The Doppler half-width is in a square root dependence on the gas temperature. In the present investigation the gas temperature has not been measured. Results published by the present research team [2] make it possible to set estimates of average gas temperature at about 2000 - 2500 K and average Doppler

half-width at about $2.2*10^{-3}$ nm. The population formula for the Doppler case is written as:

$$N = \text{const} \frac{\Delta\lambda_D}{A_{ij}\ \lambda^4} \alpha_0 \qquad (2)$$

Here $\Delta\lambda_D$ is the Doppler half-width. λ is the wavelength of the bandhead and A_{ij} is the absolute transition probability of the band. The constant dependens on the system of units used. In Fig. 4 the time dependence of the concentration of N_2^+ ions on the vibrational level v=0 is presented. To determine the total concentration of N_2^+ ions the vibrational temperature in N_2^+ ground state is to be known. The latter, however, cannot be measured directly. The vibrational temperature for N_2 ground state has been determined on the assumption of its strong correlation with the directly measurable vibrational temperature in the excited state $C^3\Pi_u$. According to our indirect data the vibrational temperature in N_2 ground state for t > 200 μs is about 5000 K. If to assume that the vibrational temperature in N_2^+ ground state has the same value due to effective V - V transitions, the total N_2^+ ion concentration reaches a value of about $2.5*10^{14}$ $1/cm^3$ at

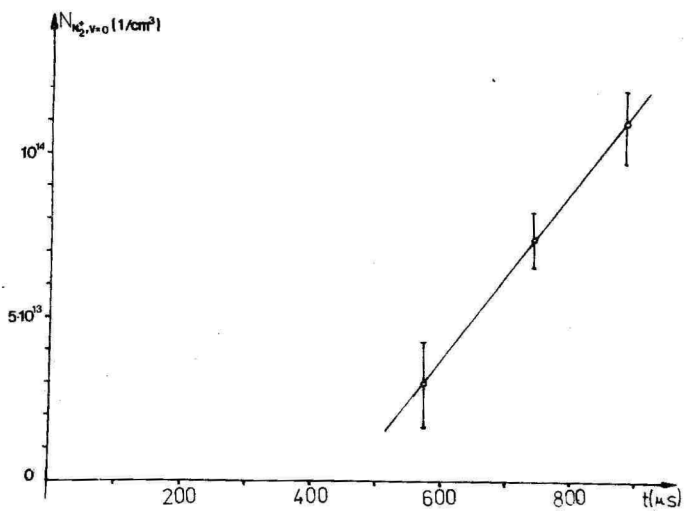

Fig. 4. The time dependence of the concentration of N_2^+ ions on the vibrational level v=0.

the end of the radiopulse.

It should be noted, that N_2^+ are not the only kind of ions in any nitrogen discharge. Due to the conversion

$$2N_2 + N_2^+ \rightarrow N_4^+ + N_2 \qquad (3)$$

and dissociative recombination of both N_2^+ and N_4^+ (the latter having the dissociative recombination rate coefficient about an order of magnitude greater than N_2^+), there is a certain balance of concentrations of these two kinds of ions. Applying the conversion rate coefficients presented in [3], it can be concluded that at later states of the discharge the relative concentration of N_4^+ ions is not higher than 10 %. N_3^+ ions are not likely to play a significant part in the process because of relatively low dissociation degree.

As is seen in Fig. 4, the N_2^+ ion concentration has been determined only for later states of the discharge channel propagation. The $B^2\Sigma_u^+$ state of N_2^+ is excited mostly by collisions of N_2^+ ions in the ground state with the vibrationally excited molecules in the ground state of N_2. Therefore at the initial state of the discharge with lower vibrational temperature there is practically no 1 system radiation. The method has been successfully used to determine the concentration of the N_2 $B^3\Pi_g$ state [4]. It became possible because the $C^3\Pi_u$ state is excited by various mechanisms and the $N_2\,2^+$ $0 \rightarrow 0$ band radiates throughout the radiopulse. A suitable method to determine N_2^+ ion concentration at earlier states of the discharge seems to be LIF (Laser-Induced Fluorescence).

In conclusion it should be mentioned that the investigation detected a growth in the ionization degree at the later state of the discharge. The fact is highly interesting as the reduced field strength E/N (N being the concentration of neutrals) in the discharge did not rise at $t > 500\ \mu s$, having a relatively low value of 20 Td. The phenomenon has no satisfactory empirically tested explanation.

REFERENCES

1. Фриш С. Э. Определение концентрации нормальных и возбужденных атомов и сил осцилляторов методом испускания и поглощения света. – В кн.: Спектроскопия газоразрядной плазмы/ Под ред. С. Э. Фриш. – Л.: Наука, 1970. – с. 7-62.
2. Laan, M. and Susi, J. Optical diagnostics of the propagating HF discharge in nitrogen // Acta et comm. Univ. Tartuensis. – 1987. – No. 755. – pp. 3-9.
3. van Koppen P.A.M., Jarrold M.F., Bowers M.T., Bass L.M., Jennings K.R. Ion-molecule association reactions: A study of the temperature dependence of the reaction $N_2^+ + N_2 + M \rightarrow N_4^+ + M$ for M = N_2, Ne and He. Experiment and theory // J. Chem. Phys. – 1984. – Vol. 81. – No. 1. – pp. 288-297.
4. Laan, M., Susi, J. Determination of N_2 $C^3\Pi_u \rightarrow B^3\Pi_g$ 0 → 0 band absorption in the propagating HF discharge channel // XVII ICPIG. Budapest. – 1985. – Vol. 2. – pp. 1014-1016.

ОПТИЧЕСКОЕ ОПРЕДЕЛЕНИЕ КОНЦЕНТРАЦИИ ИОНОВ В ВЫСОКОЧАСТОТНОЙ ПЛАЗМЕ АЗОТА: ИЗМЕРЕНИЕ ПОГЛОЩЕНИЯ

М.Р. Лаан, П.П. Парис, Я.А. Сузи

Р е з ю м е

Методом измерения относительного поглощения излучения перехода 0 → 0 первой отрицательной системы азота определяется концентрация ионов N_2^+ в канале нестационарного ВЧ разряда. Исследовали импульсный ВЧ разряд (длительность импульса I мс, несущая частота 20 МГц) с остриевого электрода в азоте атмосферного давления. Метод одного зеркала позволяет определить кинетику концентрации ионов N_2^+ на поздних стадиях распространения разрядного канала (t > 500 мкс). Для ранних стадий разряда указанный метод неприменим из-за отсутствия излучения первой отрицательной системы азота. Наблюдается рост степени ионизации к концу импульса разряда несмотря на уменьшение значения приведенной напряженности электрического поля E/N.

THE DISCHARGE IN ARGON AT ATMOSPHERIC PRESSURE IN THE POINT-TO-PLANE DISCHARGE GAP

H. Korge, U. Kuusk and M. Laan

Discharges in rare gases in strongly inhomogeneous field at atmospheric pressure have been discussed in a relatively small number of publications [1]. At the same time this type of discharge is a convenient object to investigate the mechanisms of contraction. The present paper is our first step in this direction.

The experimental setup was the same as that in [2]. A hemispherically capped platinum rod with a diameter of 1 mm and a plane nickel disc with a diameter of 20 cm were mounted at a distance of 4 cm in a stainless steel vacuum chamber with quartz windows. The chamber had a volume of about 20 litres. The chamber was evacuated to $8*10^{-8}$ Torr and filled with pure argon. The gas pressure in the system was set at 770 Torr. Recording the discharge current-voltage characteristics high voltage was supplied to the point electrode over a 10 MΩ ballast resistance.

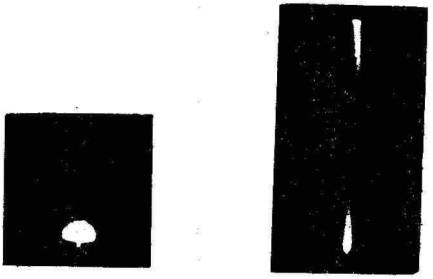

a) b)

Fig. 1. Appearance of the discharge in the case of negative point: a) diffuse discharge form b) constricted discharge form.

At the negative point the discharge took two characteristic forms of discharge (see Fig. 1.). For lower

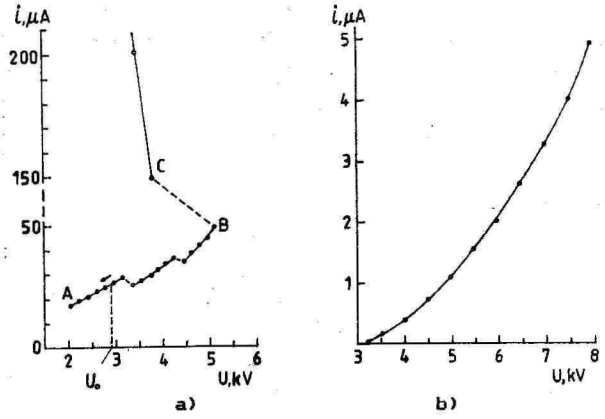

Fig. 2. Current-voltage characteristics of the discharge in the point-to-plane discharge gap in argon at a pressure of 770 torr (gap distance 4.0 cm; ballast resistance 10 MΩ) a) at the negative point and b) at the positive point.

currents up to the point B (see Fig. 2,a) the distribution of luminosity was of a diffuse type (see Fig. 1,a), whereas only the more intense luminosity around the point was registered on photo. Actually faint diffuse luminosity can be seen in the whole discharge gap except for the region near the point with a bright narrow channel of a length of less than 1 mm. Around the point electrode a conical light boundary can be observed. The notches on the curve AB (see Fig. 2,a) correspond to the change in the location of the point.

As a rule higher voltage causes the channel to be located on the lateral surface of the point. At B more intense luminosity regions near the plate electrode can be seen. After transition from B to C the discharge had a shape of a diffuse bright channel bridging the gap (see Fig. 1,b), whereas the distribution of diffused luminosity in the gap remained unchanged.

It is revealing to compare the current-voltage characteristics of argon and nitrogen [2]. Identical characteristic parts can be seen on these curves, but at the same

time there is a considerable quantitative difference connected with different distribution function of electrons in inert and molecular gases. For argon the onset potential (U = 2,9 kV) did not coincide with the offset potential (U = 2,1 kV) which leads to the conclusion that already for the part AB (see Fig. 2,a) the stepwise ionisation mechanism plays an important role.

The current-voltage characteristic for the positive point was measured up to 8 kV (see Fig. 2,b). The onset potential U = 3,2 kV coincided with the offset potential and was approximately equal to the potential of the negative point.

The discharge could be observed as a steady feeble red glow covering the point tip. Burst pulses or streamers were not registered. The currents at the threshold were of the order of 10^{-8} A. Thus the results are similar to those obtained by Das ; Wessler who used considerably purer discharge conditions did not obtain a corona before spark breakdown at 3,5 kV [1].

Both, diffuse and constricted discharge forms at the negative point were investigated spectroscopically (see Figs. 3 and 4.).

Spectra were registered over a wavelength range from 250 to 800 nm by means of photomultipliers FEU-140 and FEU-83 and a monochromator MZD-2. Radiation from the bright narrow channel region was focussed on the input slit of the monochromator by means of glass and quartz optics. Spectral

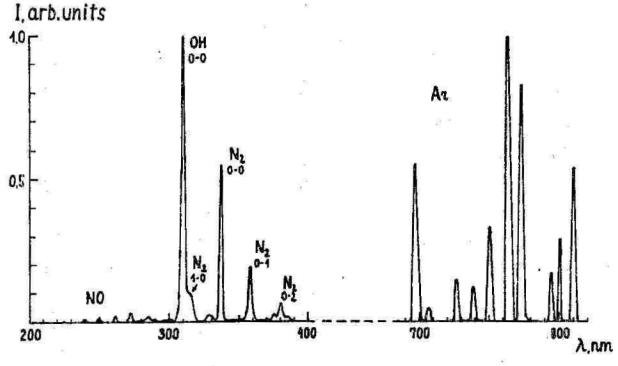

Fig. 3. The spectrum of the discharge in argon at the negative point.

sensitivities of different optical setups employed were determined with a tungsten gauge lamp.

In addition to the argon lines (transition 4p-4s) (see Fig. 3) the bands of the second positive system of N_2, an OH band and weak traces of NO were detected. Line intensities registered from red and violet parts of the spectrum are not related in Fig. 3.

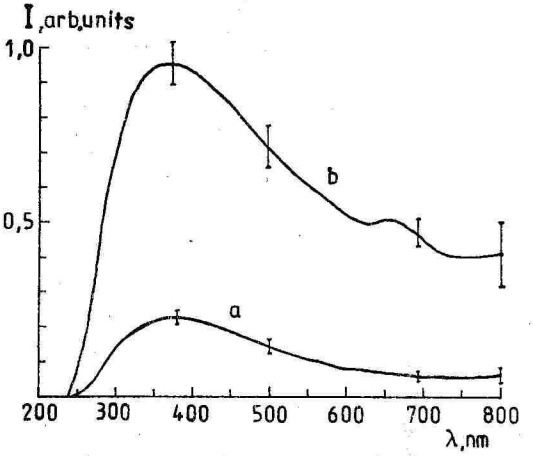

Fig. 4. The spectral intensity distribution of Ar continuum in a) diffuse discharge form b) constricted discharge form.

Characteristically, the line spectrum was superimposed upon the continuous spectrum (see Fig. 4). This type of spectrum is well-known in the case of positive column of rare gas medium-pressure glow discharges.

The radiation continuum has been thoroughly investigated in both, diffuse and constricted glow discharge forms and its bremsstrahlung origin has been proved [3,4]. In addition to the bremsstrahlung continuum mechanism, a continuum determined by a transition between bound and dissociative molecular states is possible. The molecular continuum has been observed in the afterglow of low pressure discharge [5]. Data on discharges at atmospheric pressure have been presented in [6], where the study was carried out in a high current regime

under impure conditions. In the present experiment the spectral intensity distribution in both discharge forms (see Fig. 4.) was similar to the distribution in [3,4].

References

1. Loeb, L.B. Electrical coronas // Berkeley and Los Angeles, University of California Press, 1965.
2. Korge, H., Kudu, K., Laan, M. The discharge in pure nitrogen at atmospheric pressure in point-to-plane discharge gap // 3rd Int. Symp. High Voltage Eng., Milan, 1979, Paper 31.04.
3. Pfau, S., Rutscher, A. Continuum Radiation of Positive Column of Rare Gas Discharges // Proc. IX Conf. on Phenomena in ionized Gases, Bucharest, 1969. - p. 586.
4. Pfau, S., Rutscher, A. On the origin of visible continuum radiation in rare gas glow discharges // Physica 81 C, 1976. - p. 395-402.
5. Герасимов Г.Н., Малешин М.Н. Молекулярный спектр ксенона в области 200-1000 нм // Оптика и спектроскопия. - 1985. - том 58, вып. 5. - с. 1029-1033.
6. Королев Ю.Д., Хузеев А.П., Шемякин И.А. Сильноточный диффузный разряд в аргоне //Изв. вузов сер. физика. - Томск, 1983. - No. 6736-83Деп.

РАЗРЯД В АРГОНЕ ПРИ АТМОСФЕРНОМ ДАВЛЕНИИ В РАЗРЯДНОМ ПРОМЕЖУТКЕ ОСТРИЕ-ПЛОСКОСТЬ

Х.И. Корге, У.И. Кууск, М.Р. Лаан

Р е з ю м е

Разряд возбуждался в аргоне при атмоферном давлении в разрядном промежутке острие-плоскость. Вольт-амперная характеристика разряда снята при отрицательном и положительном напряжениях острия. Описаны внешние формы разряда. В случае отрицательного острия установлено существование двух форм разряда - диффузного и контрагированного, для которых сняты спектры вблизи острия. Спектр контрагированного разряда лишь интенсивнее спектра диффузного разряда, качественных различий не обнаружено.

THE SPECTRUM OF RADIO NOISE GENERATED IN CORONA DISCHARGE ON MODEL ANTENNAE

V. Smirnov

It is known that corona discharges generated at the edges of surfaces in strong electric fields are sources of radio noise. This fact is of particular interest primarily in connection with thunderstorm clouds and highvoltage power lines [3-6]. The information available on the frequency spectrum of such radio noise characterizes a relatively narrow frequency interval (10^6...10^8 Hz) predominantly for the alternating current corona without the analysis of the physical nature of the radio noise.

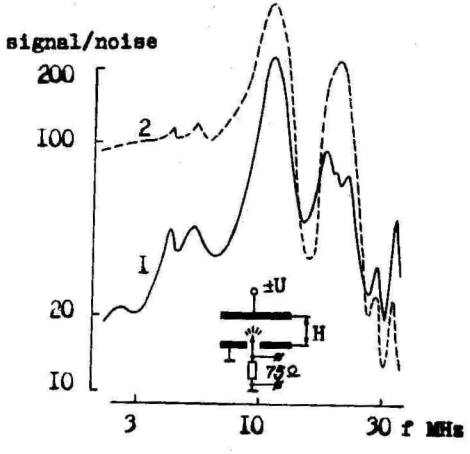

Fig. 1. Frequency track of the signal r.m.s. value for the negative (I) and positive (2) corona from 1 mm diameter point in 3 kV/cm field. The detector bandwidth is 5 kHz.

This paper presents the results of an experimental study of 10^4...10^9 Hz frequency spectrum of signals induced by unipolar corona points in the electric fields up to $3*10^3$ V/cm in the plane gap under strictly controlled conditions (fixed geometry of the gap and antenna, absence of pollutants in the air, absence of air movement, etc.).

The design of the experiment is presented in Fig. 1. The

discharge gap was formed by 30 cm diameter brass disk electrodes with adjustable gap up to 15 cm. The model antennae were 5-30 mm diameter metallic rods with various angles of edge slope (from 30° to 5°). The ratio between rod and gap lengths was 3...15. The MCP-30 selective microvoltmeter (Syden-Telec, France) was used as a measuring receiver conforming to the international standard CISPR. The experiment included the measurements of the amplitude - frequency spectrum of the signals emitted by Ohmic loading of 75Ω on the corona electrode, whereas the sign and magnitude of the capacitor upper plate potential were changed with respect to grounded bottom disk on which the corona antenna was located. It should be noted that the geometry of the gap and the antenna did not significantly influence the noise spectrum structure at moderate field values ($E \leq 3 E_o$, where E_o is the corona of onset field strength).

The typical measurement results of amplitude - frequency characteristics (AFC) of unipolar corona discharge signal on 1.5 cm antenna in 8 cm gap for 3-60 and 60 kHz...800 MHz frequency intervals, respectively, are brought in Figs. 1 and 2. Output signals of AM ($F \leq 30$ MHz) and FM detectors were registered by a rms voltmeter.

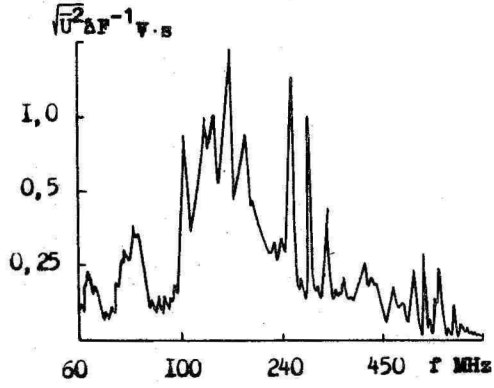

Fig. 2. The noise signal spectrum of the positive corona normalized to the radio set bandwidth. The electric field strength is 2 kV, the gap is 80 mm.

From these figures it follows that generally, in contrast to the available data [4,6], the signal spectrum is not continuous but bandpass. For 100-800 MHz interval the line structure was more typical. The band locations do not practically depend on the corona polarity. The largest signal amplitude corresponds to 10 MHz frequencies. Intense bands can also be found in 50 kHz, 5, 20, and 150 MHz ranges. The polarity of the corona appears mainly as differences in noise amplitudes at the spectrum edges. The negative corona signal amplitude decreases more quickly as the frequency decreases with respect to maximum. At high frequencies the positive corona amplitude falls more rapidly. From this follows a practically important recommendation concerning the dependence of optimal frequencies of radio reception on the polarity of the contraelectrode potential.

The signal level is in a complex dependence on the frequency tuning of the receiver. As is seen in Fig. 3, each frequency value has its corresponding maximum of the signal and higher frequencies have higher values of the potential at which the amplitude maximum is reached. This effect, unknown in the literature, may be of practical importance as it makes it possible to optimize the problems not only over the polarity of the contraelectrode, but over the absolute values

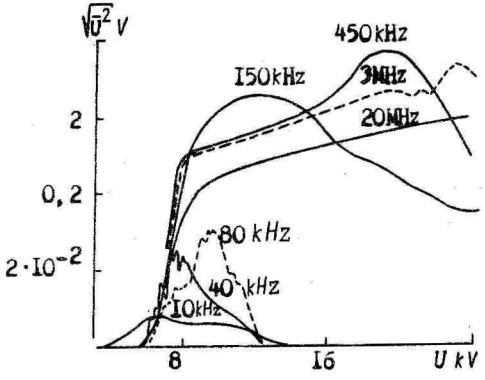

Fig. 3. R.m.s. amplitude of signal as a function of field strength in the discharge gap of 80 mm length and frequency of AM receiver tuning. The corona is negative.

of the field strength in the discharge gap. It should be emphasized that similar regularities are supported for the values of the relation between antenna length and discharge gap from 0.5 to 10 practically independently of the electrode form. The variation of the electrode radius r_o influences only the signal frequency variation at the output of the detector at moderate field strengths ($E \approx E_o \ldots 2E_o$), increasing approximately linearily with decreasing r from 100 to 10 μm.

Let us attempt to obtain a radiotechnical analog of a signal form from the data on the effective frequency bandwidth occupied by the signal (at the noise-signal ratio of about 3 the width is 600 MHz) and the mean duration of the discharge pulse $\tau \approx 10^{-7}$ s [2]; and to determine in the ordinary way the form index K through frequency band and signal duration: $K = \tau/(2\,\Delta f) \approx 20$. This value is between the indexes for the cosine-cubic (K = 5,2) and right-angled (K = 33) pulses. It can be seen that this is in agreement with the commonly used "oscillographic" model of discharge pulse - dual exponent with constant time of increase and decrease of 10^{-8} and 10^{-7} s.

Let us consider the character of corona discharge signal sequences that can give more valid information on the nature of the noise. Correlation analysis is known to be a reliable way for revealing interrelations in a system. A DISA correlator 55D70 was used to obtain cofunction on the basis of multiplication analog version realization.

$$\hat{K}(\tau) = \frac{1}{T}\int_0^{T-|\tau|} [\overline{x(t)} \cdot \overline{x(t+\tau)}]\, dt,$$

where τ is the correlation interval ($0 \leq |\tau| \leq T$). The correlator was connected to the linear output of a "video" measuring receiver. In Fig. 4. examples of some realizations for various discharge gap potentials at 7 MHz frequency are presented.

The case of the positive corona is of particular interest because, as noted in [1], there is no universally recognized single opinion about the degree of discharge periodicity. As is seen in Fig. 4 the signals in the positive corona have some periodicity at certain values of the gap potential. It appears more sharply at potentials which are slightly higher

than the corona onset threshold (~8 kV) typical of the pre-onset streamer regime [1]. Under these conditions the interference (noise) signal maximum is achieved at carrier frequencies of 100 kHz. The correlation function for narrow 9±0.5 kV interval of the positive corona potentials corresponds to the correlation function of the uniform sequence of smoothed bipolar rectangular pulses, and for the rest of the values of U it corresponds to unipolar impulses with very small on-off time ratio.

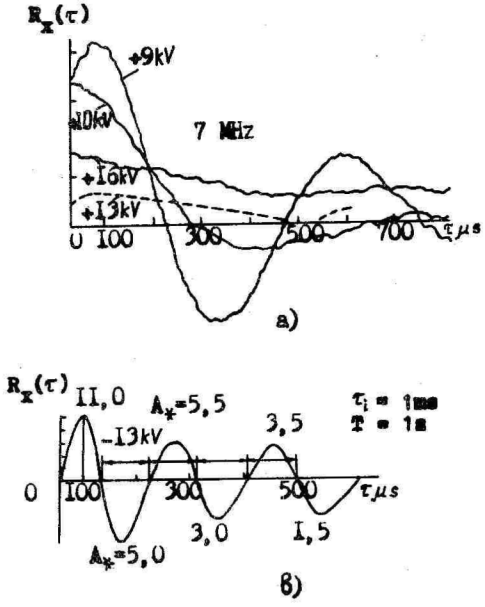

Fig. 4. The noise correlation functions of the positive (a) and negative (b) corona in the point to plane gap. The carrier frequency is 7 MHz. MCP-30 receiver (Syden Telec, France). 55D70 correlator (DISA, Denmark). The correlation time is 10^{-3} s, the integration time is 1 s. Numbers along the R_x function characterize relative amplitudes of the correlator signal.

In the negative corona regimes ($U \leq 1{,}2\ U_o \ldots 3U_o$) and at bipolar ionization in the positive corona of the discharge

contour (circuit) produced by two ^{239}Pu plates, total current of 10^{-6} A varied the regime considerably (Fig. 4b). Here the correlation function resembles the correlation functions for low-pass white noise:

$$R(\tau) = a * \Delta f * \sin(2\pi \Delta f)/2\pi \Delta f * \tau,$$

where a is a coefficient. The spectral density of such signal power $G_x(\tau) = 4\int_0^\infty K(\tau)\cos(2\pi f \tau)d$ on the O,f axes is a rectangle with the sides of a and Δf.

Thus, in the general case, the corona discharge signals induced on a metal rod of random configuration and length, have at the detector output features of white noise limited by the radio set bandwidth. The noise level decrease at a given electric field value can be achieved by optimal carrier selection of the reception frequency. To achieve an even greater decrease it is reasonable, considering the nature of the corona discharge, to strobe the receiver input circuit by an interval of at least 3τ, where τ is the discharge pulse duration ($\sim 10^{-7}$ s).

Conclusions

1. The noise signal generated in the electric circuit of the discharge gap, produced by a conductive disk under a static potential and by a point-antenna, exceeds the noise level of radio receivers used in $10^4 - 10^9$ Hz range $10^2 \ldots 10^4$ times.

2. The amplitude - frequency signal characteristics of both, positive and negative corona discharge are not continuous, as has been supposed in the literature, but have a band and line structure. The main bandwidths are in the range of 4 ± 2 MHz, 19 ± 2 MHz, 25 ± 2 MHz, and 150 ± 20 MHz. Some lines can occur inside the bands. Experimental estimates of the centres of the above frequency bands are in agreement with the results derived from the analysis of the fine structure of corona discharge pulses measured in [2]. Thus , the main 15 MHz and 150 MHz bandwidths (signal repetition rates about 70 ns and 7 ns, respectively) are in good agreement with the discharge pulse duration values (~ 70 ns) and head front duration (~ 5 ns). The 25 MHz bandwidth is likely to be the second harmonic of the discharge pulse.

3. Low frequency bandwidths (below 100 kHz) are typical of the low strength regimes of the electric field ($E \approx E_o$). The contribution of UHF harmonics increases together with the strength. With increasing E the main bandwidths of 12 MHz and 150 MHz slightly grow in amplitude which indicates the conservatism of discharge pulse characteristics (forms, duration, charge) in a wide interval of the field strength.

4. The noise recorded at the detector output of the AM/FM receiver with corona antenna has white noise features, and it results from the expansion of discharge pulses in harmonics in the radio set circuits.

References

1. Kudu, K.F. On the initial (pre-onset) stage from the point discharge to the air // Tartu: Tartu State University. - 1960, 56 p. (in Russian).
2. Laan, M.P. Field distribution calculation in case of continuous corona impulses // Research Notes of the Tartu University, 1979. - Issue 479, - pp. 77-106 (in Russian).
3. Riser, Y.P. Gas discharge physics // M.: Nauka. - 1987, - pp. 505-511 (in Russian).
4. Perelman, L.S. and Chernoborodov, M.I. Study on the positive corona impulses and radionoise from the conductor under natural conditions // Electricity, 1966. - No. 4, - pp. 62-66 (in Russian).
5. Khalifa, M.M., Kamal, A.A., Zeitoun, A., Radwah, R., E.C.-Bedwainy, S. Correlation of radio noise and quasi-peak measurement to corona pulse randomness // IEEE Trans. of power appar. and systems, 1969. - Vol. 88. - No. 10, - pp. 1512-1521.
6. Nigol, O. Analysis of radio noise from high-voltage lines // IEEE Trans. of power appar. and systems, 1964. - Vol. 83, - pp. 534-535.

О СПЕКТРЕ РАДИОШУМОВ,ВОЗНИКАЮЩИХ ПРИ КОРОНИРОВАНИИ МОДЕЛЬНЫХ АНТЕНН

В.В. Смирнов

Р е з ю м е

Изучаются амплитудно-частотные характеристики радио-сигналов в интервале частот 10 кГц...1ГГц, возникающих при коронировании электродов-антенн, как функции полярности короны и напряженности электрического поля. Указывается на преимущественно полосовую структуру помехи. Положение центров полос (15, 150 МГц и др.), независимое от полярности и величины поля интерпретируется как результат спектрального разложения в трактах радиоприемника импульсов коронного разряда типа двойной экспоненты, имеющих средние значения длительности переднего фронта около 7 нс и длительности на полувысоте 70 нс. Анализ автокоррелограммы помехового сигнала подверждает наличие высоко периодических режимов в отрицательной и, частично, положительной короне.

AIR ION OBSERVATORY AT TAHKUSE: INSTRUMENTATION

U. Hõrrak, F. Miller, A. Mirme, J. Salm, and H. Tammet

Introduction

The system is designed for continuous recording of atmospheric electrical and meteorological parameters at an observation station. It is installed at Tahkuse village situated 27 km NE from Pärnu, Estonian SSR, USSR [1,2]. The design of the system is based on the research in [3,4,5]. In addition to the air ion mobility spectrum in a wide range of $3*10^{-4}$ ...3 $cm^2/(V*s)$ the system is able to measure and record basic meteorological parameters, electric field strength, intensity of atmospherics, etc.

General layout of the system

Principal components of the system are depicted in Fig.1.

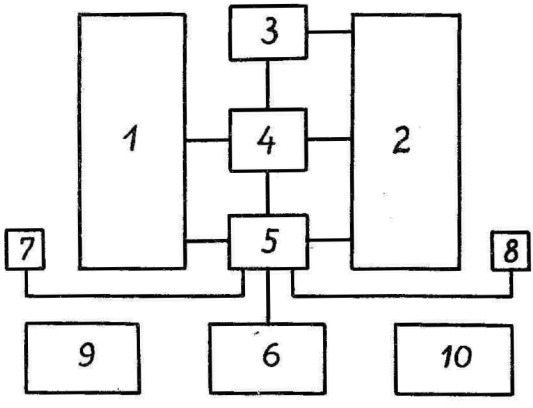

Fig. 1. Block-diagram of the system

The air ion mobilities are measured by a six-channel (1) and a ten-channel (2) spectrometer (abbreviations S-6 and S-10, respectively). One of the measuring capacitors of S-10 is equipped with a charger (3) to obtain some extra infor-

mation about aerosol particles. Direct voltage for each measuring capacitor (MC) is provided by the voltage supply (4) controlled by the controller (5). Besides the control of the components of the system the controller is responsible for the reception and tranmission of signals. The controller is operated by an Elektronika D3-28* computer (6). The computer program controls the measurement, preliminary data processing and storage.

In addition to the spectrometers, the system has sensors for meteorological parameters (7). The control panel (8) is used to control the display of current results and, if necessary, to change operation modes. Both spectrometers are in the same air tract (9) with a common fan. As a precaution against possible power cuts the computer, the controller, and the voltage supply have an autonomous power supply (10). The above devices, excluding the meteorological sensors, are enclosed in a thermally insulated stable-climate chamber which makes it possible to use the equipment throughout all four seasons.

Six-channel air ion spectrometer

The measuring capacitor of S-6 is identical to the one described in [5]. The electrometric amplifiers are described in [6]. The feedback circuit of the amplifier consists of parallel resistor (about 1 TΩ) and capacitor (about 50 pF). The exact values of resistance and capacitance are determined for each amplifier.

S-6 has six collector electrodes, the respective channels are numbered from 0 to 5 according to the air flow.

The incoming air flow is divided into two parts by a preliminary capacitor. The outer coaxial layer is deionized, while the central flow passes through retaining its natural condition. To ensure efficiency of the preliminary capacitor, the polarity and value of the voltage are chosen in line with the recommendations in [7,8].

---

* Henceforth the originally Cyrillic letters used in the designations of apparatus types have been transliterated into the Latin alphabet.

The total flow rate is 9900 cm^3/s. The flow rate of the outer deionized layer is 8200 cm^3/s. Limiting mobilities for each channel can be computed by means of the geometrical average of the total flow rate and the outer layer flow rate (this average is 9000 cm^3/s). Air ion spectrum will be presented in mobility bands (subintervals) with boundaries close to the limiting mobilities. The boundary mobilities are presented in Table 1.

Table 1

Boundary mobilities of S-6, in $cm^2/(V*s)$

Channel No		0	1	2	3	4	5
at 47.5 V	from	2.5	2.0	1.6	1.26	1.0	0.8
	to	3.2	2.5	2.0	1.6	1.26	1.0
at 150 V	from	0.8	0.63	0.5	0.4	0.32	0.25
	to	1.0	0.8	0.63	0.5	0.4	0.32

The limiting mobility of the preliminary capacitor is two times lower than the minimum limiting mobility of the MC.

An approximate description of the dependence of the signal on the mobility inside subintervals can be given by a triangular graph where maximum sensitivity is located in the geometrical centre of a subinterval and where sensitivity decreases towards the limits of the subintervals [9].

Ten-channel air ion spectrometer

Basic characteristics of S-10 are idential to those published in [3]. The only significant modification are preliminary capacitors added at the entrances to MCs. These preliminary capacitors give the spectrometer the characteristics of a differential spectrometer of the second order [9]. The preliminary capacitor is depicted in Fig. 2.

Electrodes 1 and 3 are grounded, electrode 2 is given DC voltage. The air between electrodes 1-2 and 2-3 is deionized, whereas the air passing electrode 1 retains its natural condition. In S-10 (as well as in S-6) effective filtration is achieved by the selection of voltage polarity and value on electrode 2 in accordance with the recommendations in [7,8].

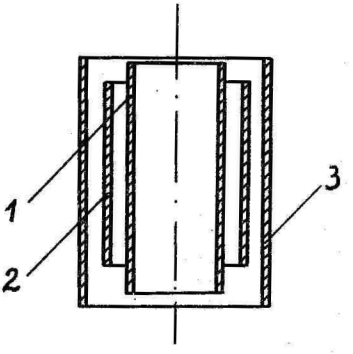

Fig. 2. Preliminary capacitor for S-10. 1,2,3 - the electrodes.

S-10 has two measuring capacitors: MC_i for small and intermediate ions (channels 6...10) and MC_l for large ions (channels 11...15). The voltage on MC_i is 406 V, the total air flow rate is 4750 cm^3/s, the flow rate of the outer layer is 2350 cm^3/s and the geometrical average of the flow rates is 3340 cm^3/s. The voltage on MC_l is 890 V, the total flow rate is 1210 cm^3/s, the flow rate of the outer layer is 600 cm^3/s and the geometrical average of the flow rates is 850 cm^3/s.

The boundaries of the mobilities for S-10 are presented in Table 2.

Table 2

Boundary mobilities of S-10, in $cm^2/(V*s)$

Channel No		6	7	8	9	10
MC_i	from	0.4	0.15	0.07	0.032	0.015
	to	∞	0.32	0.15	0.07	0.032
Channel No		11	12	13	14	15
MC_l	from	0.007	0.0032	0.0015	0.0007	0.00032
	to	0.015	0.007	0.0032	0.0015	0.0007

Channel 6 has integral characteristic, while the other channels are differential with approximate triangular apparatus functions [9]. The limiting mobilites of the preliminary ca-

pacitors are 8 and 4 times smaller than the respective minimum limiting mobilites of MC_1 and MC_4.

Charger

The charger makes it possible to control the charging of aerosol particles in order to obtain extra information on the size spectrum of the atmospheric aerosol and on electrical parameters of the atmospheric aerosol. A computer program can turn the charger on/off. Depending on the program, the charger can charge particles either with negative or positive small air ions.

The charger was to meet two main conditions. First, it had to guarantee an opportunity for theoretical calculation of the aerosol particle charging processes in the device. Second, it has to achieve a good approximation to an ideal unipolar diffusion charging of particles with small air ions. As a basis for the attainment of these two aims the theoretical model of ideal transverse charger proposed in [10] was used.

The layout of the charger is illustrated in Fig. 3.

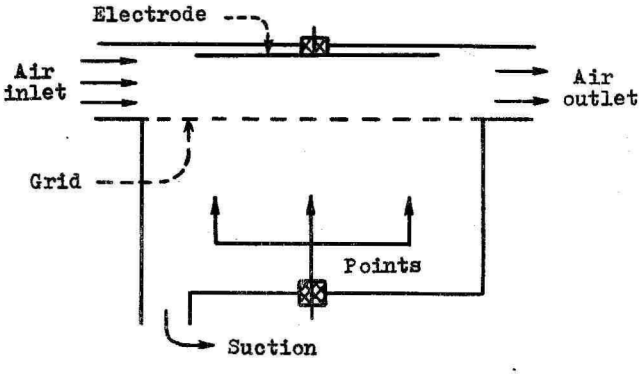

Fig. 3. Diagram of the charger

From above the charging zone is limited by a plane electrode connected with an electrometric amplifier, from below it is limited by a plane grid through which small air ions are fed. The length of the zone is 20 cm, the width is 12 cm and the heigth is 5 cm. The flow rate of inlet air is about

1500 cm^3/s; the flow rate of outlet air is about 1200 cm^3/s. Approximately 300 cm^3/s is sucked away through the grid. The suction is carried out in order to suppress the transport of corona products into the charging zone. The voltage between the electrode and the grid is 200 V, the respective field strength is 40 V/cm. When the net is dust-free, and the voltage on the points is 3 kV, the value of the dimensionless charging parameter $\propto$ (cf.[10]) is approximately 20, or $n_0 t$ is approximately $8*10^6 s \cdot e/cm^3$. When the net is contaminated with dust and/or hair the value of the parameter $\propto$ decreases.

The actual value of the dimensionless charging parameter is computed using the effective value of the strength of small air ion current through the upper electrode of the charger which is obtained and recorded by the system.

Voltage supply

The voltage supply provides the measuring capacitors, the preliminary capacitors, and the charger with high-stability voltages of 400 V, 890 V, 1.8 kV and 3 kV.

Stabilized direct voltage is obtained by the rectification of HF voltage provided by a stabilized generator. Final stabilization is carried out by means of parametrical stabilizers on corona stabilitrons SG301S and SG302S.

A voltage of 890 V on the measuring capacitors is given by one and the same highly-stable supply through a voltage divider with a total resistance of 61 MΩ.

The voltage supply is controlled by a controller which turns it on/off and switches the polarities. For physical switching of high voltage a special relay is used.

Controller and control panel

The controller used in the present system is an analogy of the device described in [4]. The controller comprises a control block, a relay commutator for analog signals, an analog-digital converter (ADC), a protection circuit for the electrometric amplifiers of the spectrometers, triggers and relays for commutation, a timer, and a preliminary amplifier with an amplification coefficient of 100.

According to the commands of a Elektronika D3-28 computer the controller performs various functions: controls the

shorting of relay switches at the input of the electrometric amplifier through the protection circuit, switches the voltages of the preliminary and measuring capacitors and of the charger, performs commutations necessary for regular zero-control of several sensors.

According to the commands of the computer the controller obtains signals from different sensors and from the electrometric amplifiers of the spectrometers, subsequently the signals are transformed into a code and transmitted to the computer.

The control panel is used for the selection of operation mode and for current indication of results on the display of the computer, as well as for labeling the record.

To suppress noises the controller is connected to the computer via a unit of galvanic isolation.

The measurement range at the input to the ADC is -10 V...10 V. The digitization increment is 5 mV for signals with an absolute values higher than 1 V and 0,5 mV for the signals with absolute values lower than 1 V. A preliminary amplifier with an amplification coefficient of 100 can be added to any measuring channel.

The measurement time for one channel is about 20 ms, whereas the span cannot be reduced due to the inertia of the electromagnetic relays of the commutator.

Air tract

The inlet opening for the investigated air is in the southern side of the observatory building, at a height of 5 m from the ground. Protection against precipitation is provided by a metal shelter. A metallic channel with a cross section of 0.02 m^2 leads the air to the two spectrometers (S-6 and S-10). The time of air travel in the channel is about 1.5 s. To suppress turbulence the channel is provided with lengthwise walls as well as with directing blades at bends and at the outlet. The channel grows narrower in the direction of the flow.

The flow is created by a sucking fan. Distribution chamber at the inlet end of the fan provides calibrated air flows through MCs (S-6, MC_1, MC_1) and the charger. To suppress the effect of wind on the flow rate the outlet of the fan takes place at the same side of the building with the inlet.

Autonomous power supply

The device for uninterrupted power supply consists of a reference 50 Hz generator, a low frequency amplifier, a power supply, and floating batteries.

Before being used by the load connected to the device the signal of the reference generator is amplified by a 200 W amplifier with automatic adjustment of output voltage to 220 V. The generator and the amplifier operate on the mains (220 V) through the power supply and floating batteries with a voltage of 24 V and a capacitance of 120 Ah.

The computer, the controller and the voltage supply are fed through the above device. It ensures the stabilization of short-term fluctuations in the voltage supplied from the mains, it also warrants the integrity of the program and automatic resumption of operation after power cuts lasting less than 3 hours.

Sensors

According to functions the sensors of the measurement system can be divided into three groups: the sensors of meteorological parameters, the sensors of atmospheric electricity parameters, and the sensors monitoring technological parameters of the measurement system itself.

The first group comprises the sensors of:

(1) direction and velocity of the wind (anemorhumbometer M63M-1 [11] with a supplementary device for electrical output);

(2) relative humidity of the air (hygrometer GS-210 and a hair hygrometer equipped with a potentiometric converter);

(3) the temperatures of the air and earth (graduated temperature-sensitive resistors MMT-4 with a nominal resistance of 15 kΩ);

(4) atmospheric pressure (a unified sensor of pressure, system KRAMS [11,12]);

(5) meteorological visibility RDV-2([11,12]);

(6) total radiation (thermal electrical pyranometer M-80M [11],.

The sensors of temperature and humidity are in a channel provided with a fan and situated near the inlet of the main

air tract. The photometric unit of the sensor RDV-2 is in a special shelter at a height of about 2 m, the prism reflector with an additional metallic protection shield is elevated on a concrete support pillar to a height of 3.5 m; the support with the reflector is 100 m away from the photometric unit RDV-2. The sensor of wind direction and velocity is at the top of a 10 m support.

The second group is made up a Pole-2 field strength sensor [13] and a sensor of close thunderstorms. The latter has been built on the analogy of the KRAMS-system sensor [12], it has two sensitivity limits for thunderstorms at a distance up to 10 km, or 30 km, respectively. These sensors have been positioned separately from each other and from the other sensors in accordance with their operational requirements.

The sensors of the third group, monitoring the technological parameters of the system, comprise the sensor of current strength of the charger, the sensor of minimal voltage from the mains, and the sensor of temperature in the thermal-insulation chamber.

The above set of sensors is open to alteration and addition as the controller can cope with 12 additional sensors.

The computer program controlling the system is thoroughly described in the present volume [14].

Acknowledgements

The above measurement system would not have materialized without the efforts of the whole staff of the Air Electricity Laboratory at Tartu University. The authors express their sincere gratitude to their colleagues at the Laboratory as well as to Y. Georgiyevsky, R. Sepp, T. Sinimäe, V. Smirnov and M. Sulev.

References

1. Таммет Х.Ф., Ихер Х.Р., Миллер Ф.Г. Спектр подвижности односекундных легких аэроионов в природном воздухе // Уч. зап. Тарт. ун-та. – 1985. – Вып. 707. – С. 26-36.
2. Хыррак У.Э., Таммет Х.Ф., Ихер Х.Р., Сальм Я.Й. Зависимость спектра аэроионов от ветра (по измерениям в Тахкузе в 1985 году) // Уч. зап. Тарт. ун-та. – 1988. –

Вып. 809. – С. 79–86.

3. Сальм Я.Й. Десятиканальный спектрометр аэроионов // Методы и приборы биоинформации и конторолля параметров окружающей среды. Межвуз. сб. – Вып. 150. – Л.: ЛЭТИ, ЛИАП, 1981. – С. 34–38.

4. Мирме А.А. Гранулометр аэрозоля на линии с мини-ЭВМ "Электроника Д3–28" // Уч. зап. Тарт. ун-та. – 1982. – Вып. 631. – С. 111–118.

5. Таммет Х.Ф. и др. Аппаратура и методика спектрометрии подвижностей легких аэроионов // Уч. зап. Тарт. ун-та. – 1987. – Вып. 755. – С. 18–28.

6. Миллер Ф.Г. К разработке электрометров прямого усиления для многоканальных спектрометров аэроионов // Уч. зап. Тарт. ун-та. – 1981. – Вып 588. – С. 124–132.

7. Устройство для определения спектра аэроионов: А.с. 938336 СССР, Н 01 J 39/36 / Я.Й. Сальм; Заявл. 14.11.80; Опубл. 23.06.82; Бюл. No. 23.

8. Сальм Я.Й. Модификация дифференциального спектрометра аэроионов // Методы и приборы контроля параметров биосферы. Межвуз. сб. – Вып.171. – Л.: ЛИАП, 1984. – С. 6–9.

9. Таммет Х.Ф. Аспирационный метод измерения спектра аэроионов // Уч. зап. Тарт. ун-та. – 1967. – Вып. 195.– С. 1–232.

10. Таммет Х.Ф. К технике электрической гранулометрии аэрозолей // Уч. зап. Тарт. ун-та. – 1980. – Вып. 534. – С. 55–79.

11. Стернзат М.С. Метеорологические приборы измерения. – Л.: Гидрометеоиздат, 1978. – 392 с.

12. Автоматическая станция КРАМС / Под ред. Л.П. Афиногенова и М.С. Стернзата. – Л.: Гидрометеоиздат, 1974. – 218 с.

13. Гордюк В.П. Исследование принципов построения приборов для измерения напряженности электрического поля в приземном слое атмосферы // Тр. ГГО. – 1981. – Вып.442. – С. 96–102.

14. Tammet, H. Air Ion Observatory at Tahkuse : Software // See this volume, pp. 44–51.

ОБСЕРВАТОРИЯ АЭРОИОНОВ ТАХКУЗЕ: АППАРАТУРА

У.Э. Хыррак, Ф.Г. Миллер, А.А. Мирме,
Я.И. Сальм, Х.Ф. Таммет

Р е з ю м е

Аппаратура, предназначенная для регистрации атмосферно-электрических и метеорологических величин, содержит шестиканальный и десятиканальный спектрометры подвижности аэроионов, источник высокостабильных напряжений, контроллер, ЭВМ "Электроника Д3-28", автономный источник питания и ряд датчиков. В настоящее время осуществлена регистрация спектра подвижности в диапазоне от $3*10^{-4}$ до 3 $см^2/(В*с)$ в 20 фракциях, а также основных метеорологических величин.

AIR ION OBSERVATORY AT TAHKUSE : SOFTWARE

H. Tammet

Introduction

The control of measurement and recording of results at Tahkuse Air Ion Observatory is carried out by means of a computer [1] and the structure of observations and recordings is determined by a computer program. It is possible to consider the program as an addition to the instrumentation which can be either partially or totally changed according to current needs of the user. This approach cannot guarantee uniformity of observation methods and uniform structure of the data. Uniformity, however, contributes significantly to the value of data obtained in a permanently active observatory . For this reason the basic software used at Tahkuse is considered an integral part of the system which should be able to support longtime operation without major changes.

The basic software consists of an observation program and a service program. Regular observations are controlled by the observation program, whereas the service program carries out regular checkups on the state of air ion spectrometers, as well as the operations necessary for setting up and transforming the apparatus table. For the operation of the service program regular observations are interrupted. The observations are interrupted also for the operation of special programs which can be devised for temporary tasks.

The software is designed for the Elektronika D3-28 computer. The computer has a relatively poor general software. For high level languages only a Basic interpreter is accessible. The power of the computer and its inventory of operators are insufficient for the execution of the required algorithms with a Basic interpreter. Therefore the following approach to programming has been adopted:

- the Basic interpreter has been enlarged by an additional operator for data exchange with the controller which directly controls the measurement devices (an interpreter program for this operator was developed by A. Mirme),
- external machine-code subroutines have been written for three additional input/output operations,

- an initial variant of the program was written in Basic and debugged at a slow measurement rate.
- the speed was increased by the translation of some segments of the program into machine code.

Elektronika D3-28 computers have their own numerical displays and keyboards. During the execution of the measurement program the computer is used without the external CRT display. The service program has both, CRT display and no-display, options.

Below attention will be paid to basic structures and operations of the observation program and the checkup procedure. The discussion presupposes familiarity with the paper [1] where the equipment of the Tahkuse Observatory is described.

The structure of observations

The duration of one full period of measurement and data processing is one hour. During this period the data are accumulated in RAM. At the end of every period the data are statistically processed and the results are recorded on a tape. For recording ordinary audio compact cassettes are used, one C90 cassette accommodates the data of one month's uninterrupted observations.

Every one-hour period consists of twelve 5-minute cycles. The internal structure of the cycles is identical for all the cycles but the first cycle has additional functions of statistical processing and recording of the data gathered in the preceding one-hour period.

Optionally, the data of every 5-minute cycle may be recorded in addition to the period data (this option can be selected by pressing a button on the control panel). This option is used only as an exception as it brings about a tenfold increase in tape consumption.

Each 5-minute cycle consists of five one-minute phases. The air ion spectrometer (see [1]) measurement modes are varied in different phases according to Table 1.

The structure of operations within a one-minute phase analogous to that described in [2] is presented in Table 2.

Table 1

Spectrometer modes in the order of phases

Phase	6C spectrometer voltage	10C spectrometer voltage	charger mode and polarity
-	- 45.5 V	-	off
- -	- 150.5 V	-	on -
Z	0	0	off
+ +	+ 150.5 V	+	on +
+	+ 45.5 V	+	off

Table 2

The structure of a one-minute phase

Second	O p e r a t i o n
1	Blocking of electrometers in spectrometers. Switch of per-minute control relay to position A. Switch of mode according to Table 1. Primary data processing of the preceeding minute.
12	Deblocking of electrometers in spectrometers.
20	Measurement and storage of results into vector A. Swich of per-minute control relay to position B. If the first minute of a cycle, then intermediate data processing of the preceeding cycle and if the 5-minute recording option, then recording on tape. If the first minute of a period and the preceeding period has been complete, then statistical processing and recording on tape. Indication of current measurements on display.
60	Measurement and storage of results into vector B. Beginning of the next one-minute phase according to Table 1.

Primary data processing

One phase yields vectors A and B as measurement results, the vectors correspond to signals from all the channels. The channels are divided into four categories:

- channels of spectrometer,
- channels of sensors without zero control,
- channels of sensors with per-minute zero control,
- channels of sensors with per-hour zero control.

Per-minute zero control is carried out every minute by means of relay contacts the switching of which is described in Table 2. The formal operation is written as $X = A - B$ or $X = B - A$ depending on the relay position that switches the sensor to zero control. Per-hour zero control is carried out by the contacts of the other relay which operates with the period of one hour.

Spectrometer channel signals are reduced to steady-state values obtained by a method described in [3]. Formal calculation is done according to formula

$$X = a \cdot A + b \cdot B \qquad (1)$$

where a and b are coefficients dependent on the time constant of the electrometer.

Formula 1 is universal in allowing non-spectrometric channels zero correction, for this purpose $a = 1$, $b = -1$ or $a = -1$ $b = 1$ are to be selected. For sensors without zero control $a = b = 0.5$ can be used. On the basis of the aforementioned considerations formula (1) has been adopted as a universal formula for primary processing of data from all channels.

Apparatus table

To contribute to the universality of the measurement program, information about the parameters of spectrometers and sensors has been brought together in an apparatus table. The apparatus table is written on the tape independently of the program and can be updated according to changes in the devices without making any changes in the program itself.

The equipment at the Tahkuse Observatory has 17 channels for spectrometer and of up to 19 channels for sensors. Thus,

the apparatus table comprises 94 numbers, the meanings of which are explained in Table 3.

Table 3

The structure of the apparatus table

Number	M e a n i n g
1...19	Physical numbers of sensor channels.
20...55	Constant a for primary processing.
56...91	Constant b for primary processing .
92	Actual number of sensors of range 10 V.
93	Actual number of sensors of range 10 mV.
94	Number of the apparatus table.

The numbers in the apparatus table appear in the order of logical numbers of the channels. Discrimination between physical and logical numbers makes possible arbitrary addition of sensors to the controller with subsequent respective corrections in the apparatus table. The physical numbers of sensor channels with per-hour zero control are labelled with a minus in front of the number of the channel.

Input of the apparatus table will take place immediately when the program is started.

Secondary data processing

After the accumulation of primary data of a 5-minute cycle the following operations are executed:

- six statistical sums for every spectrometric channel (the sums of signals of all phases and the sum of squares of Z phase signals) are accumulated,
- two statistical sums for every sensor channel (the sum of signals and the sum of squares of signals) are accumulated.

After the accumulation of statistical sums for the whole one-hour period:

- means and standard deviations are computed,
- data are formatted and written on tape,
- all statistical sums are set to zero.

Results of one-hour periods or 5-minute cycles are written as a separate block of data. Every block is written twice. Data are presented as two-byte decimal numbers. Each block contains (in the order of appearance) : number of the day with the count starting on March 1, 1984, number of the minute with the count starting at the beginning of the day, number of apparatus table, code of the keys of the control panel. In the case of hourly recording these parameters are followed by:

- 17 standard deviations of zero for spectrometric channels,
- 4 x 17 hourly means of spectrometer signals for four modes - , -- , + , ++ ,
- N hourly means of sensor signals,
- N standard deviations of sensor signals.

N signifies the number of sensors. In the case of 5-minute storage the above parameters are modified to:

- 4 x 17 values of spectrometer signals for four modes -, -- , + , ++ ,
- N values of sensor signals.

The encoding of numbers in a record block is oriented to processing by a two-computer system described in [4].

In every storage cycle data are set to zero by the Z phase signal. Empirical results have given indications of small shifts not eliminated by the zero correction. Therefore the observation technique requires special observations with the air flow through the measurement capacitors cut off; such special observations should be conducted at three-month intervals. The results should be taken into account during the processing and analysis of the data carried out outside the framework of the present observation and storage system.

Diagnostics of spectrometers

For diagnostic measurements observations are interrupted, the fan is switched off, and inner covers of the measuring capacitors are connected to a computer-controllable voltage source.

To determine the state of the spectrometers the voltage on the inner covers will be modified from one stable level to

another, after that the transition processes in the electrometers of all the channels are investigated. If the electrometers have no faults, then the actual transition process is in good correlation with the theoretical exponential model. The jump of the electrometer signal and the time constant of the transition process make it possible to calculate the measuring capacitance and resistance of the electrometer. The calculation is based on the effective capacitance of the measuring capacitor. The effective capacitance can be measured with high accuracy during the calibration of spectrometers, as it does not undergo subsequent changes.

The diagnostics takes about one hour. In this time the transition processes are investigated in 10 runs for each electrometer. In addition, several other experiments are carried out. Having completed the necessary computations the computer will issue a table with the results of diagnostics. In the table the following data are indicated for every spectrometer channel :

- measuring resistance of the electrometer,
- measuring capacitance of the electrometer,
- zero point of the deblocked electrometer,
- zero shift at deblocking,
- ionization chamber current in the measuring capacitor of the spectrometer.

All the above parameters are provided with standard deviations computed according to the differences in the results of the series of runs.

The values of measuring resistance and capacitance can be used for the calculation of coefficients of formula (1). Information about the zero point and the zero shift is necessary to estimate current technical conditions of the electrometers and the insulators of the measuring capacitors. The current of the ionization chamber gives information about radioactive contamination of the measuring capacitor.

Acknowledgement

The author is indebted to A. Mirme who wrote the computer programs for data exchange with the controller. Appreciation goes to U. Hõrrak for his help in debugging and running the programs.

References

1. Hõrrak, U., Miller, F. a.o. Air ion observatory at Tahkuse : Instrumentation. See this volume pp. 33-43.
2. Таммет Х.Ф., Миллер Ф.Г. и др. Аппаратура и методика спектрометрии подвижностей легких аэроионов // Уч. зап. Тарт. ун-та. - 1987. - Вып. 755.- С. 18-28.
3. Таммет Х.Ф. К технике электрической гранулометрии аэрозолей // Уч. зап. Тарт. ун-та. - 1980. - Вып. 534. - С. 55-79.
4. Бернотас Т.П., Кольк Э.Э. и др. Система сбора и обработки данных в спектрометрии аэрозолей и аэроионов // Уч. зап. Тарт. ун-та. - 1985. - Вып. 707. - С. 46-53.

ОБСЕРВАТОРИЯ АТМОСФЕРНЫХ ИОНОВ ТАХКУЗЕ: ПРОГРАММНОЕ ОБЕСПЕЧЕНИЕ

Х. Таммет

Р е з ю м е

Структура наблюдений и некоторые элементы методики наблюдений с помощью аппараратуры [1] определяются через программу управляющей ЭВМ. Для обеспечения единообразия рядов наблюдений программа рассматривается как фиксированная составляющая системы наблюдений. Описываются программа наблюдений и самостоятельная процедура диагностики состояния аппаратуры. Программы реализованы для ЭВМ "Электроника Д3-28".

Период операции в программе наблюдений - один час. Статистические сводки результатов наблюдений за каждый час записываются на магнитофонную кассету. Одна кассета достаточна для размещения записей за один месяц. Одночасовой период измерения распределяется на 12 пятиминутных циклов и один цикл на 5 одноминутных фаз, описанных в табл. 1. Структура действий внутри фазы описана в табл. 2. Первичная обработка данных в каждой фазе по формуле (1) позволяет редуцировать сигналы электрометров на установившиеся значения [3] и скорригировать на нулевой отчет сигналы датчиков, имеющих режим проверки нуля. Параметры аппаратуры фиксируются раздельно от программы аппаратурной таблицей, структура которой описана в табл. 3.

ON THE NATURE OF NEGATIVE SMALL AIR IONS OF AN AGEING TIME OF ONE SECOND

T. Parts

Introduction

Numerous reactions between gaseous, liquid, and solid particles (neutral, charged, excited) occur in the air. Theoretical studies have been made of various chemical reactions with the participation of negative ions, and of the influence of impurities on the composition of air ions [1-3]. In addition, there are numerous experiments with artificial gas mixtures similar to the air [4-6]. Nevertheless, the precise nature of the processes connected with ion composition of the air is not clear. Only fragments and parts of possible reactions have been investigated, whereas a considerable number of thermodynamic characteristics of reactions in the gas phase are not known [5].

According to the data of mass-spectrometric measurements the composition of dominant negative air ions in ground level air should be described by the formula $NO_3^-(HNO_3)_m(H_2O)_n$ [7]. The ageing of such ions can be some hundred seconds but the composition of air ions is dependent on their ageing. Primary negative ions O_2^-, O^-, OH^- transform into the ions $O_2^-(H_2O)_n$, $CO_4^-(H_2O)_n$, $O_3^-(H_2O)_n$, $CO_3^-(H_2O)_n$, $OH^-(H_2O)_n$, $NO_2^-(H_2O)_n$, $NO_3^-(H_2O)_n$, etc. in $5 \cdot 10^{-4}$ s. Some theoretical calculations predict that in the age group of about 1s the ions $O_2^-(H_2O)_4$ and $O_2^-(H_2O)_5$ are dominant [1, 2]; on the other hand, the ions $CO_4^-(H_2O)$, $NO_3^-(H_2O)$ ... have been suggested [3, 6]. The values of the relative humidity and concentration of NO_2 play important role in the evolution of negative ions [2, 6].

Mobility spectrometry is one of the methods for the investigation of air ions [8-11]. The present work is an attempt to explain the change of mobility spectra of small negative air ions under the influence of different impurities added to the air. It has been presumed that physical-chemical characteristics of impurities and air constituents may determine the nature and composition of air ions. In a recent paper [11] an identical research on positive air ions has been carried out.

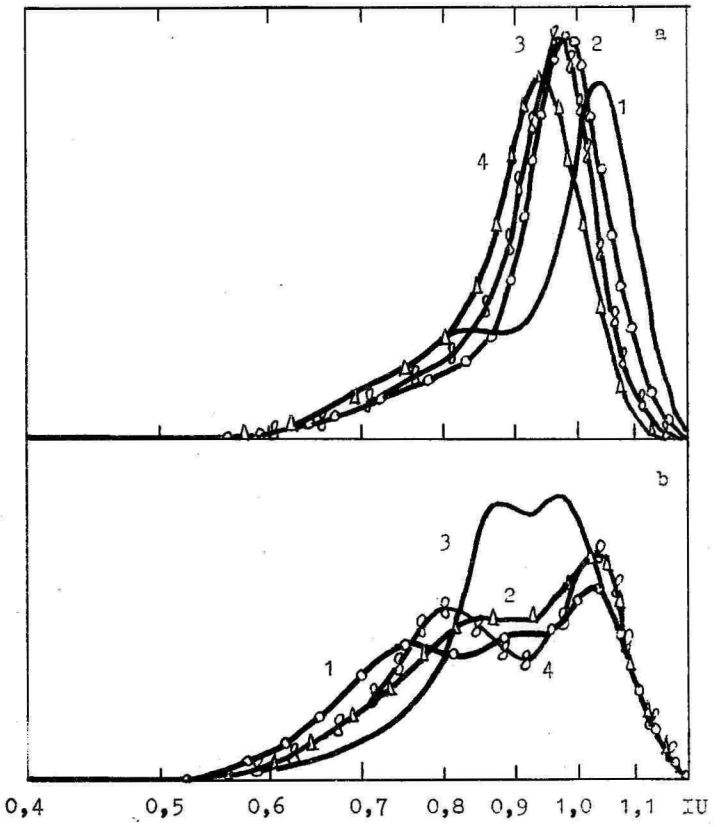

Fig. 1. Mobility spectra of negative small air ions of an ageing time of 1s in a clean laboratory room.

a) Typical : 1 - March 1986 (average), relative humidity (R) ≤ 40%, 2 - 06.05.86, R ~ 40%, 3 - 03.06.88, R > 60%, 4 - 29.12.88, R > 85% (artificially),

b) Exceptions : 1 - 03.05.88, R ~ 42%, 2 - 16.08.88, R ~ 66%, 3 - 16.10.85, R ~ 68% (people present in the room), 4 - 18.03.86, R ~ 88%.

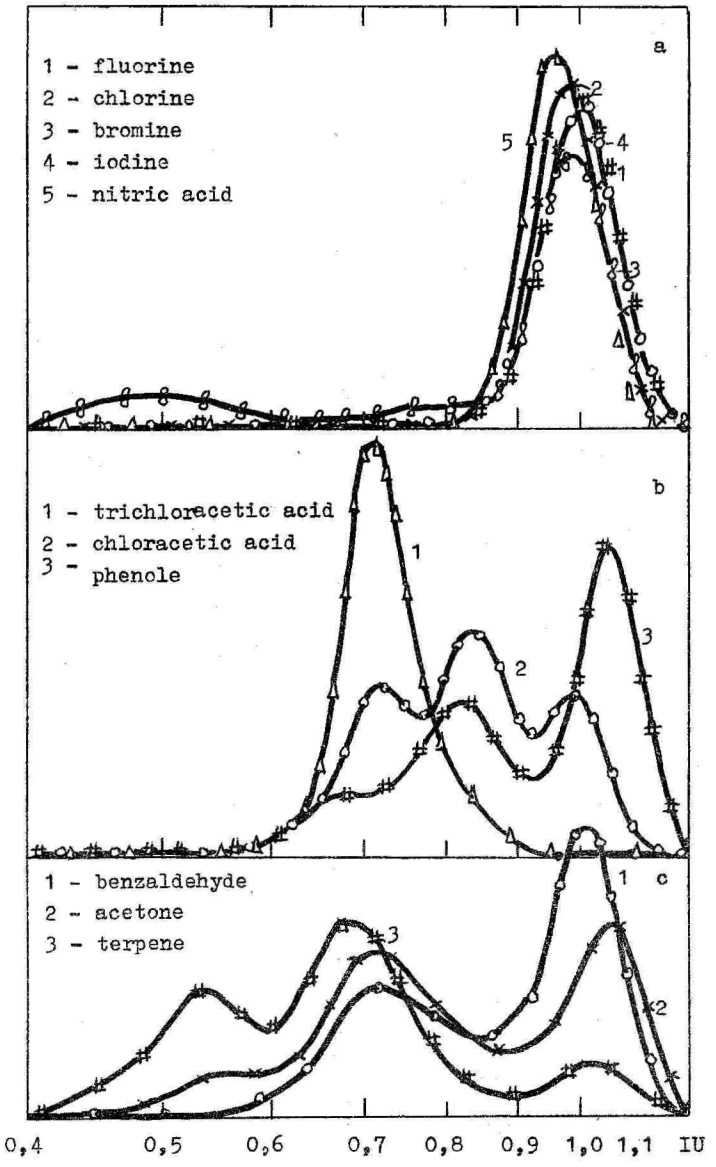

Fig. 2. The influence of the impurities on the mobility spectra of small negative air ions.

Measurement results

Over 1000 mobility spectra of negative air ions of an age of 1s were measured in a clean laboratory room [10]. The measurements were carried out under different climatic conditions, the varied parameters being the temperature, the pressure, the relative humidity, and the composition of the air. The concentrations of the impurities released in the air were estimated by the area of evaporation [11].

Background spectra without controlled influence of impurities are presented in Fig. 1 (a, b). Usually these spectra have a sharp maximum at about 1.0 IU (1 IU = 1.8 $cm^2/V*s$). In winter when the relative humidity in heated rooms falls below 40%, the maximum shifts towards greater mobilities. In summer the maximum shifts towards smaller mobilities, the same happens when the humidity is increased artificially. Such an effect of humidity is inverse to its effect on the mobility spectrum of positive ions [11]. In isolated cases negative ion spectra had two maxima (Fig. 1b).

Controlled influence of various impurities can substantially change the mobility spectra (Fig. 2a,b,c). The influence of impurities can be divided into three types: (1) admixtures yielding a cleancut maximum at about 1.0 IU (Fig. 2a); (2) impurities yielding maxima at about 0.7 (which may be dominant) and about 0,85; 1,0 IU; (3) impurities yielding maxima at about 0.7, 0.55 and 1.0 IU (Fig. 2c).

The first type includes mainly halogens, halogen hydrides, some halogenated hydrocarbons, nitric acid, and some organic acids (e.g. lactic acid). The second type includes strong Lewis acids, e.g., trichloroacetic acid, trifluoroacetic acid and some weaker Lewis acids (e.g. phenol). The third type includes mainly various terpenes in turpentine, acetone, benzaldehyde, 2,5-lutidine. It should be pointed out that all cleancut maxima (except 0.55 IU) (Fig. 2) are observed also in the background spectra (Fig. 1), whereas the patterns of the maxima depend on the concentration of admixtures and humidity.

Discussion

It has been noticed that several admixtures influence the spectrum of negative ions of an ageing time of 1s [8, 9]. The exact nature and mechanism of the influence are not clear. The composition of air ions responsible for the spectrum has not been elucidated. Estimates can be made on the basis of the masses of ions on the assumption of validity of the de-

Table 1

Mobilities of small ions, masses, and some possible negative ions responsible for them

IU	k, $cm^2/V \times s$	m, AMU	Small ions	m, AMU
0,4	0,7	800		
0,5	0,9	500		
			$NO_2^- (HNO_3)_3 (H_2O)_9$	411
			$NO_3^- (HNO_3)_3 (H_2O)_6$	357
0,6	1,05	300		
			$NO_3^- (HNO_3)_2 (H_2O)_6$	294
			$NO_3^- (HNO_3) (H_2O)_6$	233
0,7	1,25	200		
			$NO_3^- (HNO_3) (H_2O)_4$	197
			$NO_3^- (HNO_3) (H_2O)_3$	179
			$OH^- (H_2O)_9$	179
			$NO_3^- (HNO_3) (H_2O)_2$	161
0,8	1,45	150		
			$NO_3^- (HNO_3) (H_2O)$	143
			$NO_3^- (H_2O)_4$	134
			$NO_3^- (H_2O)_3$	116
0,9	1,6	100		
			$NO_3^- (H_2O)_2$	98
			$OH^- (H_2O)_4$	89
1,0	1,8	85		
			$NO_3^- (H_2O)_3$	80
			$OH^- (H_2O)_3$	71
1,1	1,95	70		
			$OH^- (H_2O)_2$	53
1,2	2,15	50		
			$OH^- (H_2O)$	35

pendence of mobility on mass presented in [12].

Table 1 presents the mobility interval of small ions and the masses of ions according to [12]. The last column contains several possible small air ions of these masses.

Table 2 presents a couple of physical-chemical characteristics of the admixtures and gases contained in the air. At the end of Table 2 data on clusters in the air can be found. For larger clusters there is no data on electron affinity ,

Table 2

Some physical-chemical characteristics of air constituents

No.	Compound		Mol.mass AMU	Ionization potential V	Electron affinity eV
1.	Nitrogen	(N_2)	28	15,5	-
2.	Oxygen	(O_2)	32	12,1	0,9
3.	Carbon dioxide	(CO_2)	44	13,8	-
4.	Sulphur dioxide	(SO_2)	64	12,3	1,1
5.	Nitrogen dioxide	(NO_2)	46	9,8	2,0/3,8
6.	Water	(H_2O)	18	12,6	0,9
7.	OH-radical		17	13,0	1,8
8.	Nitrogen monoxide	(NO)	30	9,3	0,43/0,91
9.	NO_3-radical		62	-	3,9
10.	Fluorine	(F_2)	38	17,4	2,6
11.	Chlorine	(Cl_2)	71	13,0	1,7
12.	Bromine	(Br_2)	160	11,8	2,6
13.	Iodine	(J_2)	254	9,4	2,4
14.	Hydrate	$OH(H_2O)$	35	-	2,65
15.	"	$OH(H_2O)_2$	53	-	3,3
16.	"	$OH(H_2O)_3$	71	-	4,0
17.	"	$NO_2(H_2O)$	64	-	2,9
18.	"	$NO_2(H_2O)_3$	100	-	3,8
19.	"	$NO_3(H_2O)$	80	-	4,25
20.	"	$NO_3(H_2O)_2$	98	-	4,7
21.	"	$O_3(H_2O)$	66	-	2,3
22.	"	$CO_4(H_2O)$	94	-	1,72

at the same time it is exactly these clusters that may play an important role in the mobility spectrum below 1.6 $cm^2/V \cdot s$.

In the chemistry of negative air ions electron affinity has a great importance. Among gaseous components of the air nitrogen and oxygen compounds deserve attention due to their wide spread. NO_2, NO_3, OH, and their hydrates form ions of greatest electron affinity (Table 2). NO_2, and NO_3 are connected with nitric acid [13], OH is connected with H_2O [14]. Air humidity has an effect on the concentrations of HNO_3 in the air, it also influences the relation of the concentrations of HNO_3 in gaseous and liquid phase.

When the concentration of HNO_3 is increased (Fig. 2a), the mobility spectrum is moved towards smaller mobilities and has only one cleancut maximum. Ions are likely to be dominant, estimates by mass and electron affinities indicate that these ions can be $NO_3^- (H_2O)_2$ with additional $NO_3^- (H_2O)$ and $OH^-(H_2O)_3$. When the concentration of HNO_3 in the air is decreased, $OH^-(H_2O)_3$ may be dominant and the mobility is increased at a smaller mass of an ion.

Ions OH^- as strong basics have an important part in the chemistry of gas phase, e.g. reacting with a Lewis acid [5]:

$$OH^- + CH_2 = CH - CH_3 \rightarrow [CH_2 = CH - CH_2]^- + H_2O \,. \quad (1)$$

In the presence of water the reactions of OH with organic compounds can lead to the formation of clusters of water, e.g.

$$OH^- + \text{(cyclic ether)} \xrightarrow{H_2O} OH^-(H_2O)_n \,. \quad [5] \qquad (2)$$

Hydrates $OH^-(H_2O)_3$ may be present in the air, if to take into account their electron affinity (Table 2). In addition, the formation of ions OH^- in water vapours has been proved in electronic bombardment, whereas some physical characteristics of ions O_2^- and OH^- coincide [14].

Thus it can be supposed that mobility maxima at 1.0 – 1.1 IU corresponding to ion masses below 85 AMU can be connected with the balance of air ions, where $NO_3^- (H_2O)$, m = 80 and $OH^-(H_2O)_3$, m = 71 are dominant. It is known that ions

$OH^-(H_2O)_3$ are the most stable among hydrates $OH^-(H_2O)_n$ [15].

Air ions of lower mobilities than 0,8 IU are observed when impurities are added to the air (Fig. 2). The mechanisms of the effect of impurities are likely to be analogous to reactions (1) and (2) where other ions except OH^- may be participate, e.g., NO_3^-

$$RCOOH + NO_3^- (H_2O)_n = RCOO^- + HNO_3 + H_2O \ . \qquad (3)$$

The higher the dissociation constant of RCOOH, the stronger the acid and the greater its influence on the mobility spectrum. Reactions (1) and (3) lead to increased concentrations of H_2O and HNO_3. The possibility of the formation of larger clusters with HNO_3 also increases. The mobility maxima at 0.55 IU, 0.7 IU can be explained by the presence of clusters of the type $NO_3^- (HNO_3)_3 (H_2O)_6$, m = 357 AMU, $NO_3^- (HNO_3)(H_2O)_3$, m = 179 AMU and $NO_3^- (HNO_3)(H_2O)$, m = 143 AMU and with other clusters of the type $NO_3^- (HNO_3)_m (H_2O)_n$ which should be prevalent in the air.

Conclusions

1. It is suspected that the air ions responsible for mobility spectrum maxima both in the background and contaminated air are composed of the same ions, whereas the impurities shift the balance in favour of either $NO_3^- (HNO_3)_m (H_2O)_n$ or $OH^-(H_2O)_n$.

2. Proton transfer reactions have an important role in the chemistry of negative ions. Being sources of protons, strong Lewis acids influence the mobility spectra and thus also the composition of negative air ions.

Further studies of the nature of negative air ions should be connected with the precise determination of the concentrations of HNO_3, H_2O and other components of the air.

References

1. Huertas, M.L., Fontan J., Gonzalez J. Evolution times of tropospheric negative ions // Atm. Env. – 1978. – Vol. 12. -- pp. 2351-2362.
2. Лутс А.М., Сальм Я.И. Кинетика образования отрицательных легких аэроионов в тропосфере // Уч. зап. Тарт. ун-та.

- 1988. - Вып. 809. - С. 60-67.

3. Kawamoto, H., Ohawa, T. Negative ion composition in the lower atmosphere // Proc. 8th Int. Conf. Atm. Electricity. - 1988. - Uppsala. - pp. 124-129.

4. Fehsenfeld, F.C., Ferguson, E.E. Laboratory studies of negative ion reactions with atmospheric trace constituents // J. Chem. Phys. - 1974. - Vol. 61. - No. 8. - pp. 3181-3193.

5. De Puy, C.H., Bierbaum, V.M. Formation of anions in the gas phase // Structure/Reactivity and Thermochemistry of Ions. Ed. by P. Ausloos, Sh.G. Lias. - 1987. - D. Reidel : Dordrecht. - pp.279-303.

6. Лившиц А.И., Портнов Ф.Г., Шмидт А.Б. Влияние влажности на химический состав ионов в воздухе //Изв. АН Латв. ССР, сер. хим. - 1983.Вып. 4. - С. 449-451.

7. Eisele, F.L. Identification of tropospheric ions // J. Geophys. Res. - 1986. - Vol. 91. - No. D7. - pp. 7897-7906.

8. Таммет Х.Ф. Зависимость спектра подвижности легких аэроионов от микропримесей воздуха // Уч. зап. Тарт. ун-та. - 1975. - Вып. 348. - С. 3-15.

9. Ихер Х.Р., Сальм Я.И. Зависимость спектра подвижности легких аэроионов от химических примесей в воздухе // Уч. зап. Тарт. ун-та. - 1982. - Вып. 631. - С. 27-34.

10. Партс Т.М., Сальм Я.И. Воздействие пиридина и некоторых его гомологов на спектр подвижности положительных легких аэроионов // Уч. зап. Тарт. ун-та. - 1988. - Вып. 809. С. 71-78.

11. Партс Т.М. О природе положительных легких аэроионов односекундного возраста // Уч. зап. Тарт. ун-та. - 1988. - Вып. 824. - С. 69-77.

12. Kilpatrick, W.D. An experimental mass-mobility relation for ions in air atmospheric pressure // Proc. 19th Conf. Mass Spectrometry. - 1971. - Atlanta. - pp. 320-325.

13. Fehsenfeld, F.C., Howard C.J., Schmeltekopf A.L. Gas phase ion chemistry of HNO_3 // J. Chem. Phys. - 1975. - Vol. 63. - No. 1. - pp. 2835-2841.

14. Compton, R.V., Christophorou L.G. Negative ion formation in H_2O and D_2O/ Phys. Rev. - 1967. - Vol. 154. - No. 1. - pp. 110-116.

15. Белл П. Протон в химии // - 1977. - М. Мир. - 382 с.

О ПРИРОДЕ ЛЕГКИХ ОТРИЦАТЕЛЬНЫХ АЭРОИОНОВ ОДНОСЕКУНДНОГО ВОЗРАСТА

Т.М. Партс

Р е з ю м е

Известно, что спектрометрия подвижности легких аэроионов может быть в некоторых случаях использована для определения загрязнения воздуха [8-10]. При этом учитывается изменение спектров подвижности или положительных или отрицательных аэроионов. Механизмы действия примесей на ионный состав воздуха до конца не ясны. Отсутствует целый ряд термодинамических данных о реакциях в газовой фазе. В данной работе делается попытка объяснить изменение спектров подвижности отрицательных легких аэроионов односекундного возраста под влиянием загрязнителей. Наибольшее влияние оказывают сильные льюисовские кислоты, имеющие высокую константу диссоциации в газовой фазе. Сделан вывод о существенной роли реакций переноса протона в изменении ионного состава воздуха. Понижение подвижности аэроионов может быть связано с ростом кластерных ионов типа $OH^-(H_2O)_n$ и $NO_3^-(HNO_3)_m(H_2O)_n$. Дальнейшие исследования должны быть связаны с точным определением концентрации газовых составляющих воздуха.

INFLUENCE OF POLLUTION ON ELECTRIC PARAMETERS OF THE AIR

L. Visnapuu and R. Priiman

Conductivity and polar charge density are basic electrical parameters of the air. These parameters are determined by the quantity and quality of free electric charges (air ions). The quality and the quantity of free electric charges are expressed by mobility and charge density, respectively. Air ions have certain mobilities and their distribution by the mobilites yields the air ion spectrum. Air ions can be divided into two main groups: small ions with the limiting mobility $k \geqslant 0.1$ $cm^2/(V \cdot s)$ and large ions with $k < 0.1$ $cm^2/(V \cdot s)$. The total polar charge density of air ions is usually determined by air ion counters.

Conductivity in the air is mostly due to small air ions. When the air contains pollutants such as vapours and aerosol particles, small air ions and free electrons are precipitated to the pollutants. In this process part of small ions are transformed into large ions and thus the mobility spectrum undergoes a change. The lower the conductivity in the air and the smaller the part of small ions in the spectrum, the more polluted the air. This fact makes it possible to estimate pollution by the conductivity and the air ion mobility spectrum. Additional information about this feature of the air is given by chemical composition of the pollutants.

Polar charge density measurements of small and large ions have been carried out in the city of Tartu since 1937 [1]. Dominant pollution sources in the city are industries and traffic. In the last decades the influence of both pollution sources has been rapidly growing [2].

The Table presents average data of spring/summer measurements of polar charge densities of small and large ions in Tartu in the years 1937-1988.

It can be seen that average charge densities for small air ions have been rapidly decreasing, whereas for large ions the average charge densities have grown. This is a result of constantly increasing atmospheric pollution.

The measurements indicate that the charge density of large ions in recreation and health resort areas is by an order lower than in industrialized areas. The reverse holds for

small ions. A partial explanation can be found in the ability of green plants to absorb pollutants causing increased charge density of large ions.

Table 1

Average charge densities of small and large ions e/cm^3 in Tartu in 1937-1988

years	$k \geq 0.1$ $cm^2/(V \cdot s)$		$0.001 < k < 0.1$ $cm^2/(V \cdot s)$	
	−	+	−	+
1937	850	1050		
1951	750	1000		
1960-1963	500	600	1760	2120
1980	450	550	1860	2130
1988	290	310	2500	2400

The leaves of plants absorb gases and dust from the environment. There are different mechanisms of detoxication of toxic compounds. Some compounds are bound by the cytoplasma of plant celle and disinfected while others are transformed into non-toxic products. High efficiency of forests in cleaning the environment of toxic compounds is also conditioned by the fact that trees facilitate turbulent scattering of poisonous gases.

In the processes of photosynthesis the plants emit oxygen and a number of volatile organic compounds (etheric oils, terpene hydrocarbons, aldehydes, ketons and others). These substances enter into various reactions with pollutant admixtures which results in disinfection of the air. All the above processes bring about changes in the electrical state of the air. The latter has numerous natural causes.

We have studied volatile phyto-organic compounds in the form of sprayed solutions of pine extraction and peppermint extraction with regard to their effect on the mobilities of the air ions.

Solutions of 1% were sprayed in laboratory rooms by a general purpose "Comfort" spray during 30 min. The concentration of phyto-organic compounds after the spray achieved an order of 10^2 mg/m^3 (the total of terpene hydrocarbon was determined by fine-layer chromatography). Polar space charge density was measured by an air ion counter

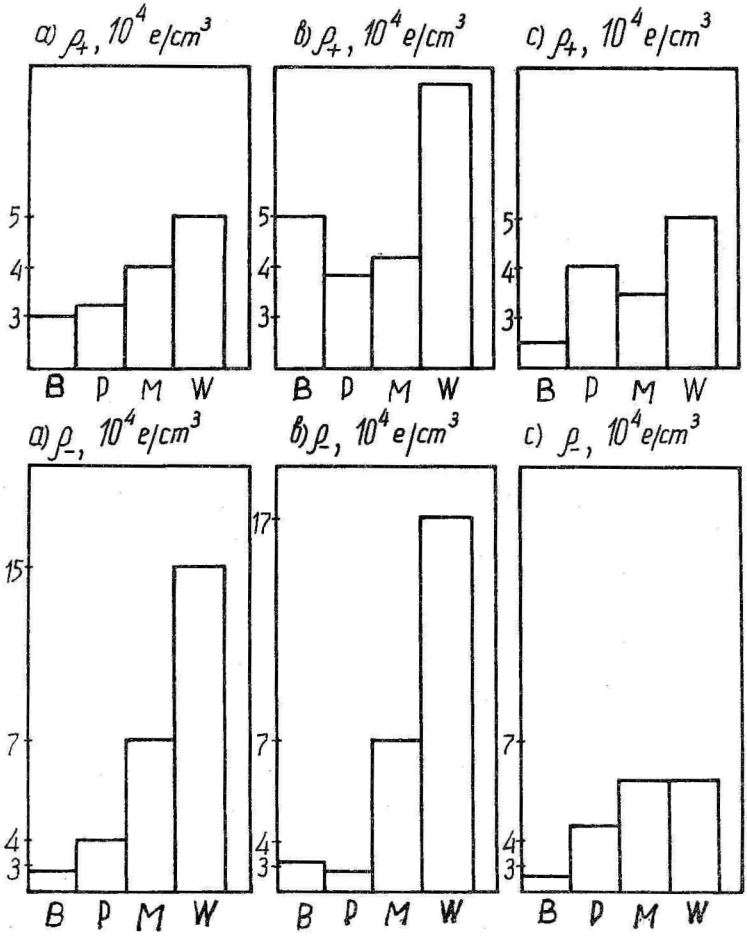

Figure 1. Polar space charge densities e/cm^3 large air ions ($k \geq 10^{-3}$ cm^2 /(V·s)) at various sprays:
solution M – 1% peppermint extraction,
solution P – 1% pine extraction,
W – tap water
a) in the middle of the room,
b) far from window,
c) near an opened vent window,
B – background.

of the type UT-8401. The counter was located at the window, in the middle, and the corner of the room; the limiting mobilities were 10^{-1} and 10^{-2} $cm^2/(V*s)$. Before every spray cycle background charge density was measured at the same limitng mobilities. Results of the measurements are presented in the Figure 1.

The data clearly indicate an increase in the charge density after the spray of water or water solutions in the air. This is a natural result of the balloelectrical effect. A comparison of charge densities of large ions shows that peppermint and pine extraction solutions brought about several times smaller growth of charge density than the spray of tap water. In a more modest degree, analogous phenomenon was observed in the behaviour of small ion charge density.

Considering these processes under natural conditions in foul weather, it can be supposed that volatile phyto-organic compounds cause a lowered charge density for both, small and large ions. In natural conditions the influence of plantgenerated phyto-organic compounds is of a more complex nature, especially in foul weather.

The experiments make it possible to draw a conclusion that man-produced pollutants are cleaned or neutralized more rapidly near fountains, mountain streams, waterfalls, and areas of plant growth, than at open landscapes without plantlife. Volatile phyto-organic compounds released from plants decrease air pollution with large ions. Thus, air ion charge density measurements help to estimate aerosol pollution of the atmospheric air.

References

1. Митт А. Колебания плотности молионов в атмосфере города Тарту за 1937 год // Уч. зап. Тарт. ун-та. - 1946.- Вып. 2. - С.42. (На эстонском языке).
2. Прюллер П.К. Исследование спектра атмосферных ионов, гигиеническое и биометеорологическое значение ионизации атмосферы по данным измерений в г.Тарту. - Уч. зап. Тарт. ун-та. -1970.- Вып. 240. - С. 3-31.

О ЗАВИСИМОСТИ ЭЛЕКТРИЧЕСКИХ ХАРАКТЕРИСТИК ВОЗДУХА ОТ ЕГО ЗАГРЯЗНЕННОСТИ

Л.Ю. Виснапуу, Р.Э. Прийман

Р е з ю м е

Рассмотрены изменение спектра электрических подвижностей аэроионов при загрязнении воздуха и оценка загрязненности воздуха по этому спектру. Приведены средние данные весенне-летних измерений полярных плотностей заряда легких и тяжелых аэроионов в г.Тарту в 1937-1988 гг. Показаны постоянное уменьшение средних плотностей заряда легких аэроионов и увеличение средних плотностей заряда тяжелых аэроионов, обусловленные ростом загрязнения атмосферного воздуха. Рассмотрена очистка воздуха от различных загрязняющих примесей летучими компонентами выделений растений.

ANALYSIS OF MEASUREMENT METHODS OF AEROSOL SIZE SPECTRUM WITH ELECTRICAL ANALYZER TSI 3030

M. Noppel

Abstract

The paper evaluates through mathematical modeling the exactness of two approaches to the processing of signals of the electrical analyser TSI-3030. A model of "one-peak" average spectrum of atmospheric aerosol has been used as the initial spectrum. A traditional method involving scaling transformation is found to give two spurious peaks in the resulting spectra. The matrix approach eliminates the spurious peaks and the initial spectrum is restored better. It is pointed out that the signal in the device is elicited not only by the particles in the measurement range but also by larger particles. In the case of fogs this can cause considerable errors. Distortions in results caused by device adjustment imprecision and parameter fluctuation is studied. Apparatus matrix for the transformation of channel signals into aerosol particle fraction concentration is found by fitting to empirical data the parameters of the proposed mathematical model of the spectrometer. Two different TSI 3030 devices are compared and significant discrepancies in results found.

Introduction

The electrical method is one of the widely used methods for aerosol spectrum measurements. The method allows in situ measurements and yields data on fine particles which cannot be studied with optical devices. Electrical aerosol analyzers TSI 3030 (EAA) manufactured by Thermo-Systems Inc. have found worldwide application in the 5...500 nm range [1]. At the same time, there are considerable discrepancies in the size distributions obtained by electrical methods (higher particle concentration in the range of small sizes) and other methods [2]. Usually the TSI-3030 signals are processed by a mathematical model which presupposes that for every channel the signal (current difference) y_i is proportional to the aerosol concentration N_i in the nominal size range cor-

responding to that channel - $Y_i = A_i N_i$. Experimental determination of the coefficients A_i (calibration) has shown that the latter relation is not valid [3]. Monodisperse aerosols elicit signals not only in their "own" channel but also in the neighboring channels. In [4] an interpolation of experimental results in [5] (apparatus records of 16 different average sizes of aerosol particles) has been used to determine the response of TSI-3030 to 61 monodisperse aerosols. The average values of aerosol particle radii were geometrically uniformly distributed by size from 1.6 nm to 500 nm. Regarding every aerosol as a superposition of these 61 monodisperse aerosols it is possible to calculate the response of EAA to this aerosol. It has been established that the above scaling transformation may lead to errors amounting to 200-300% for some fraction concentrations. In [6, 7] a new mathematical model has been proposed. The spectrometer is described by a linear apparatus equation - $y = H\varphi$, where H - apparatus matrix, y - set of channel signals, φ - set of numbers characterizing the size spectrum, e.g., fraction concentrations. Ways of determining the apparatus matrix are considered in [8, 9, 10, 11].

The present paper attempts to study the exactitude of these two methods for signal processing by means of numerical modeling. In addition, the influence of the precision in construction and assembly, as well as the impact of deviations in adjustable parameter values on the exactitude of results will be analysed. In the latter case two aspects should be pointed out. First, the precision in manufacturing and in adjustment of parameters like flow rates, precipitation voltage, etc.; and second, the stability of the regime parameters. The question of precise adjustment of regime parameters arises when old calibrations are used after repairs or extended to newly-manufactured spectrometers, as calibration is a complex and time-consuming procedure. Errors ensue also from fluctuations of regime parameters, the average values of which are determined in adjustment of the device. These errors are added to the systematic errors of adjustment. Another negative factor is the noise of current measurements.

Numerical modeling of EAA

At building the present model, a theoretical spectrometer model proposed in [10] has been used. The behaviour of aerosol passing through the charger and the measuring capacitor has been described according to the theory of the aspiration method [12]. The aerosol flow in the charger can be regarded as consisting of narrow sheaths, whereas inside every sheath the charging conditions are considered uniform. The charge distribution of particles in the sheaths is calculated by the algorithm [13, 14] created on the basis of the theory of Fuchs [15, 16], and the numerical solution of the equation of particle charging in external electric field. It is a complicated task to determine, either experimentally or theoretically, the exact values of conductivity and strength of the electric field in the actual chargers of the spectrometers. Therefore in the theoretical model the charging conditions are described by the inclusion of respective parameters. The values of these parameters can be determined by fitting the theoretical spectrometer signals for standard aerosols with the experimental ones. Applying the above approach, a calibration procedure of electrical spectrometers, i.e., a procedure to determine the apparatus matrix H has been proposed in [10]. In the present paper the procedure is used for the EAA. The method has been modified in comparison with the one used in [10], where on the basis of theoretical and experimental signals the authors computed the central channel, the standard deviations by channels and the average levels of signal in the channels for every test aerosol. Next, fitting was carried out by these parameters. In the present investigation, however, the fitting has been done directly by the channel signals. The fitted parameters of the model included: 3 coefficients of parabolic approximation of the electric field distribution, 3 respective coefficients for air conductivity in the charging area, 1 parameter for the description of particle precipitation in the charger and the capacitance of the preliminary part of the measuring capacitor. Differently from [10] the parameter describing the influence of possible residual turbulence in the measuring capacitor was omitted. Experimental channel signals are presented in [3, Table 2] (cf. also Table 1, ibid.). According to the experimental calibration of the EAA [3] the test aero-

Table 1

Relative distribution of experimental and theoretical signals of EAA by channels for test aerosols with log-normal distribution (σ_g = 1.05 ; in experiment, if r_g = 3.75 nm, 6.67 nm, then σ_g = 1.5), with various particle sizes (r_g)

Channel	Channel average in nm	r_g in nm	3.75	6.67	11.9	21.1	37.5	66.7	119	211	375
2	3.75		0.11	0	0	0	0	0	0	0	0
			(1)	(0)	(0)	(0)	(0)	(0)	(0)	(0)	(0)
3	6.67		0.89	1	0.10	0	0	0	0	0	0
			(0)	(1)	(0.08)	(0)	(0)	(0)	(0)	(0)	(0)
4	11.9		0	0	0.90	0.52	0.01	0	0	0	0
			(0)	(0)	(0.92)	(0.49)	(0)	(0)	(0)	(0)	(0)
5	21.1		0	0	0	0.06	0.16	0	0	0	0
			(0)	(0)	(0)	(0.07)	(0.14)	(0)	(0)	(0)	(0)
6	37.5		0	0	0	0.42	0.67	0.24	0	0	0
			(0)	(0)	(0)	(0.44)	(0.65)	(0.42)	(0)	(0)	(0)
7	66.7		0	0	0	0	0.10	0.57	0.28	0.01	0
			(0)	(0)	(0)	(0)	(0.17)	(0.49)	(0.22)	(0)	(0)
8	119		0	0	0	0	0.03	0.15	0.45	0.31	0.10
			(0)	(0)	(0)	(0)	(0.02)	(0.09)	(0.48)	(0.31)	(0.11)
9	211		0	0	0	0	0.02	0.01	0.15	0.32	0.30
			(0)	(0)	(0)	(0)	(0.02)	(0)	(0.20)	(0.36)	(0.28)
10	375		0	0	0	0	0	0.01	0.05	0.18	0.26
			(0)	(0)	(0)	(0)	(0)	(0)	(0.06)	(0.18)	(0.25)
Calcul. sensitivity A_1, nA/(10^6 particles/cm^3)			0.149×10^{-3}	2.34	6.64	12.3	23.4	42.6	76.5	140	264
Experim. sensitivity A_2, nA/(10^6 particles/cm^3)			0.105	2.40	6.00	11.5	22.5	41.5	81.0	150	285
A_1/A_2			0.0014	0.98	1.11	1.07	1.04	1.03	0.94	0.94	0.93

sols are considered in the calculations to be log-normal with geometrical standard deviation 1.05, and with geometrical averages of the radii corresponding to the channel averages. The concentrations of test aerosols have been chosen so that the sum of channel signals of an aerosol would be independent of particle sizes. Table 1 presents relative channel distributions of the signals calculated on the basis of the results of fitting and the experimentally obtained signals (in brackets). It can be seen that the numerical model well describes the properties of the spectrometer.

The discrepancies between the experimental and the calculated sensitivities do not exceed 11% (except for channel 2). The difference is greatest for channel 2 where the experimental sensitivity exceeds the theoretical one by a factor of 700. For practically occurring concentrations of particles of $r < 5$ nm size and at the sensitivity equal to the theoretical sensitivity, the particles do not elicit signals exceeding noise current (10^{-15} A [1]) .This means that according to the theoretical model channels 1 and 2 lack signals. The model explains the lack of signals in the first two channels by the precipitation of particles in the charger. In channel 2 signal can be elicited only by particles with radii close to the upper boundary of the channel (5 nm). The manufacturers of TSI-3030 do not recommend the use of the first two channels. The high experimental sensitivity of channel 2 can be explained by the wide distribution ($\sigma_g = 1.5$) of the aerosols of smog chamber, used

Table 2

Matrix H_o of transformation $N = H_o y$, where y - signals of the EAA from channel 3 to channel 10 (in 10^{-15} A), N - fraction concentrations (in cm^{-3}).

376.48	-19.36	19.77	-3.47	1.08	-0.50	-0.08	0.52
47.69	130.17	-132.97	23.35	-7.30	3.51	0.03	-2.96
-10.11	18.55	171.00	-33.40	10.47	-5.08	0.12	4.08
2.03	-3.71	2.54	55.93	-17.82	9.08	-1.72	-5.47
-0.96	1.76	-12.38	3.40	34.10	-17.08	3.22	8.54
0.17	-0.30	3.10	-3.27	0.86	24.90	-7.13	-12.12
-0.049	0.09	-1.118	1.556	-3.928	6.215	3.873	1.692
0.012	-0.022	0.280	-0.396	1.104	-3.582	4.003	4.458

for the gradation of the first channels. The largest particles of this aerosol may pass through the charger without precipitation. At the same time this contradicts the experimentally observed concentration of wide aerosol signal in one nominal channel only.

Apparatus matrix of EAA

Table 2 presents the matrix H_o connecting the fraction concentrations of aerosol N to channel signals $y - N = H_o y$. The division of the size scale into subintervals corresponds to the division used in the EAA. In the computation of this matrix it has been assumed that the spectrum of the investigated aerosol can be presented as a linear combination of elementary spectra $\varphi = \sum_i a_i \varphi^i$. Spectra proposed in [7] were used as elementary spectra φ^i. In the scale 1/r these elementary spectra φ^i are triangular and their linear combination is a piecewise-linear function. The points that determine the location of the triangles on the scale correspond to the following values of particle radii (in nm) 4.65; 8.89; 15.8; 28.1; 50; 88.9; 158; 281; ∞. Seven elementary spectra have been used. Channel signals y_k^i (channels k = 3,..., 10) of elementary spectra φ^i have been computed by the theoretical model. With reasonable precision electrical spectrometers can be considered linear. The size spectrum, as a linear combination of elementary spectra $\sum_i a_i \varphi^i$ is juxtaposed with a linear combination of signals $\sum_i a_i y_k^i$. The method of least square (the minimized value is $\sum_k (y_k - \sum_i a_i y_k^i)^2$, where y_k - empirical channel signals), leads to a linear system of normal equations: $\sum_i a_i \sum_k y_k^i y_k^j = \sum_k y_k y_k^j$ or, in a shortened form $Y^T Y a = Y^T y$; where Y-matrix with elements y_k^i , T - transposition sign. The solution of the system $a = (Y^T Y)^{-1} Y^T y$. Fraction concentrations are calculated by integrating the linear combination of the size spectrum over the subintervals of particle radii

$$N_L = \int_{r_L}^{r_{L+1}} \sum_i a_i \varphi^i dr = \sum_i a_i \int_{r_L}^{r_{L+1}} \varphi^i dr = \sum a_i \Phi_{Li}$$

or

$$N = \Phi a,$$

thus $$N = \Phi (Y^T Y)^{-1} Y^T y = H_o y \quad .$$

Comparison of the matrix approach and the traditional scaling method of signal processing

In the traditional scaling transformation of signals the results depend on the measured spectrum [4]. In the present study the initial spectrum is the Smerkalov distribution [17] obtained by averaging empirical spectra measured by different researchers. The concentration of particles has been chosen

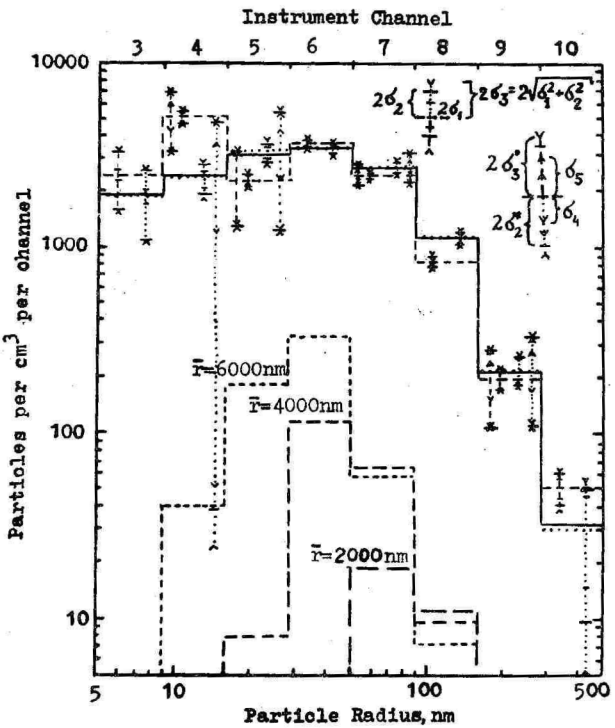

Fig. 1. Modeling of TSI-3030 output for the incoming aerosol with the Smerkalov distribution and for fogs with gamma-distribution

—— initial spectrum; --- restitution according to TSI-3030; ... piecewise linear restitution; σ_1 – adjustment errors; σ_2 – regime parameters fluctuations and noise 10^{-15} A; σ_4 – noise 6×10^{-15} A; σ_5 – noise 12×10^{-15} A; σ_2^* – regime parameters fluctuations and noise 6×10^{-15} A; $\sigma_3^* = \sqrt{\sigma_2^{*2} + \sigma_1^2}$

so that 15000 particles in cm^3 would be found in the measurement range of TSI-3030 5...500 nm.

The response of model spectrometer to this distribution is computed. After that the distribution is restored in the shape of fraction concentrations by scaling transformations $N_i = a_i y_i$, where $a_i = 1/A_i$ - model scale coefficients taken from Table 1. The restitution has been carried out also using the matrix H_o (Table 2). The results are presented in Fig. 1.

It can be seen that the traditional scaling transformation leads to the appearance of a spurious peak (+108%) in fraction 4 (r = 9...16 nm) and a depression (- 28%) in fraction 5 (n = 16...28 nm), thus the spectrum acquires a bimodal shape. The decrease in channel 5 can be observed already in the model channel signals. At precipitating voltages on the collector rod used in the EAA (these voltages determine channel limits) particles with radii in the vicinity of 21 nm (nominal size of channel 5) elicit signal basically in channel 6, if they have one elementary charge, and in channel 4, if their charge is equal to two elementary charges (see also Table 1). The scaling transformations are executed on the assumption of one-to-one dependence between particle size and the charge acquired by the particle in the charger. The method does not allow to take into account discrete particle distribution according to charge which in the above case results in spurious peaks. The appearance of the spurious peaks is also suggested by the results in [4] obtained for artificial aerosol. The spurious peaks are avoided and the exactness of distribution restitution is increased, if for model signals the approach presented in the previous section is used instead of the traditional method. When matrix H_o is applied to real spectrometer signals, the exactness of results depends on the correspondence of the mathematical model to the real spectrometer, i.e. on the closeness of the model signals to real signals. Assuming that real signals are different from the model signals in the same way as experimental sensitivities differ from theoretical (see Table 1), we obtain a one-modal spectrum with fraction concentration errors from the 3th channel onwards 3%, -12%, 5%, 6%, 4%, 5%, 21%, -17%. When the errors of channel signals ε_j modulo are below 10^{-15} A, then the maximum errors of fraction concentrations $\sum_j |H_{oij}\,\varepsilon_j|$ have the following values (in cm^{-3}): 420; 450; 250; 98; 81; 52; 19; 14. Maximum errors are increa-

sed together with the errors of channel signals and the spurious peaks are possible in the limits of these errors.

The influence of regime parameter stabilization errors and preliminary adjustment on exactitude

In the determination of errors caused by deviations in manufacturing precision and variations of regime parameters the deviations and variations are considered to be random and characterized by covariant matrixes C_1 and C_2.

Matrix C_1 describes possible deviations arising in preliminary adjustment of regime parameters and also the differences in technical parameters of different devices. The following parameters have been considered F_1 - flow of pure air; F_2 - aerosol flow; C - effective capacitance of the measuring capacitor; $\alpha_o = \lambda t/\varepsilon_o$ - charging parameter, where λ - conductivity in the charging zone, t - charging time, ε_o - electric constant; U_i - precipitating voltages determining channel limits; E_o - average field strength in the charger; Q - parameter of precipitation. To model precipitation in the charger, the precipitating effect has been taken to be equal to the effect of the preliminary capacitor. The precipitating effect of the preliminary capacitor is determined by parameter Q , i.e., the effective charge of the preliminary capacitor. Errors of the above parameters are considered independent of each other with the standard deviations being 1% of the average values (10% for E_o and Q , taking into account the data in [1]). The average values of parameters F_1 , F_2 , U_i , C are taken from [1] or obtained by fitting.

Matrix C_2 describes the influence of the fluctuations of regime parameters α_o, U_i , E_o , Q (precipitation depends on the strength of the electric field in the charger and on the speed of the particles passing through the charger, i.e. F_2). The fluctuations of the latter parameters are considered independent of each other. All the air flows in the EAA are created by one pump and consequently changes in the operation of the pump bring about simultaneous changes in all the air flows. Flows F_1 and F_2 are viewed as components of a random variable which are increased or decreased simultaneously. The standard deviations for α_o , U_i , F_1 , F_2 are elected to be equal to 1% of the average (for E_o , Q - 10%).

For small changes δp_i of regime parameters p_i and for one

and the same aerosol (Smerkalov's distribution) the changes δy in the vector of channel signals y can be considered linearly dependent on changes δp_i:

$$\delta y = \sum_i \left(\frac{\partial}{\partial p_i} y \right) \delta p_i = \left(\sum_i \frac{\partial H_o}{\partial p_i} \delta p_i \right) \varphi .$$

For linear transformation $\mathcal{L}$ of a random vector its covariational matrix C is transformed according to formula $C' = \mathcal{L}\, C\, \mathcal{L}^T$, where C' - covariational matrix of a random vector obtained by linear transformation. Fraction concentrations of aerosol N are linearly related with the channel signals y according to equation $N = H_o y$. In the case of scaling transformation matrix H_o is diagonal and the scaling coefficients are located across the diagonal.

The standard deviations of fraction concentration errors are determined by the diagonal elements of the matrix $H_o (\frac{\partial y}{\partial p}) C_i (\frac{\partial y}{\partial p})^T H_o^T$, where $\frac{\partial}{\partial p} = (\frac{\partial}{\partial p_1}, \frac{\partial}{\partial p_2}, \ldots, \frac{\partial}{\partial p_n})$ is applied to every element of vector y ($\partial y/\partial p$ - matrix). C_i has the value C_1 (adjustment errors) or C_2 (fluctuations). The deviations δy of the signal for 1% (E_o, Q - 10%) changes of all the above parameters are proportional to the concentration of the incoming aerosol. Greatest influence on the channel signal is exerted by changes in the air flow F_1. When F_1 is changed by 1%, the signal in channel 3 is changed by 2.5%, in channel 9 - 3%, in channel 10 - 4%. Simultaneous changes in flows F_1 and F_2 cause the signal in channel 9 to change by 4% and in channel 10 by 5%. A change of effective capacitance by 1% causes 3% changes in channel 9 and 4% changes in channel 10. A 10% increase in the precipitation parameter leads to a 9% decrease in channel 3. For the rest of the channels and for a change of other parameters by 1% (E_o - 10%) the signal change does not exceed 1%. According to [3] the channel noise current is in the order of 10^{-15} A. The noise is independent of aerosol concentration. The present paper will not deal with current (signal) fluctuations caused by aerosol concentration fluctuations during measurement. It has been assumed that the noise currents (10^{-15} A) in the channels are independent. The respective covariational matrix C_n has been added to the matrix $(\frac{\partial y}{\partial p}) C_2 (\frac{\partial y}{\partial p})^T$, i.e., in addition to the influence of the fluctuations of different parameters also the noise current is considered. The contribution of the noise current to the error in fraction concentrations depends on the concentration of the measured aerosol and increases

with the decrease of the latter. In Fig. 1 the fraction concentration errors are depicted in the range of 2 standard deviations $\pm 2\sigma_1$ ($\sigma_{1i} = \sqrt{[H_o(\frac{\partial y}{\partial p})C_1(\frac{\partial y}{\partial p})^T H_o^T]_{ii}}$); $\pm 2\sigma_2$ ($\sigma_{2i} = \sqrt{\{H_o[\frac{\partial y}{\partial p}C_2(\frac{\partial y}{\partial p})^T + C_n]H_o^T\}_{ii}}$); $\pm 2\sigma_3$ ($\sigma_{3i} = \sqrt{\sigma_{1i}^2 + \sigma_{2i}^2}$). Here H_o means either the matrix in Table 2, or the diagonal matrix of scaling coefficients. These changes can also be viewed as changes within the limits of one standard deviation, whereas the respective errors of technical and regime parameters should be considered twice as large. As is seen in Fig. 1, the deviations are slightly smaller in the case of scaling transformation as compared with matrix signal processing. The errors σ_3 in per cent of the mean in the case of scaling transformation are (from channel 3 onwards) : 18%, 4.3%, 5%, 3%, 3%, 4%, 7.3%, 11%. For matrix processing the respective figures are 21%, 10%, 6%, 3%, 3%, 4.3%, 8%, 35%. Largest errors can be noticed in the first and the last channel.

In [18] measurements of monodisperse particles have been conducted with one EAA device. From the presented printout it follows that for that particular device the current noise has had the order of 6×10^{-15} A. Fig. 1 presents fraction concentration errors for channel 4, 5 and 7 in the limits of two standard deviations $\pm 2\sigma_2^*$, $\pm 2\sigma_3^*$, if the current noise is 6×10^{-15} A. The same figure contains also fraction concentration errors caused only by a noise of 6×10^{-15} A ($\pm\sigma_4$) and 12×10^{-15} A ($\pm\sigma_5$). It is evident that the increase of noise has a noticeable influence on the errors, especially in the first and the last channel. Matrix processing in these channels is significantly sensitive to the amount of noise.

Influence of particles larger than the EAA measurement range

The nominal measurement range of the EAA is from 5 nm to 500 nm radius. The signals are elicited not only by the particles of a certain range, but also the particles of larger sizes which may cause the multiplication of results. Due to the electric field in the charger the mobilities of large particles ($r > 1000$ nm) coincide with these of the measurement range. In the present study the response of the EAA to gamma-distribution with average values $\bar{r}$ = 2000 nm, 4000 nm, 6000 nm and with the parameter of distribution $\mu = 6$ is calculated. A gamma-distribution with such parameter value describes the distribution of droplets in radiation fogs

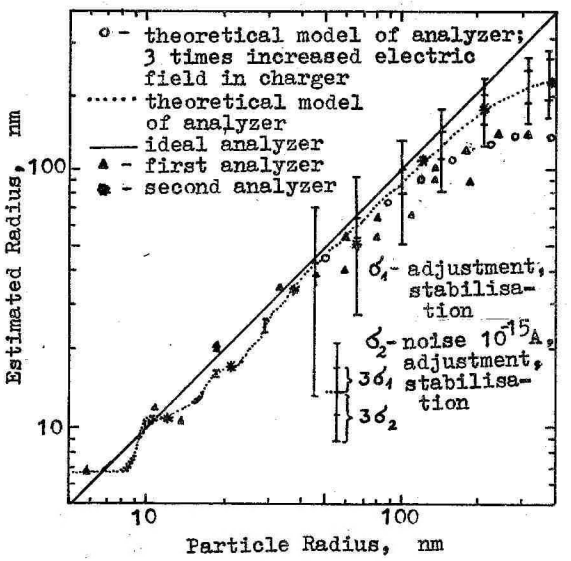

Fig. 2. Average particle size estimates of test aerosol by the readings of two EAA devices. Theoretical size estimates are obtained by numerical modeling of one EAA.

[19]. The number of droplets varies between 1 and 600 particles/cm^3 depending on the size and intensity of the fog. For the sake of convenience the concentrations of fogs used in the calculations have been set at one particle per cm^3 . Visibility S, where only the light scattering effect of fog droplets has been taken into account, has the following values S = 110 km for $\bar{r}$ = 2000 nm, S = 31.4 km for $\bar{r}$ = 4000 nm, S = 14.6 km for $\bar{r}$ = 6000 nm. The number of particles is inversely proportional to the visibility. In Fig. 1 it can be seen that distortions due to fog droplets increase with the size. Scaling transformation was used to obtain fraction concentrations. The erroneous concentration increase caused by fog droplets is manifest mainly in channels 5, 6 and 7 . When the drops grow, the distortion effects move towards the first channels. In thick fogs and for low concentrations of particles of the size r = 5...500 nm the EAA can give erroneous results. The EAA should be used with caution in aerosol

chambers where artificial fogs are generated.

Comparison of two EAA devices

In [18] the EAA has been used for the measurement of monodisperse particles. Average particle sizes have been estimated by the fraction concentrations, whereas fractions located far from the main maximum have not been considered. In the present investigation the respective results for one EAA are presented by the triangles in Fig. 2.

The data presentation format is identical to the one used in [18]. The dotted curve represents the estimate of average size of log-normal aerosols ($\sigma_g \approx 1.05...1.1$.) calculated on the basis of the theoretical model. The asterisks stand for the estimates of average particle size obtained by the second EAA [3]. The estimates have been calculated on the basis of experimental data (in brackets) in Table 1. These data have also been used in fitting of the parameters of the theoretical model. For the second device there is a good agreement between the experimental and the theoretical results. It should be pointed out that the discrepancy between the asterisks and the theoretical curve at r = 67 nm corresponds to the irregularity in the experimental data [4]. Fig.2 gives possible errors of average size estimates in the limits of three standard deviations on the theoretical curve. The standard deviation σ_1 describes the variability of average size estimates caused by technical manufacturing imprecision of 1%, by adjustment faults of 1% (10% for E_o and Q), and an instability of regime parameters of 1%. In the deviation σ_1 noise in the channels is not taken into account. The influence of noise has been found by adding normal-distribution random numbers to the theoretical signals, the mean of the numbers was zero and the standard deviation was 6×10^{-15} A. For the first EAA the noise was in the order of 6×10^{-15} A. The concentration of monodisperse particles was set at 1000 particles in a cm^3 . The estimates of average particle size were computed by the methods described in [18]. Repeated computation gave sufficient data for the computation of standard deviations of the estimates. The standard deviations σ_2 in Fig. 2 are results of addition of the above dispersions (with the dispersion due to the noise added to the dispersion of σ_1^2). It can be seen in Fig. 2 that the deviation of average

size estimates increases with the decrease of size. The charge on the particles decreases together with the particle size and thus, if the particle concentration remains constant, the signal/noise ratio deteriorates. At the same time the deviation δ_1 is decreased together with the decreasing particle size. The triangles signifying the data of the first EAA are outside the range determined by the theoretical curve and the deviations $\pm 3\delta_2$. This EAA had been in use for many years without supplementary calibrations and adjustment. It is evident that in the region of large particles its calibration had been shifted, although the shift had not been detected by the built-in checking systems. One of the possible causes may be the growth of field strength in the charger.

In Fig. 2 the circles designate the estimate of the average size of the model spectrometer, whereas field strength in the charger has been increased three times. It can be seen that the circles are in better correspondence with the data of the first EAA.

To estimate the applicability of matrix H_0 (Table 2) for the first EAA [18], channel signals have been calculated first at unchanged field strength in the charger and then at a three times increased field strength. Smerkalov's distribution [17] is used as a size spectrum of the input aerosol. Using matrix H_0 fraction concentrations have been computed. The ratios of fraction concentrations of the modified model and the concentrations for the initial model have the following values: 1.00; 0.99; 1.05; 1.10; 1.21; 1.34; 0.77; -1.43. The ratios of respective channel signals (or fraction concentrations calculated by scaling transformation) are 1.00; 1.03; 1.07; 1.13; 1.23; 1.16; 0.77; 0.46. It can be seen that the application of scaling coefficients or matrix H_0 of the second device to the model signals which approximately describe the first device leads to considerable errors. For matrix H_0 the concentration of the last fraction acquires a negative value. The transfer of the calibration (matrix H_0) of the second device to the first device gives unsatisfactory results. According to model calculations, a 3% change made separately in any of the parameters described in the preceding section causes greatest error in fraction concentration (45%) in channel 10. In the rest of the channels the errors are within 10%. If these changes in the parameters are added up as dispersions of ran-

dom independent variables (modeling of adjustment imprecision), then the errors in fractions 5...8 have the order of 10%, in fractions 3, 4, and 9 the order is 20%; and in fraction 10 the order is 80%.

References

1. Liu, B.Y.H., Pui, D.Y.H., Kapadia, A. Electrical analyser: history, principle, and data reduction // Aerosol measurement / Ed. D.A. Lundgren et al. - Gainesville: University of Florida, 1979. - P. 341-383.
2. Phalen, R.F., Ho, A.T., Kenoyer, J.L. Comparison of electron microscopy and the electrical aerosol size analyzer for determination of size distribution of a submicronic salt aerosol // Aerosol measurement / Ed. D.A. Lundgren et al. - Gainesville: University of Florida, 1979. - P. 480-487.
3. Pui, D.Y.H., Liu, B.Y.H. Electrical aerosol analyzer : calibration and performance // Aerosol measurement / Ed. D.A. Lundgren et al. - Gainesville: University of Florida, 1979. - P. 384-399.
4. Richards, L.W. The reduction of data from the electrical aerosol analyzer // Aerosol measurement / Ed. D.A. Lundgren et al. - Gainesville: University of Florida, 1979. - P. 438-450.
5. Liu, B.Y.H., Pui, D.Y. On the performance of the electrical aerosol analyzer // J. Aerosol Sci. - 1975. - Vol. 6. - P.249-264.
6. Таммет Х.Ф. Об электрической гранулометрии аэрозолей // Уч. зап. Тарт. ун-та. - 1975. - Вып. 348. - С. 30-34.
7. Таммет Х.Ф. Кусочно-линейная модель спектра в аэроионных и аэрозольных измерениях // Уч. зап. Тарт. ун-та. - 1980. - Вып. 534. - С. 45-54.
8. Таммет Х.Ф. Калибровка электрического гранулометра аэрозолей по распределению осажденных частиц // Уч. зап. Тарт. ун-та. - 1983. - Вып. 648. - С. 52-58.
9. Кикас Ю.Э., Мирме А.А., Пейль И.А., Тамм Э.И., Таммет Х.Ф. Экспериментальная градуировка электрического спектрометра аэрозолей методом эталонных аэрозолей // Уч. зап. Тарт. ун-та. - 1985. - Вып. 707. - С. 54-71.
10. Ноппель М.Г., Х.Ф. Таммет. Метод и алгоритм вычисления аппаратной матрицы электрического спектрометра

аэрозолей// Уч. зап. Тарт. ун-та. – 1987. – Вып. 755. – С. 62–70.

11. Мирме А.А. О калибровке электрического спектрометра аэрозолей // Уч. зап. Тарт. ун. – 1987. – Вып. 755. – С.71–79.

12. Таммет Х.Ф. Аспирационный метод измерения спектра аэроионов // Уч. зап. Тарт. ун-та. – 1967. – Вып. 195. – 232 с.

13. Ноппель М.Г. О распределении зарядов на аэрозольных частицах при униполярной зарядке их легкими аэроионами // Уч. зап. Тарт. ун-та. – 1983. – Вып. 648. – С. 32–40.

14. Noppel, M. Algorithm for rapid approximate calculation of the charge distribution of conductive aerosol particles charged in a strong electric field // Уч. зап. Тарт. ун-та. – 1985. – Вып. 707. – 84–93.

15. Фукс Н.А. О величине зарядов на частицах атмосферных аэроколлоидов // Изв. АН СССР. Сер. геогр. и геофиз. – 1947. – Т. 11 – No. 4. – С. 341–348.

16. Фукс Н.А. О стационарном распределении зарядов аэрозольных частиц в биполярно ионизированной атмосфере // Изв. АН СССР. Сер. геофиз. – 1964. – No. 4. – С. 579–586.

17. Смеркалов В.А. Аппроксимация среднего распределения аэрозольных частиц по размерам // Изв. АН СССР. Физ. атмосф. и океана. – 1984. – Т. 20. – No. 4. – С. 317–321.

18. Мирме А.А., Рейнарт А.Э., Кикас Ю.Э., Тамм Э.И., Дубровин М.А., Бернотас Т.Н., Пейль И.А. Измерение спектров калибровочных аэрозолей. Сравнение анализатора TSI со спектрометром ТГУ // Уч. зап. Тарт. ун-та. – 1987. – Вып. 755. – С. 80–88.

19. Зуев Б.Е., Кабанов М.В. Оптика атмосферного аэрозоля. – Л.: Гидрометеоиздат, 1987. – Т. 4. – 254 с.

АНАЛИЗ МЕТОДОВ ИЗМЕРЕНИЯ СПЕКТРА РАЗМЕРОВ АЭРОЗОЛЯ ЭЛЕКТРИЧЕСКИМ АНАЛИЗАТОРОМ TSI-3030

М.Г. Ноппель

Р е з ю м е

В работе численным моделированием изучается точность предложенных в литературе двух подходов к обработке сигналов электрического анализатора TSI-3030. В качестве исходного спектра размеров использовалась одномодальная модель среднего спектра атмосферного аэрозоля. Распространенный способ вычисления спектра размеров путем масштабного преобразования канальных сигналов приведет к появлению двух ложных пиков в результатах. При матричном подходе к обработке сигналов ложные пики устраняются, точность восстановления исходного спектра повышается. Из-за наличия электрического поля в зарядниках, сигнал в приборе вызывают не только частицы из области измерения, но и частицы, размер которых больше верхней границы области. В случае туманов это может привести к значительным погрешностям в получаемом спектре.

Изучено влияние погрешностей настройки прибора и флуктуации значений режимных параметров на точность измерения спектра. Путем подгонки теоретических канальных сигналов прибора к экспериментальным сигналам определены значения параметров теоретической модели. По модели вычислена аппаратная матрица для перевода значений канальных сигналов в фракционные концентрации частиц аэрозоля. Проведено сравнение двух экземпляров прибора TSI-3030. Сравнение выявило заметное расхождение в результатах измерения.

SIZE DISTRIBUTION DYNAMICS OF RURAL AND URBAN AEROSOLS

Ü. Kikas, A. Mirme and E. Tamm

Introduction

Atmospheric aerosol is extremely changeable. It is influenced by the circulation and turbulence of the air, meteorological parameters, and the chemical composition of the air. On the other hand, the behaviour of the aerosol is determined by the laws of physics.

At the present stage, the most important task of atmospheric aerosol measurements is to find regular patterns on the background of fluctuations. In situ measurements have enabled the authors of [1, 2] to establish some regularities in aerosol dynamics: different forms of nighttime and daytime spectra, dependence of the stability of aerosol fractions on the average size of the fractions, etc. In order to establish the degree of applicability of these results further aerosol spectra measurements were carried out under different conditions. The present paper will lay out and compare the results of three such measurement periods.

Conditions of the measurements of spectra

The measurements of spectra were carried out automatically by the original electrical spectrometer of Tartu University [3]. The records of particle spectrum took place in every 5 min. The diameter range from 10 nm to 10 μm was divided into 12 fractions. All three measurement periods were conducted in summer under relatively similar meteorological conditions. Two measurement periods were conducted in the countryside: in a station of the Institute of Atmospheric Physics of the Soviet Academy of sciences in Zvenigorod, 35 km from Moscow and in a station of Tartu University in Voore, 60 km from Tartu, Estonia. Period 3 was carried out in the city of Tartu. Table 1 characterizes the conditions of observation. The duration of one measurement period was about 8 days. After preliminary processing the respective numbers of analysed spectra for the three periods were 1661, 1600 and 1695.

Table 1

The conditions of observation

	Zvenigorod	Voore	Tartu
T i m e	13–22 June 86	19–26 Aug 87	9–16 July 87
Sunrise	4 : 50	6 : 50	5 : 20
Sunset	23 : 00	21 : 55	23 : 25
Temperature C			
day	20...29	9...23	–
night	11...17	8...18	–
Pressure mm Hg	742...755	757...764	–
Rel. humidity %			
day	25...60	70...100	–
night	70...100	85...100	–
Elevation of spectrometer above ground m	1.2	3	7
Wind velocity m/s	5...8	1.5...3	–

Daily variation of the aerosol state

Aerosol particle concentration undergoes strong fluctuations. Therefore isolated measurements do not provide reliable and representative data which would characterize the aerosol state. A more adequate picture of the aerosol in certain locality can be obtained by the analysis of a more extensive corpus of measurement data. Such data, if the measurements have been carried out for several days, give information on the dynamics of the aerosol for the period. Fig. 1 presents average daily variations of numerical and volume concentrations of particles with diameters from 10 nm to 10 μm.

It can be seen that in different locations the aerosols differ both in numerical and volume concentrations. In the city there were several times more aerosol particles than in rural locations, whereas at Zvenigorod which is situated near a metropolis, the particle content was slightly higher than at Voore. The daily variation of particle concentration in the city was wide, while the variations of different days

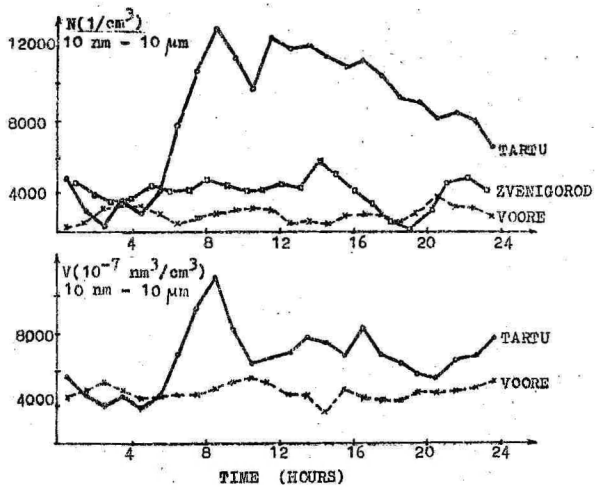

Fig. 1. Average daily variations:

N - numerical concentrations of particles 10 nm...10 μm,

V - volume concentrations of particles 10 nm...10 μm.

were similar. The average daily variation of N was very weak at Voore and weak at Zvenigorod, the variations of different days in the countryside were weakly correlated (~20%).

Nevertheless, all three variations in Fig. 1 clearly exhibit trends within one-day periods. We suggest an interpretation of the trends by two factors, namely, the level of air pollution (amount of trace gases), and the intensity of solar radiation. After sunrise the trace gases which have been generated during the night will enter into photochemical reactions. The final products of these reactions can make up aerosol particles by nucleation and condensation on nuclei. In the morning hours the particle concentration will rise together with the intensity of solar radiation. Maximum concentrations were observed from 10:00 to 14:00.

After 14:00 the particle concentration usually dropped. To explain this, two hypotheses can be proposed. First, by that time the air might not contain a sufficient amount of gases capable of aerosol formation. Second, by that time the con-

centration of particles in the range 0.2...0.3 μm has been significantly increased. These particles, in their turn will "eat up" small particles in coagulation.

In the evening, as the air is cooling down, certain gases (e.g. water vapour) are saturated and their condensation will cause the evening rise in particle concentration.

In the city the variation of emission of man-produced substances coincides with the variation of solar radiation, this brings on a sharp increase in particle concentration during the morning hours. The daytime drop of the particle concentration is less steeply manifest in the city and is apparently caused by the decrease of pollutant emissions during the working hours. The influence of human activity on the state of city aerosol is explicitly demonstrated in Fig. 2 which depicts the variation of concentration N in Tartu during 6 days.

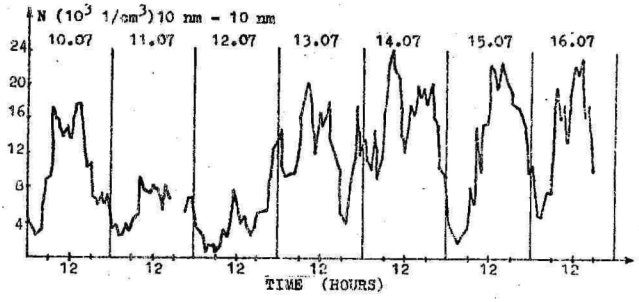

Fig. 2. Time variation of particle concentration 10 nm...10 μm in the city of Tartu

Two holidays - Saturday, July 11 and Sunday, July 12 are clearly distinguished by low particle concentrations.

The average daily variation of volume concentrations V (Fig. 1) in Tartu and Voore is largely similar to the variation of N . As V characterizes the mass of aerosol particles, and N/V characterizes their size, it can be concluded that the spectrum deformation is weak inside one-day periods. Only the growth of mean particle size in the evening can be seen clearly; then the decrease of N is accompanied by the increase of V .

Spectra of aerosol particles

Average spectra are presented in Table 2.

Table 2

Average spectra of aerosol particle number concentrations

No. frac.	Fraction boundaries d (μm)	Zvenigorod N (cm^{-3})	Zvenigorod σ/N	Voore N (cm^{-3})	Voore σ/N	Tartu N (cm^{-3})	Tartu σ/N
1	0.010–0.018	1464	1.11	625	1.93	3688	0.94
2	0.018–0.032	1592	0.75	1144	1.35	3584	0.91
3	0.032–0.056	1744	0.61	1191	0.68	2074	0.80
4	0.056–0.100	1196	0.66	985	0.50	1210	0.79
5	0.10–0.18	625	0.53	763	0.60	600	0.74
6	0.18–0.32	199	0.62	327	0.68	217	0.67
7	0.32–0.56	26	0.78	102	0.66	62	0.68
8	0.56–1.0	4.3	0.73	35	0.64	23	0.79
9	1.0–1.8	1.9	0.60	8.7	0.68	9.8	0.88
10	1.8–3.2	0.5	0.60	1.4	0.63	2.7	0.69
11	3.2–5.6	0.20	0.65	0.27	0.66	0.55	0.76
12	5.6–10.0	0.01	3.07	0.03	1.11	0.05	0.92
	0.01–10	6884	0.62	5207	0.66	11610	0.78

The spectra of different locations are clearly distinguished by the levels of fraction concentrations N and variabilities (σ/N). Concentrations of small (d < 0.1 μm) and large (d > 1 μm) particles in urban aerosols clearly exceed those in rural aerosols. Higher concentrations of small particles are apparently caused by active generation of photochemical aerosol in the more polluted urban air. It can be supposed that large fractions of urban air are made up mostly of disperse particles (dust) and that the increase in their concentration is not connected with active generation in small

fractions.

In submicron fractions (0.1 μm < d < 1 μm) the highest concentrations were observed in Voore. The reason may be a higher relative humidity in August (Table 1).

The results of [1] were confirmed, i.e., it was found that in all the cases nighttime and daytime spectra were significantly different in the region of small particles (Fig. 3).

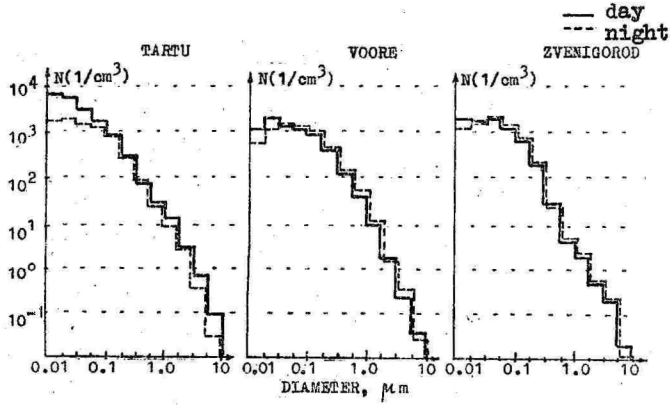

Fig. 3. Average daytime and nighttime spectra

Nighttime observations yielded spectra of aged aerosol with the maximum concentration of particles with 0.03...0.06 μm diameters. In the daytime spectra maximum concentrations were observed in the fractions of "young" particles with the diameters d < 0.02 μm. These data demonstrate the difference between daytime and nighttime particle generation rates. The difference in the particle generation rates can be best expressed by daily variations of fraction concentration relations N_1/N_2 and N_2/N_3 (Fig. 4).

In Voore, where the air was presumably the purest of the three observation sites and the amount of trace gases was determined by natural causes, the level of particle generation was lowest. At the same time N_1/N_2 was well correlated with solar radiation. Also in Zvenigorod the correlation between N_1/N_2 and UV-radiation was 36%. The respective correlations between total particle concentrations N and the radiation we-

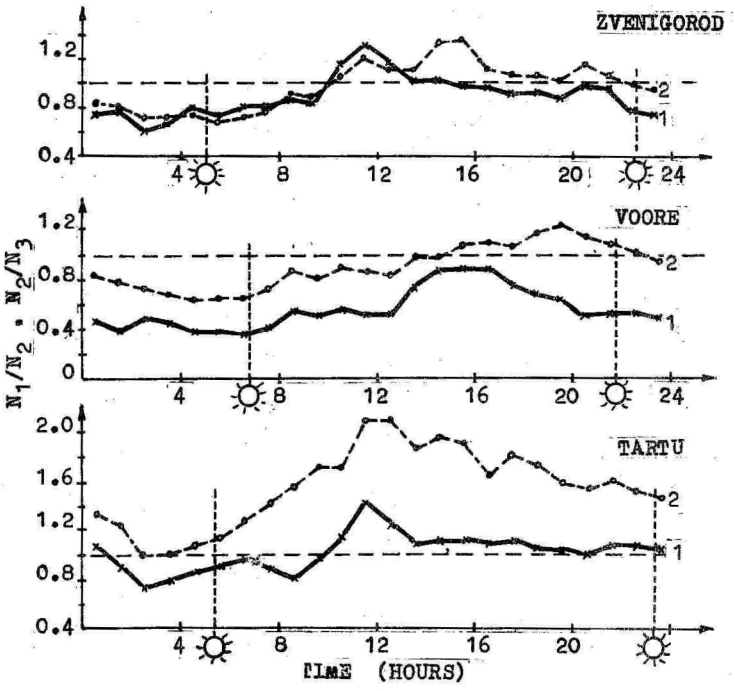

Fig. 4. Daily variation of the relations of fraction concentrations N_1/N_2 (1) and N_2/N_3 (2).

re very weak (Voore 9%, Zvenigorod 8%). This corroborates the conclusion in [1] that solar radiation influences aerosol situation mostly in the region of small particles.

Persistence of aerosol fractions

Estimates of characteristic time τ_i of autocorrelation functions for all fraction concentrations were found. As has been pointed out in [1], the variation of these autocorrelation functions describes the influence of three kinds of processes: fast, medium, and slow. The latter are the physical processes of aerosol development: coagulation, condensation, and precipitation. Characteristic time τ_i has

been determined as the time of 50% fall of the slow component of the correlation function. This parameter characterizes the stability of an aerosol fraction in a given period of time and in a given location.

All three measurement periods confirmed the dependence of τ_i on the average fraction size (Fig. 5). Fractions with particle diameters 0.2...0.6 μm were most stable; fractions with diameters 0.01...0.03 μm exhibited greatest instability, high instability was observed also in the case of large fractions with particle diameters over 3 μm.

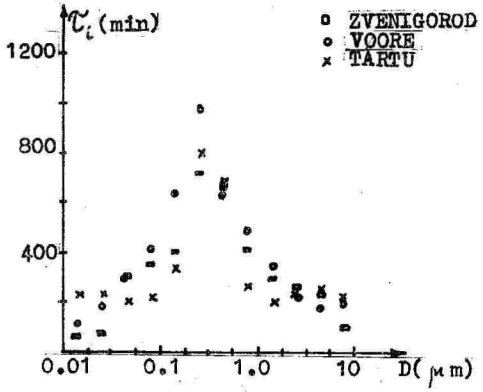

Fig. 5. The dependence of characteristic time τ_i of aerosol fraction on average fraction diameter D.

The observed variation of the functions $\tau_i(D)$ agrees with theoretical notions of the stability of atmospheric aerosol. Characteristically, the stability of fractions was only weakly dependent on location and thus also on aerosol concentration.

Conclusions

Experimental in situ measurements of atmospheric aerosol conducted in three different locations make it possible to conclude that different locations have their characteristic

aerosol situations. The concentration of particles is determined by the level of impurities, i.e., the generation is lowest in the nighttime and highest at noon. This is expressed by different forms of nighttime and daytime average spectra.

The above holds also for urban aerosols, where, however, man-generated pollution has the greatest influence. Variations in the amount of man-produced pollution determine the variation of aerosol situation in urban areas. Therefore, the processes in urban aerosols are more complex in comparison with rural aerosols.

These conclusions as such are not new in the aerosol science. On the other hand, this investigation has proved the possibility of experimental study of the regularities of highly changeable atmospheric aerosols.

References

1. A. Mirme, Ü. Kikas, E. Tamm. Time-size structure of atmospheric aerosol // Lecture Notes in Physics 309. Atmospheric aerosols and nucleation. - Springer-Verlag 1988. P. 52- 55.
2. А.А. Мирме, Ю.Э. Кикас, Э.И. Тамм. Динамика спектра атмосферного аэрозоля приземного слоя // Уч. зап. Тарт. ун-та. - 1988. - Вып. 824. - С. 109-120.
3. A. Mirme et al. Multi-channel electric aerosol spectrometer // Eleventh internat. conf. on atmospheric aerosols, condensation and ice nuclei. - Budapest, 1984. - Pre-print Vol. II. - P. 155-159.

ДИНАМИКА АТМОСФЕРНОГО АЭРОЗОЛЯ В ГОРОДЕ И В СЕЛЬСКОЙ МЕСТНОСТИ

Ю.Э. Кикас, А.А. Мирме, Э.И. Тамм

Р е з ю м е

Представлены результаты наблюдений атмосферного аэрозоля с помощью многоканального электрического спектрометра ТГУ [3].

Приведено сравнение трех измерительных серий проведенных в летнее время в сельских местностях (Вооре, Зженигород) и в городе (Тарту). В каждой серии статистически обработаны 1660 спектров в диапазоне диаметров частиц 10 нм до 10 мкм.

Уровень концентрации аэрозольных частиц и динамика спектра характерны для данной местности. Они определяются, главным образом, интенсивностью солнечного излучения и количеством следовых газов в воздухе. Фотохимическая генерация частиц происходит в мелкодисперсной части спектра ($d < 0{,}03$ мкм).

Особенностью городского аэрозоля является повышенная численная концентрация частиц в мелких и крупных фракциях и и корреляция с интенсивностью городской жизни.

Стабильность аэрозольной фракции зависит от среднего размера фракции и является наибольшей в диапазоне диаметров частиц 0,2 мкм 0,6 мкм.

CHARGE GENERATION AND SEPARATION IN THE EVAPORATION OF WATER AEROSOL DROPLETS

V. Tamme

In addition to natural generation, water aerosols are widely used in medicine, health resorts, conditioning and purification systems. In spray production of water aerosol high charges are generated on the droplets. When the droplets evaporate, the charges change the electrical state of the air, various technological processes, etc.

There are three possible ways of charge separation during evaporation [1] : a) low-temperature ion emission, b) charge emission in the strong Coulombic field of the droplets, c) electrostatic bursting the droplets when the Rayleigh instability limit is exceeded (the diameter of the evaporating droplets decreases and the surface charge density increases). After the evaporation the non-volatile substance makes up a solid particle (the so-called residual nucleus) which carries a relatively high electric charge and can survive in a suspended state for a relatively long time. These particles can be recorded by electrical methods of aerosol spectrometry.

In [2] the results of air ion counter measurements of electric charges generated in the air during the evaporation of water spray are presented. The measurement methods used, however, give no information neither about the initial charges on the droplets, nor about whether the evaporation was accompanied by electrostatic bursting of the droplets, or only by charge emise in a suspended state for a relatively long time. These particles can be recorded by electrical methods of aerosol spectrometry.

In [2] the results of air ion counter measurements of electric charges generated in the air during the evaporation of water spray are presented. The measurement methods used, however, give no information neither about the initial charges on the droplets, nor about whether the evaporation was accompanied by electrostatic bursting of the droplets, or only by charge emission from the surface of the droplets.

The multiparametric process of polydisperse droplet formation in pneumatic spray and subsequent evaporation is not easily replicable, therefore for the purposes of this

investigation the droplets were charged in a Berglund-Liu monodisperse droplet generator /3/ The aim of the present study was to determine empirically the initial charges on the droplets and their further separation during the evaporation up to electrical bursting.

The block-diagram of the measurements is depicted in Fig.1.

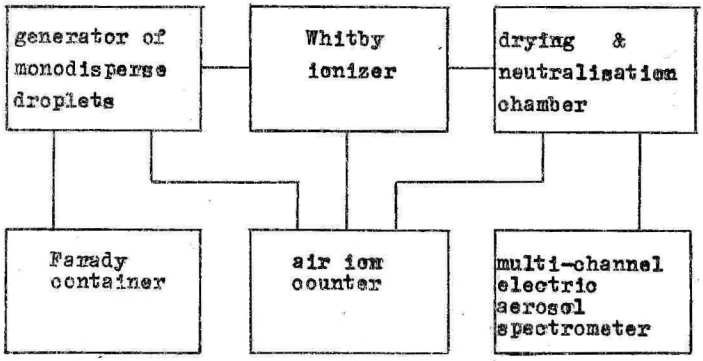

Fig. 1. Block-diagram of the measurements

A monodisperse droplet generator was used to produce droplets of diameter d = 22 μ and geometrical standard deviation σ_g = 1.06. The size and numerical concentration of the droplets were calculated on the basis of the parameters of the generator and checked with an optical microscope.

The average charge on the droplets was determined with a Faraday cylinder and an air ion counter. Both variants yielded + 10^{-15} C as an average charge on a droplet which is roughly equal to the absolute value of the charge of the droplets generated in a spray with an oscillating capillary described in [4]. Unipolar positive droplets were directed into the evaporation and neutralization chamber where they were mixed with dry air (10% RH) containing bipolar ions (10^4...10^5 e/cm^3). The diameters of the droplets decreased, the droplets lost their unipolar charges and were neutralized. Bipolar ionization in the chamber was created by a Whitby ionizer [5].

The neutralization of water aerosol at several evaporation

modes was measured by a UT-8401 air ion counter. The polar charge density of the water spray after evaporation and neutralization was measured at three limiting mobilities of the counter : 2, 10^{-1} and 10^{-3} $cm^2.V^{-1}.s^{-1}$. Average charge densities are presented in the Table, whereas the measurement modes were as follows.

A. Background measurements. 1. Dried filtered air, without neutralization, relative humidity R = 10% , time in chamber t = 6,5 s. 2. Filtered air with neutralization, R = 10% , t = 6,5 s.

B. Monodisperse spray without neutralization. 1. Spray with humid air, R = 70% , t = 38 s.

C. Spray with neutralization. 1. Monodisperse spray R = =50%, t = 19 s. 2. Polydisperse spray (without ultrasound) R = 50% , t = 19 s.

Table 1

Ion charge density levels in the air under various conditions

Mode	Polar ion charge density $P_{\pm}$, $\cdot 10^3$ e. cm^{-3} at limiting mobilities k_o					
	k_o= 2 $cm^2.V^{-1}.s^{-1}$		k_o= 0.1 $cm^2.V^{-1}.s^{-1}$		k_o= 10^{-3} $cm^2.V^{-1}.s^{-1}$	
	P_+	P_-	P_+	P_-	P_+	P_-
A.1	0.06	0.06	1.5	2.0	2.0	2.4
A.2	17	17	30	28	40	40
B.1	2.3	-	190	-	250	-
B.2	40	-	2000	-	2300	-
C.1	17	17	90	95	100	100
C.2	15	15	95	95	100	100

The Table shows that monodisperse spray in mode B1 (dry air) will cause an increase in the ionization by one order of magnitude in comparison with the spray with humid air (B2). It can be assumed that the increase is brought about by a greater relative role of electrostatic bursting in dry air. The design of the present experiment, however, does not enable us to give an unambiguous answer to this question.

In modes C1 and C2 space charge density measurements were combined with aerosol measurements with a multi-channel wide-range aerosol spectrometer EAA [6].

Measurement results are histographically presented in Fig. 2 which characterizes the dependence of channel signals (unit 10^{-15} A) on the diameter of the particles generated during evaporation and neutralization. The numerical concentrations printed above the channel signal peaks have been obtained computationally.

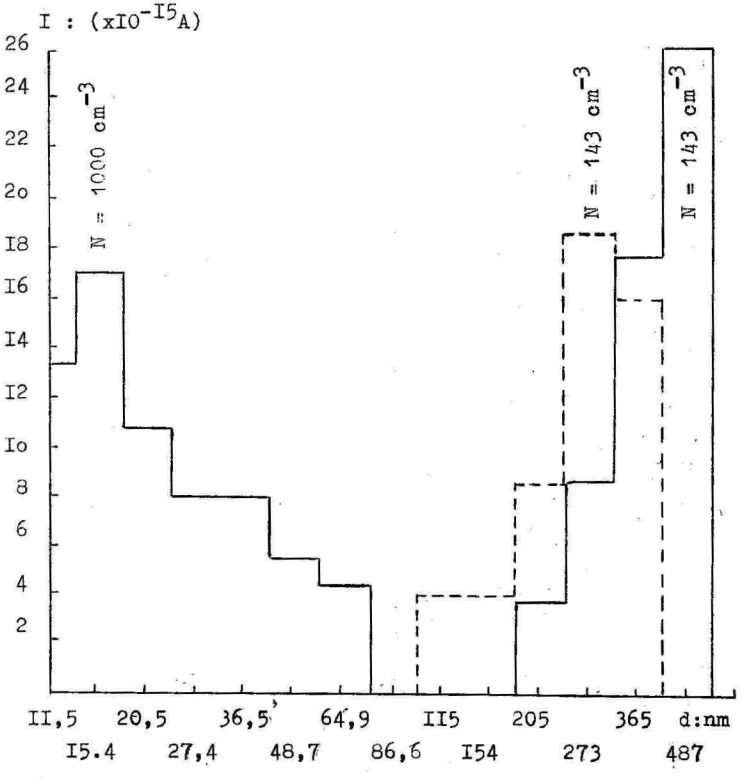

Fig. 2. Channel signal spectra of wide-range aerosol spectrometer

—— measurement in mode B.1.

---- measurement in mode B.2.

Fig. 2 shows that during evaporation in mode C2 a partial electrostatic bursting of the droplets takes place, and the maximum of burst products is recorded in channel 2 (d = 0.01...0.02 μdia).

This is caused by the widening of the droplets size spectrum at non-ultrasonic spray in a Berglund-Liu generator (σ_g = 1.06 grows to σ_g = 1.2). Consequently smaller droplets appear. In bipolar ion environment these droplets evaporate before total neutralization. The appearance of these droplets is accompanied by an increase in the surface density and finally by electrostatic bursting. As a result of these processes relatively large drops (22 μdia) are transformed into a fine aerosol with an average particle diameter of 0.01...0.02 μ dia. A comparison of the ionization measurements in modes C1 and C2 in the Table does not reveal significant differences.

It can be concluded that ordinary wet-scrubbers as well as other equipment where water is pneumatically sprayed in electric fields can act as generators of ultra-fine aerosols.

References

1. Савченко А.Б., Смирнов В.В. Ионный механизм обмена примесями между гидросферой и атмосферой // Изв. АН СССР, Физика атмосферы и океана. - 1985. - Т. 21. - Но. 1. - С. 32-41.
2. Виснапуу Л.Ю. К зависимости электризации распыленной воды от ее состояния // Уч. зап. Тарт. ун-та. - 1987. - Вып. 755. - С. 184-187.
3. Тамме В.Б., Коппелмаа И.В. Вибрационный генератор монодисперсных аэрозолей // Уч. зап. Тарт. ун-та. - 1987. - Вып. 755. - С. 113-119.
4. Контуш С.М. Поверхностные явления в физике водных грубодисперсных аэрозолей // Автореф. дис. на соиск. уч. степ. докт. физ.-мат. наук. - 1987. - С. 25.
5. Liu B.Y.N., Pui D.Y.H. Electrical neutralization of aerosol // Aerosol. Sci. - 1974. - Vol. 5. - pp. 465-472.

К ВОПРОСУ ГЕНЕРАЦИИ И РАЗДЕЛЕНИЯ ЗАРЯДА ПРИ ИСПАРЕНИИ КАПЕЛЬ ВОДНОГО АЭРОЗОЛЯ

В.Б. Тамме

Р е з ю м е

В настоящей работе экспериментально определялись начальные заряды на монодисперсных водяных каплях и последующее распределение их вплоть до электрического взрыва капли. Средний заряд капли определялся методом цилиндра фарадея и при помощи счетчика аэроионов. Оба метода давали средний заряд капли $+10^{-15}$ С.

Монодисперсное распыление с сухим воздухом повышает ионизацию на один порядок по сравнению с распылением влажного воздуха.

Наряду с измерениями ионизации проводили и дополнительные аэрозольные измерения при помощи многоканального аэрозольного спектрометра широкого диапазона. При определенных условиях в ходе высыхания водяных капель происходит их частичный электростатический взрыв, причем максимум аэрозольных продуктов взрыва регистрируется во втором канале спектромета (т.е. d = 0.01...0,02 мкм).

A UNIVERSAL CONTROLLER FOR LONG-TERM EXPERIMENTS

A. Reinart

Introduction

The wide spread of micro- and minicomputers makes it possible to distinguish two directions in the automation of experiments:

1) hierarchical systems where data collection and sensor control are executed separately from data processing which is carried out later by more powerful computer systems;
2) data collection, sensor control and processing are executed in one and the same computer.

The main shortcoming of (1) is the hierarchical structure of the system excluding on-line processing also the final results become available with delay. The drawback of (2) is the low reliability of Soviet personal computers and their high power consumption which pose difficulties in the use of these computers in field conditions and in long-term experiments.

Aerosols and air ions are complex objects of study and their spectra are connected with the signals by equation systems which are not well determined. The systems can be solved by a computer with an operational speed of at least $10^3...10^4$ float point operations per second [1].

At Tartu University Air Electricity Laboratory long-term and field experiments are conducted with hierarchical systems where data is collected in real time and later processed by a general purpose computer.

The universal controller used at the Laboratory built on the basis of the powerful Soviet 16-bit chip KR1810VM86A* makes possible to execute most of data processing on-line. Only long-term statistics and formatting (printing, graphics) are to be done later by a general purpose computer.

---

* Henceforth the original Cyrillic letters in the designations of equipment types have been transliterated into the Latin alphabet.

Design

A 16-bit KR1810VM86A chip used (its internationally known analogue is I8086A). To achieve greater universality the controller has been designed as consisting of the main board and input/output modules.

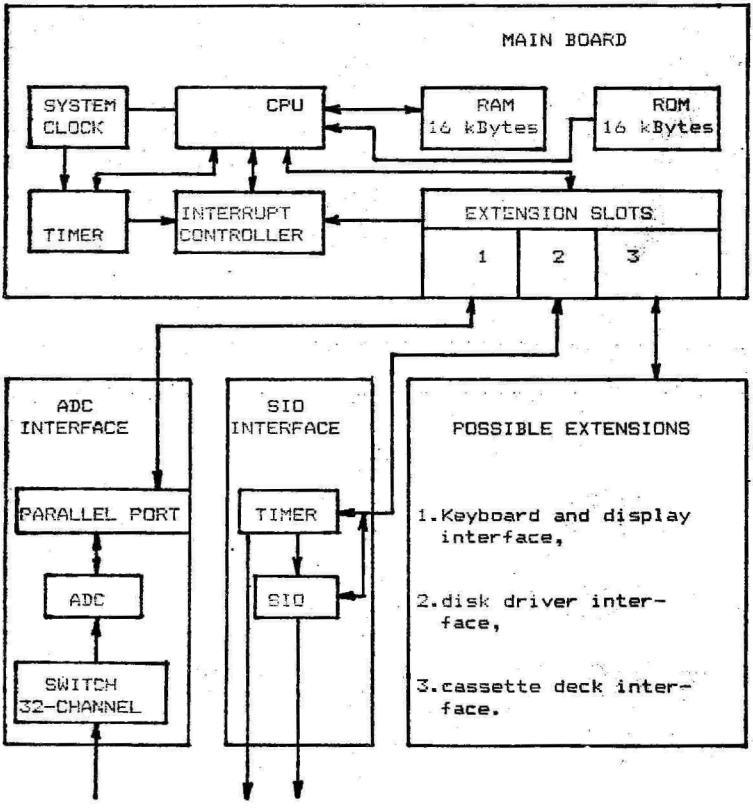

Fig.1. Block-diagram of the controller

The main board carries (Fig. 1) :

1) the microprocessor chip (CPU) with the demultiplexers and buffers of data bus and address bus,
2) system clock generator,

3) read-write memory (RAM) up to 16 kB,
4) read-only memory (ROM) up to 16 kB,
5) three 16-bit timers for real-time and other timing purposes,
6) 8-level interrupt controller,
7) extension slots for up to three extension modules.

RAM and ROM are interchangeable in the limits of 32 kB whereas the minimal value for both, RAM and ROM, is 4 kB. By an additional memory board ROM can be increased to 32 kB without limiting RAM.

Additional modules to the mother board make possible to create control systems for different experiments. To date, two additional modules have been built:

1) analog-digital converter (ADC),
2) module for serial data exchange through a standard "current loop" channel.

The ADC comprises:

1) 32-channel switch for analog voltage for the connection of any channel to input of the measurement amplifier,
2) measurement amplifier for double amplification of the voltage,
3) 10-bit ADC,
4) 24-bit (three 8-bit) parallel port for the choice of the measured channel, control of the conversion cycle and the input of the output data of the ADC to the computer.

The existing ADC makes possible to measure the input voltage in the following ranges:

1) 0...+5 V,
2) 0...+10 V,
3) -5...+5 V,
4) -10...+10 V.

An average time of one conversion is 20 μs. The input resistance of ADC is 1 MΩ.

The module for serial data exchange comprises:

1) special chip KR580VI51A to carry out serial data transmission,

2) timer for the selection of frequencies for data exchange (frequencies 100...19200 Hz).

Input/output signals of the module meet the international "current loop" standard.

The following modules are going to be built for the controller:

1) module for data storage on cassette deck,
2) module for the connection of keyboard and display,
3) control module for disk drive,
4) modules for parallel data transmission.

Programming

The choice of the KR1810VM86A chip for the controller has been conditioned by the increasingly wide spread of personal computers with these or similar chips.

Of Soviet products "ISKRA 1030" and "ES 1840" deserve mention here. The existence of such computers considerably simplifies the writing of programs for the controller. The currently used programs have been written with the macro-assembler of "ISKRA 1030" and a special floating point program library.

Preliminary debugging of the programs is carried out in a general purpose computer, then the program can be fed into the controller and final debugging can be executed. When the program is ready, it can be stored in ROM with a special programmer. The ROM-s with the program can be added to the ROM of the controller.

References

1. Бернотас Т.П., Кольк Э.Э. и др. Система сбора и обработки данных в спектрометрии аэрозолей и аэроионов // Уч. зап. Тарт. ун-та. - 1985. - Вып. 707. - С. 46-53.

УНИВЕРСАЛЬНЫЙ КОНТРОЛЛЕР ДЛЯ УПРАВЛЕНИЯ ДОЛГОВРЕМЕННЫМИ ЭКСПЕРИМЕНТАМИ

А.Э. Рейнарт

Р е з ю м е

В Аэроэлектрической лаборатории ТГУ разработан универсальный контроллер для управления долговременными экспериментами и экспериментами в полевых условиях. Контроллер позволяет осуществлять сбор данных, управление датчиками и обработку данных в реальном масштабе времени. Задачей универсальной ЭВМ остается только конечная статистическая обработка и оформление результатов.

В контроллере используется 16-битовый микропроцессор КР1810ВМ86А . На основной плате контроллера размещены микропроцессор, ОЗУ до 16 кбайт, ПЗУ до 16 кбайт, три 16-битовые таймера, 8-уровневый контроллер прерываний и разъемы для подключения к трем модулям расширения. Разработаны также 10-разрядный 32-канальный аналого-цифровой преобразователь и модуль для последовательного обмена данными.

Составление программ для контроллера производится с помощью ЭВМ "ИСКРА 1030".

ELECTROSTATIC SCATTERING OF TWO AIR ION GROUPS OF DIFFERENT MOBILITIES

A. Luts and J. Salm

This paper will discuss uniformly and unipolarily ionized gas or unipolarily charged aerosol where the process of ionization/charging has ceased. At the next stage only scattering of charged particles at the expense of their mutual Coulombic repulsion takes place in the gas. The particles carrying more than one elementary charge will not be considered. If all the ions in the gas have the same mobility the process of scattering can be described mathematically strictly [1-3]. Two discrete sets with mobilities k_1 and k_2, however, bring about considerable mathematical difficulties.

For the above system of two groups of ions the scattering equations in a dimensionless form are

$$\left.\begin{aligned} \frac{d\tilde{\varrho}_1}{d\tau} + \sqrt{\frac{k_1\varrho_{10}}{k_2\varrho_{20}}}\;\tilde{\varrho}_1\left(\tilde{\varrho}_1 + \frac{\varrho_{20}}{\varrho_{10}}\,\tilde{\varrho}_2\right) = 0 \\ \frac{d\tilde{\varrho}_2}{d\tau} + \sqrt{\frac{k_2\varrho_{20}}{k_1\varrho_{10}}}\;\tilde{\varrho}_2\left(\tilde{\varrho}_2 + \frac{\varrho_{10}}{\varrho_{20}}\,\tilde{\varrho}_1\right) = 0 \end{aligned}\right\}, \qquad (1)$$

where $\tilde{\varrho}_1(\tau) = \frac{\varrho_1(\tau)}{\varrho_{10}}$, $\tilde{\varrho}_2(\tau) = \frac{\varrho_2(\tau)}{\varrho_{20}}$ – dimensionless charge densities

$\tau = \sqrt{k_1 k_2 \varrho_{10}\varrho_{20}}\,t/\varepsilon$ – dimensionless time

$\varrho_{10}, \varrho_{20}$ – charge densities at the initial moment

t – time

ε – electrical constant (under normal conditions in gas $\varepsilon = 8.85\cdot10^{-12}$ F/m).

The relation between the charge densities given in [3] is

$$\tilde{\varrho}_1^{\,k_2/k_1} = \tilde{\varrho}_2 \,. \qquad (2)$$

Using this relation, system (1) can be transformed into independent equations, e.g.

$$\frac{d\tilde{\varrho}_1}{d\tau} + \sqrt{\frac{k_1\varrho_{10}}{k_2\varrho_{20}}}\;\tilde{\varrho}_1\left(\tilde{\varrho}_1 + \frac{\varrho_{20}}{\varrho_{10}}\,\tilde{\varrho}_1^{\,k_2/k_1}\right) = 0 \,. \qquad (3)$$

This equation has separable variables. Changing the variable $y = 1/\tilde{\varrho}_1$ we get

$$\int \frac{dy}{\sqrt{\frac{k_1 \varrho_{10}}{k_2 \varrho_{20}}}\left[1 + \frac{\varrho_{20}}{\varrho_{10}} y^{(1-k_2/k_1)}\right]} = \tau + C. \qquad (4)$$

The indefinite integral in (4) is a case of the integral of the differential binomial. When k_2/k_1 is a rational number this integral can in principle be expressed through elementary functions. However, the shape of the integral is heavily dependent on the value of k_2/k_1, and the charge density could not be expressed as an explicit function of time. To provide an illustration, let us consider the integral

$$J = \int dx/(ax^{\nu} + b).$$

When $\nu = 1/3$

$$J_{1/3} = 3\frac{b^2}{a^3} \ln(ax^{1/3} + b) - 3\left(\frac{b}{a^2} x^{1/3} - \frac{x^{2/3}}{2a}\right)$$

and when $\nu = 2/3$

$$J_{2/3} = 3b^{1/2} \arctan\left(\frac{\sqrt{b}}{\sqrt{a}\, x^{1/3}}\right) \cdot \frac{1}{a^{3/2}} + \frac{3}{a} x^{1/3} .$$

Air ion systems with multiple mobilities, where charge densities have a lognormal distribution have been dealt with in [4]. The formulas for the changes in the characteristics of the distribution, e.g. average mobility, etc. proposed in [4] have somewhat limited validity as they presuppose constancy of distribution function $\varrho = \varrho(k)$ throughout the process of scattering. Actually, the changes of the function can be considered negligible only for relatively narrow lognormal distributions, whereas already beyond the standard deviation of the scatter $\sigma_k \geq \bar{k}/5$ the distribution changes considerably. Thus, the premise of lognormal distribution does not hold throughout the process of scattering. Moreover, on the basis of [4] the rules governing the change cannot be explicitly obtained. In fact, the normal distribution does not change in the process of scattering.

Keeping in mind the mathematical difficulties, we can attempt to find approximating functions for the dependence of

the charge density on the time by means of numerical calculations. One of the more promising functions for the approximation is

$$f = (\alpha\tau + 1)^{\beta}, \tag{5}$$

which also gives a satisfactory approximation for all $\tilde{\varrho}_i$ in a system with many mobilities.

For the system with a single mobility

$$\alpha = 1\ , \quad \beta = -1 \quad \text{and} \quad f = \tilde{\varrho}\ .$$

For systems with two mobilities let us consider the functions

$$f_1 = (\alpha_1\tau + 1)^{\beta_1}, \qquad f_2 = (\alpha_2\tau + 1)^{\beta_2}, \tag{6}$$

where $k_1 > k_2$.

The parameters α_1, α_2, β_1, β_2 are determined by the minimization of error for the interval $\tilde{\varrho}_i$ from 0.01 to 1 . For a concrete set of initial parameters (k_1/k_2 , $\varrho_{10}/\varrho_{20}$) it is possible to find such α_1, α_2, β_1, β_2, that the average relative error

$$\delta = \frac{1}{n}\sum_{1}^{n}\frac{|f(\tau_i) - \tilde{\varrho}(\tau_i)|}{\tilde{\varrho}(\tau_i)}$$

in all intervals is below 5%. At the approximation of the parameters α_1, α_2, β_1, β_2 with the functions $g = g(k_i, \varrho_{i0})$ the error is slightly increased.

For the calculation of the parameters (taking into consideration that $k_1 > k_2$) we propose formulas (7) and (8)

$$\alpha_1 = \frac{1+p}{\sqrt{pq}}\left(\frac{q^{0.52}p^{0.67} + 1}{p^{0.67} + 1}\right)^{2.7}, \tag{7}$$

$$\beta_1 = -\left(\frac{p^{0.73} + 1}{q^{0.54}p^{0.73} + 1}\right)^{2.5}, \tag{8}$$

where $p = \varrho_{20}/\varrho_{10}$; $\quad q = k_2/k_1$.

In principle, these formulas can be presented in a more symmetrical form, which, however, would make practical calculations more cumbersome.

Table 1 presents the errors δ, obtained by the approximation of $\tilde{\varrho}_i$ with the function f_1, where α_1 and β_1 are computed by formulas (7) and (8), where $\tilde{\varrho}_i \in (0.02...1)$ is selec-

14*

ted as the interval. It should pointed out that the errors are increased for larger intervals and decreased for smaller intervals.

The formulas (6-8) can be used for all mobilities at $k_1/k_2 \in (1;\ 10000)$, but at $k_1/k_2 \approx 10000$ a better approximation is made possible by formula (14) in [3]. This formula has been derived under the premise that $\tilde{\varrho}_2$ is constant.

Table 1

Average relative errors for formulas (7) and (8), in %

k_1/k_2 \ $\varrho_{10}/\varrho_{20}$	46.4	21.6	10.0	4.64	2.16	1.0	0.464	0.216	0.1	0.0464	0.0216
10000	4	1	4	6	4	3	4	5	4	3	2
1000	1	1	2	4	4	3	4	5	4	3	2
464	1	0	2	4	3	3	4	5	4	3	2
216	3	1	2	3	3	3	4	5	4	3	2
100	6	2	2	3	3	3	5	5	4	3	2
46.4	7	3	1	2	3	4	5	5	4	3	2
21.6	6	2	1	1	2	4	4	5	4	2	2
10	3	3	2	1	3	5	5	4	4	2	1
4.64	6	5	4	2	2	3	5	3	2	1	1
2.16	9	8	6	3	1	1	1	1	1	1	1
1.39	5	4	3	2	1	1	1	1	1	1	1
1.11	1	1	1	1	1	1	1	1	1	2	2

Formula (2) is valid for the charge density, whereas it is generally not valid between the approximated functions f_1 and f_2 in formula (6). The function found in the present paper $f_1 = (\alpha_1\tau + 1)^{\beta_1}$ describes the scattering only in a certain time interval, for this interval formula (2) is applicable. Outside this interval, if $\tilde{\varrho}_1 \leq 0.02$, the function f_1 does not yield satisfactory approximation and calculation on the basis of this function leads to considerable errors.

To calculate the approximations of the function $\tilde{\varrho}_2$ on the basis of the function f_1, it is possible to use the formula $f_2 = f_1^{k_2/k_1}$ in the time interval τ: $f_1 \in [0.02;\ 1]$; outside this interval f_1 should be considered equal to zero, and f_2 should be calculated according to the scattering law of ions of one mobility [3]:

$$f_2 = \begin{cases} f_1^{k_2/k_1}, & f_1 \in [\Delta_1; 1] \\ \dfrac{f'_{20}}{\tau + 1}, & f_1 < \Delta_1, \quad \Delta_1 = 0{,}02 \end{cases} \tag{9}$$

where f'_{20} – function f_2 at the end of the above time interval, i.e. $f'_{20} = 0.02^{k_2/k_1}$

Table 2

Average relative errors for the approximation of the function $\tilde{\varphi}_2$ by means of formula (9), in %

$\varphi_{10}/\varphi_{20}$ / k_1/k_2	0.0216	0.0464	0.1	0.216	0.464	1.0	2.16	4.64	10.0	21.6	46.4
10000	2	2	2	2	2	2	2	2	2	2	2
1000	2	2	2	2	2	2	2	2	2	2	2
464	2	2	2	2	2	2	2	2	2	2	2
216	2	2	2	2	2	2	2	2	2	2	2
100	2	2	2	2	2	2	2	2	2	2	2
46.4	2	2	2	2	2	2	2	2	2	2	2
21.6	2	2	2	2	2	2	2	2	2	3	3
10	2	2	2	2	2	3	3	3	3	3	4
4.64	2	2	2	2	2	3	4	4	5	6	9
2,16	4	4	3	2	2	3	5	8	13	22	36
1,39	4	3	3	2	2	3	5	7	10	16	15
1.11	1	1	1	1	1	1	1	2	3	3	3

Table 2 presents the errors δ, obtained by the approxi-

Table 3

Average relative errors for the approximation of the function $\tilde{\varphi}_2$ by means of formula (9), where $\Delta_1 = 0.5\%$, in %

$\varphi_{10}/\varphi_{20}$ / k_1/k_2	0.0216	0.0464	0.1	0.216	0.464	1,0	2.16	4,64	10.0	21,6	46.4
4.64	3	2	2	2	3	5	6	6	5	5	6
2.16	9	8	5	2	2	4	5	6	7	10	15
1.39	7	6	5	3	1	1	1	1	1	1	1

mation of $\tilde{\varrho}_2$ by means of the function f_2 using formula (9). When $k_1/k_2 \approx 2$ and $\varrho_{10}/\varrho_{20} \gg 1$, the errors are considerably increased. To get a better approximation for such k_i and ϱ_{0i}, smaller values of Δ_1 (e.g. $\Delta_1 = 0.005$) should be used in formula (9). The errors for $\Delta_1 = 0.005$ are presented in Table 3.

Acknowledgements

We thank M. Noppel for his useful comments which helped us to find the form of the approximation function.

References

1. Wolodkewitsch, N. Untersuchungen über die "elektrische Diffusion" der Ionen in Gasen unipolar Beladung // Ann. Physik. - 1933. - Bd. 16.- S. 431-467.
2. Hidy, G.M., Brock, J.R. Dynamics of Aerocolloidal Systems. - New York : Pergamon Press. - 1970.
3. Сальм Я.И. Об электростатическом рассеивании аэроионов // Уч. зап. Тарт. ун-та. - 1980. - Вып. 534. - С. 95-100.
4. Верещагин И.П., Левитов В.И., Мирзабекян Г.З., Пашин М.М. Основы электрогазодинамики дисперсных систем. - М., 1974. - 480 с.

ЭЛЕКТРОСТАТИЧЕСКОЕ РАССЕИВАНИЕ ДВУХ ГРУПП АЭРОИОНОВ РАЗНЫХ ПОДВИЖНОСТЕЙ

А.М. Лутс, Я.И. Сальм

Р е з ю м е

Рассматривается однородно и униполярно ионизированный газ, в котором происходит только процесс электростатического рассеивания аэроионов (частиц аэрозоля). Рассмотрена задача о двух группах аэроионов с подвижностями k_1 и k_2. Соответствующие уравнения приведены в безразмерном виде. Для вычисления безразмерных концентраций предложены аппроксимирующие функции (6). Определены границы применения и погрешности аппроксимирующих функций.

FORMATION OF PHOTO-OXIDANTS IN THE INTERACTION OF SHORTWAVE UV-IRRADIATION AND VARIOUS VOLATILE ORGANIC SUBSTANCES

R. Priiman and L. Visnapuu

Volatile extractions emitted by plants take part in the processes of natural air purification caused by photochemical reactions. Many of these substances are strong bactericides. The mechanism of the transformation of phyto-organic volatile compounds has not been elucidated. It is known, though, that solar radiation and especially its longwave part play an important role in these reactions. Nevertheless, it is interesting to study the transformation of volatile phyto-organic substances at shorter wavelengths, as bactericidal UV-irradiation has found wide application in farming. The combination of UV-irradiation and aerosols of phyto-organic compounds makes possible to achieve a 30% higher disinfection rate, than separate application of either of the factors.

Our studies have shown that the transformation of phyto-organic substances in the presence of UV-irradiation is qualitatively and quantitatively heavily dependent on both, the concentration of the phyto-organic compound the basic ingredients of which are terpene hydrocarbons, and on the wavelength and amount of UV-irradiation.

The first products of terpene hydrocarbon transformation in the presence of UV-irradiation are often photo-oxidizers, also ozone. It should be pointed out that the formation of ozone does not have an unambiguous explanation. At bactericidal and erythemic UV-irradiation of 0,2 - 0.3 W/m^2, and in the presence of terpene hydrocarbons (α- and β-pinenes) with initial concentration of about 100 mg/m^3 the ozone concentration dropped (ozone had been formed mainly due to UV-devices, the amounts of ozone did not exceed the official limiting concentrations for industrial premises 0.1 mg/m^3).

In the experiments it was found that shortwave bactericidal UV-irradiation of the air containing certain volatile phyto-organic compounds caused the concentration of ozone to grow. Further experiments were conducted to clarify the problem.

The fact that powerful UV-irradiation is used for the disinfection of the air on farming premises (especially in

ventilation channels) lends practial importance to the study of the above problem. This paper will concentrate on the processes in the indoor air which is being influenced simultaneously by UV-irradiation and by phytoncidal phyto-organic compounds. In the experiments a stable climate chamber KTLK-1250* with an effective volume of 1200 dm^3 was used. An experimental UV-radiator DRT-400 of 400 W was placed in the chamber. In some experiments the artificial ionization was generated with a portable Riga air ionizer which at a distance of 0.5 m created a polar charge density of small ions of an order of 10^5 e/cm^3. The charge density of air ions was measured with an air ion counter UT-8401.

Air samples for the determination of ozone and nitrogen dioxide were taken in glass absorption containers filled with 1% and 8% solutions of potassium iodide. The concentrations of nitrogen dioxide and ozone were measured colorimetrically with the Griss reactive and dimethyl-n-phenyl-diamine respectively. The total of terpene hydrocarbons was measured chromatographically on a thin layer, as well as by weighing.

In preliminary measurements it was established that the generated photo-oxidizers and volatile phyto-organic compounds filled the chamber in a uniform way, as the forced concection currents mixed the air in the whole volume of the chamber. Average data of 3-5 parallel experiments on the formation of photo-oxidizers in the presence of UV-irradiation are presented in Table 1. The air pressure was 101.5 kPa, relative humidity was varied. Analogous data in the presence of certain organic compounds in the chamber is brought in Table 2.

The concentrations of phyto-organic compounds in the chamber were achieved by vaporizing the compounds in test tubes. For high concentrations the test tubes were heated in a water bath and a fan was used to increase the intensity of vaporization.

---

* Henceforth the originally Cyrillic letters used in the designations of apparatus types have been transliterated into the Latin alphabet.

Table 1

The dependence on relative humidity of photo-oxidizer concentration in the chamber in the presence of UV-irradiation, data for artificial ionization in brackets.

Relative humidity, %	Photo-oxidizer concentrations mg/m^3	
	O_3	NO_2
40	0.83	0.13
50	0.80 (0.89)	0.10 (0.30)
60	0.63 (0.72)	0.10 (0.30)
80	0.42	0.10

It can be seen that the concentrations of nitric dioxide are several times higher than these permitted by official norms for living areas. The norm of nitric dioxide for industrial premises and areas is 2 mg/m^3 , for living areas the maximum is 0.09 mg/m^3 , and daily average is 0.04 mg/m^3 .

The concentration of nitric dioxide was considerably increased when the air underwent simultaneous artificial ionization and UV-irradiation. It was found that the increase was steeper for drier air. The presence of the above phyto-organic compounds in the air slightly weakened the formation of nitric dioxide. The organic thinners, on the other hand, increased the concentration of nitric dioxide. Phyto-organic compounds and UV-irradiation increased the formation of ozone. This effect was observed selectively depending on the initial concetration of the phyto-organic agent. It was noticed that weak UV-irradiation (0.2-0.4 W/m^2) combined with admixtures of pine extraction and terpene hydrocarbons supressed ozone formation. This can be explained by the fact that ozone which is formed in small amounts is consumed in the oxidation of terpene hydrocarbons. An analogous process takes place at high concentration of ozone, but a large part of ozone is left unconsumed and ozone formation is slowed down by certain oxidation products.

It can be supposed that at ozone concentrations several times exceeding the official limit the oxidation of phyto-organic compounds is more intense and the oxidation products

Table 2

Concentrations of volatile phyto-organic compounds, organic thinners and photo-oxidizers in the presence of UV-irradiation at different humidities in the test chamber.

Relative humidity, %	Concentration of phyto-organic admixtures and photo-oxidizers, mg/m^3 Phyto-organic admixtures	O_3	NO_2
	peppermint extraction		
60	220	1.34	0.16
60	110	0.84	0.15
	turpentine		
60	150	0.73	0.10
70	100	0.31	0.14
	mixture of etheric oils		
60	140	1.56	0.03
70	100	0.59	0.08
	chlorophorm		
60	110	1.16	0.30
	pine extraction		
60	120	0.66	0.13
60	40	0.07	0.10
	α, β -pinenes		
60	130	0.82	0.13
60	50	0.19	0.10
	ethanol		
60	120	0.71	0.20

inhibit ozone formation in UV-irradiation.

Under the above conditions a considerable amount of ozone is formed in the air and it increases the disinfection effect in combination with UV-irradiation.

For such disinfection people and animals should be removed from the premises. It has been found that chlorophorm vapours increase ozone concentration, but as one of the oxidation products of chlorophorm is phosgene which is highly toxic, it is harmful to use chlorophorm even in small quantites.

К ОБРАЗОВАНИЮ ФОТООКСИДАНТОВ ПРИ ВЗАИМОДЕЙСТВИИ КОРОТКОВОЛНОВОГО УФ-ИЗЛУЧЕНИЯ И НЕКОТОРЫХ ЛЕТУЧИХ ОРГАНИЧЕСКИХ ВЕЩЕСТВ

Р.Э. Прийман, Л.Ю. Виснапуу

Р е з ю м е

Экспериментально установлено, что при облучении воздуха в малых закрытых объемах, содержащего летучие фитоорганические соединения, коротковолновым и бактерицидным УФ-излучением образуются повышенные концентрации озона. В работе рассматриваются процессы, протекающие в воздухе закрытых помещений при совместном применении УФ-излучения и аэрозолей фитоорганических композиций, обладающих фитонцидными свойствами. Приведены измеренные концентрации фитоорганических примесей, озона и диоксида азота в камере в случае УФ- излучения при разной относительной влажности и степени ионизации воздуха. Показано, что при УФ-излучении с уменьшением влажности воздуха и увеличением плотности заряда аэроионов концентрациии озона и диоксида азота повышаются. С увеличением концентрации фитоорганических примесей концентрация озона растет, а концентрация диоксида азота изменяется неоднозначно (например, в случае экстрактов мяты и хвои, растворов α, β- пиненов растет, а при скипидаре, смеси эфирных масел падает). Повышение концентрации озона в сочетании с УФ - излучением усиливает эффективность обеззараживания воздуха.

A PICOAMMETER FOR LOW AC MEASUREMENTS

M. Anso, L. Kärner

The electrometer is designed for low AC (10^{-12} ... 10^{-10} A) measurements in a frequency band of 3...100 kHz with a background DC of 2×10^{-10} ... 2×10^{-8} A in outer space. The latter circumstance demands that the picoammeter be of simple design, high reliability, low power consumption (240 mW), and small size (25x60x65 mm). The present article does not describe the narrow band filter for noise separation at the picoammeter output.

The picoammeter (Fig. 1) is an integrator-differentiator and its transfer function W(p) can be written as

$$W(p) = \frac{C_3R_5}{C_1} \cdot \frac{K_1(p)\gamma_1(p)}{K_1(p)\gamma_1(p) + 1} \cdot \frac{K_2(p)\gamma_2(p)}{K_2(p)\gamma_2(p) + 1}, \qquad (1)$$

where

$\gamma_1(p) = Z_{in}(p)/(Z_{in}(p) + Z_1(p))$,
$Z_{in}(p) = 1/C_{in}\cdot p$,
$Z_1(p) = 1/C_1 p$,
C_{in} – capacitance of the signal source,

$\gamma_2(p) = Z_2(p)/(Z_2(p) + Z_3(p))$,
$Z_2(p) = 1/C_3(p)$,
$Z_3(p) = R_5$,

$K_1(p)$ – voltage gain of amplifier A_1,
$K_2(p)$ – total voltage gain of amplifiers A_2 and A_3.

Formula (1) does not take into account the low stray capacitance of resistor R_5 which has been decreased by shielding. Neither does formula (1) include resistor R_1 (100 MΩ) which has been chosen so that the background DC of 2×10^{-8} A together with the maximum AC would not fill the the whole dynamic range of the integrator (i.e. that the measurement would take place in the linear range of the picoammeter). In addition, the condition $(2\pi\cdot R_1C_1) < 3\times10^3$ Hz must be fulfilled. Lower resistance cannot be selected for R_1 and R_5 as this would

increase picoammeter noise.

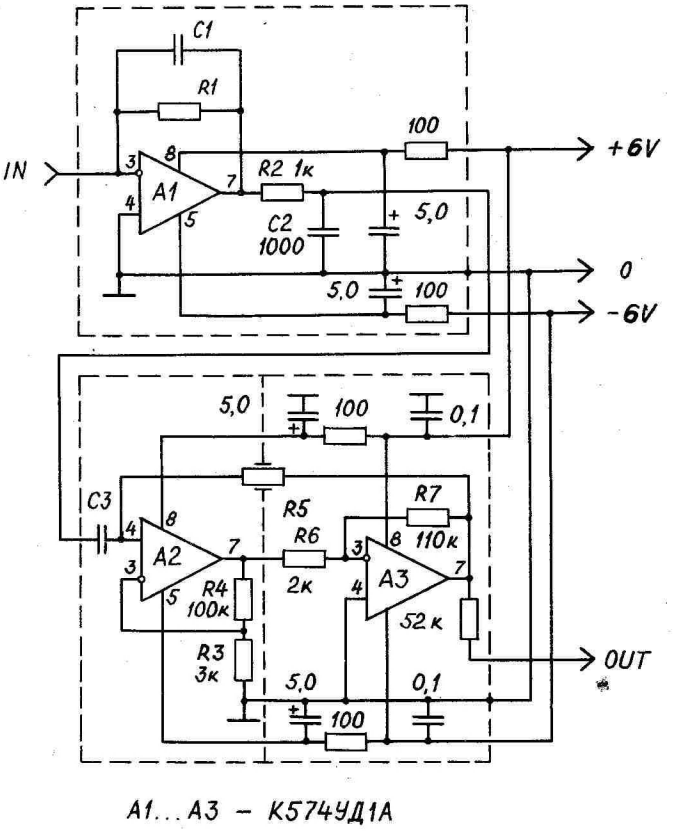

Fig. 1. The picoammeter

The voltage drop on resistor R_1 (i.e. direct voltage at the output of amplifier A_1) is proportional to the direct component of the input of the picoammeter.

The first fraction in formula (1) C_3R_5/C_1 describes the transfer function of an ideal integrator-differentiator. The second fraction has no influence on the dynamics of the picoammeter, as up to a frequency of 200 kHz it is for practical purposes equal to 1. The dynamics of the picoammeter (the transfer function for higher frequencies) is determined by the third fraction which determines the dynamics and sta-

bility of the differentiator. To ensure both, the dynamics and stability, it was expedient to build the amplifier of two operational amplifiers; $K_2(p)$ could be optimized by adjustable feedback depth. The optimum capacitance of C_3 influencing the dynamics of the picoammeter through the member $\gamma_2(p)$ was found to be 560 pF.

In the case of above two-amplifier variant it is possible to totally shield the capacitance between the input and output of the differentiator, otherwise, as was the case with the stray capacitance of R_3, it would limit piccoammeter dynamics.

There are several problems connected with the picoammeter noise. One of its sources is the thermal noise of R_1 and R_5

$$\overline{i^2_{R_1}} = \frac{4kT}{R_1} d\omega, \tag{2}$$

$$\overline{i^2_{R_5}} = \frac{4kT}{R_5} d\omega. \tag{3}$$

In addition, there are the noise voltages of operational amplifiers A_1 and A_2, and the drop noise of the leak currents at the amplifier input

$$\overline{i^2_I} = 2eI_I \cdot d\omega, \tag{4}$$

$$\overline{i^2_D} = 2eI_D \cdot d\omega, \tag{5}$$

where I_I and I_D are the input currents to A_1 and A_2, respectively. In a frequency range from 3 to 100 kHz all sources can be considered independent of frequency. The spectrum density of the total noise current at input can be expressed as

$$d\overline{i^2_n}(\omega) = \left\{\overline{i^2_I} + \overline{i^2_{R_1}} + \omega^2 C_\Sigma^2 \overline{e^2_I} + \frac{C_1^2}{C_3^2}\left[\overline{i^2_{R_5}} + \overline{i^2_D} + \overline{e^2_D}\left(\frac{1}{R_5^2} + \omega^2 C_D^2\right)\right]\right\} d\omega, \tag{6}$$

where C_{in} is the capacitance of the signal source. Formula (6) demonstrates that $\overline{i^2_{R_1}}$ reduces to input with the coefficient 1, $\overline{i^2_{R_5}}$ – with the coefficient C_1^2/C_3^2. The resistors R_1 and R_5 should be selected in such a way that the contribution of their thermal noise would be kept to minimum

over the whole range. Application of the measurement results presented in Fig. 2 makes it possible to make estimates with a correct order of magnitude

$$\sqrt{\overline{i^2_{R_1}}} \lesssim 10^{-14}\ \mathrm{A\cdot Hz^{-1/2}}, \qquad \sqrt{\overline{i^2_{R_5}}} \lesssim \frac{C_3}{C_1}\cdot 10^{-14}\ \mathrm{A\cdot Hz^{-1/2}}.$$

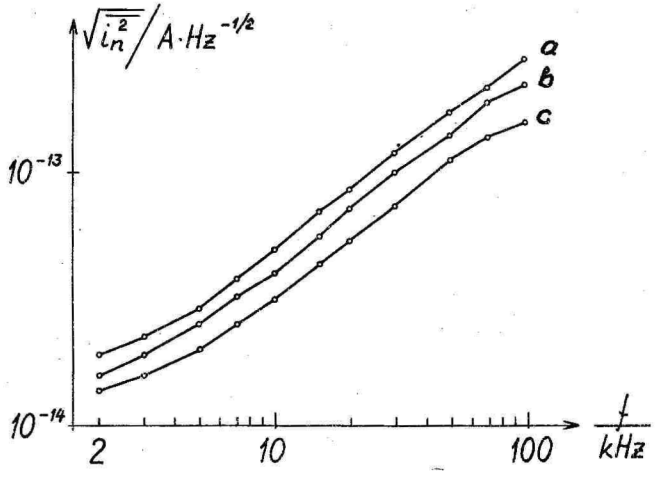

Fig. 2. Noise current at the picoammeter input

In the investigated model C_1 = 4...10 pF, C_3 = 560 pF; the order of magnitude of the coefficient is consequently $\approx 10^{-2}$. The relations (2) and (3) yield requirements for R_1 and R_5

$$R_1 \gtrsim 2\cdot 10^{-8}\ \Omega, \qquad R_5 \gtrsim 2\cdot 10^{4}\ \Omega.$$

Analogously the limitations of the drop noises of A_1 and A_2 can be obtained

$$\sqrt{\overline{i^2_I}} \lesssim 10^{-14}\ \mathrm{A\cdot Hz^{-1/2}}, \qquad \sqrt{\overline{i^2_D}} \lesssim \frac{C_3}{C_1}\cdot 10^{-14}\ \mathrm{A\cdot Hz^{-1/2}},$$

and according to (4) and (5) for the leak currents at the input

$$I_I \lesssim 3\cdot 10^{-10}\ \mathrm{A},$$
$$I_D \lesssim 3\cdot 10^{-6}\ \mathrm{A}.$$

Operational amplifier K574 UD 1A+ with a guaranteed input current $5 \cdot 10^{-10}$ A meets these conditions reasonably well.

In the case of an optimal choice of R_1 and R_5, and low leak currents I_I and I_D, the main noise sources in the investigated frequency range are $\overline{e_I^2}$ and $\overline{e_D^2}$. The relation between $\overline{e_I^2}$ and $\overline{e_D^2}$ is determined by the capacitances C_Σ and C_1 :

$$d\overline{i_n^2}(\omega) = \omega^2 \left(C_\Sigma^2 \overline{e_I^2} + C_I^2 \overline{e_D^2} \right) d\omega . \qquad (8)$$

The contribution of e_D^2 can be decreased by the selection of $C_1 \ll C_{in}$ which yields

$$d\overline{i_n^2}(\omega) = \omega^2 C_{in}^2 \overline{e_I^2} . \qquad (9)$$

Fig. 2 presents the measured noise spectra at the following values of C_{in} and C_1 :

a) $C_{in} = 0$, $C_1 = 16.4$ pF
b) $C_{in} = C_1 = 8.2$ pF
c) $C_{in} = 0$, $C_1 = 8.2$ pF .

The approximately proportional dependence of $\sqrt{\overline{i_n^2}}$ on the frequency $f = 2\pi\omega$ testifies that the main contributors to the total noise are $\overline{e_I^2}$ and $\overline{e_D^2}$, i.e. formula (8) is valid for the present circuit elements. In the case (a) noise level is higher than in the case (b) as the concentration of the whole capacitance in the integrator gives prominence to the voltage noise $\overline{e_D^2}$ of A_2.

+ The original Cyrillic letters in the designation have been transliterated into the Latin alphabet.

ИЗМЕРИТЕЛЬ МАЛЫХ ПЕРЕМЕННЫХ ТОКОВ

М.Х. Ансо, Л.П. Кярнер

Р е з ю м е

В работе описан измеритель малых токов (ИМТ), предназначенный для переменного тока 10^{-12} ...10^{-10} А в частотном диапазоне 3...100 кГц на фоне постоянного тока $2 \cdot 10^{-10}$ ...$2 \cdot 10^{-8}$ А в условиях открытого космоса. ИМТ представляет собой интегратор-дифференциатор. Основными факторами, ограничивающими быстродействие ИМТ, являются паразитная емкость резистора дифференциатора и малость коэффициента усиления операционных усилителей, из которых составлен дифференциатор, на высших частотах. Главным источником шума при емкости источника сигнала, превышающей емкость интегрирующего конденсатора, является шумовое напряжение операционного усилителя в интеграторе. Спектральная плотность приведенного ко входу шумового тока ИМТ пропорциональна частоте и емкости источника сигнала.

УДК 537.525.2

РАСПРОСТРАНЕНИЕ ОДНОЭЛЕКТРОДНОГО ВЧ РАЗРЯДА В ВОЗДУХЕ. М.Х.Айнтс, К.Ф.Куду // Уч.зап. Тарт. ун-та. -1990.- Вып.880. - С.5-12.

Представлены экспериментальные кривые зависимости скоростей распространения ВЧ разряда с остриевых электродов от расстояния, пройденного разрядом, при разных значениях ВЧ напряжения на частотах 10-20 МГц в воздухе атмосферного давления. Обнаружено сильное влияние влажности воздуха на форму разрядных каналов, от чего время перекрытия промежутка может изменяться более чем на порядок величины. Дается качественное обьяснение влияния влажности.

Илл.-3. Библ.-14. Рез. русск.

УДК 537.523.2:533.9.082.5

ОПТИЧЕСКОЕ ОПРЕДЕЛЕНИЕ КОНЦЕНТРАЦИИ ИОНОВ В ВЫСОКОЧАСТОТНОЙ ПЛАЗМЕ АЗОТА: ИЗМЕРЕНИЕ ПОГЛОЩЕНИЯ. М.Р.Лаан, П.П.Парис, Я.А.Сузи // Уч. зап. Тарт. ун-та. -1990.- Вып.880.- С.13-19.

Методом измерения относительного поглощения излучения перехода $0 \rightarrow 0$ первой отрицательной системы азота определяется концентрация ионов N_2^+ в канале нестационарного ВЧ разряда в азоте атмосферного давления.

Илл.-4. Библ.-4. Рез. русск.

УДК 535.35
537.523.2

РАЗРЯД В АРГОНЕ ПРИ АТМОСФЕРНОМ ДАВЛЕНИИ В РАЗРЯДНОМ ПРОМЕЖУТКЕ ОСТРИЕ–ПЛОСКОСТЬ. Х.И.Корге, У.И.Кууск, М.Р.Лаан // Уч. зап. Тарт. ун–та. – 1990. – Вып.880.– С.20–24.

Разряд возбуждался в аргоне при атмосферном давлении в разрядном промежутке острие–плоскость. Вольт–амперная характеристика разряда снята при отрицательном и положительном напряжениях острия. Описаны внешние формы разряда. В случае отрицательного острия установлено существование двух форм разряда – диффузного и контрагированного, для которых сняты спектры вблизи острия. Спектр контрагированного разряда лишь интенсивнее спектра диффузного разряда, качественных различий не обнаружено.

Илл.–4. Библ.–6. Рез. русск.

УДК 537.523.3

О СПЕКТРЕ РАДИОШУМОВ, ВОЗНИКАЮЩИХ ПРИ КОРОНИРОВАНИИ МОДЕЛЬНЫХ АНТЕНН. В.В.Смирнов // Уч.зап. Тарт.ун–та. –1990. – Вып.880.– С.25–32.

Изучаются амплитудно–частотные характеристики радиосигналов в интервале частот 10 КГц...1 ГГц, возникающие при коронировании электродов–антенн, как функции полярности короны и напряженности электрического поля E, а также отношения длин промежутка H и острия l_0. Указывается на преимущественно полосовую структуру помехи. Положение центров полос (12, 25, 150 МГц) и их устойчивость при изменении E и H/l_0 интерпретируется как результат спектрального разложения в приемном тракте разрядных импульсов типа двойной экспоненты, имеющих длительность переднего фронта ~ 5 нс и общую длительность на полувысоте ~70 нс. Анализ автокоррелограмм помехового сигнала указывает на наличие высоко периодических режимов в отрицательной короне и, частично, положительной короне.

Илл.–4. Библ.–6. Рез. русск.

УДК 551.594

ОБСЕРВАТОРИЯ АЭРОИОНОВ ТАХКУЗЕ: АППАРАТУРА. У.Э.Хыррак, Ф.Г.Миллер, А.А.Мирме, Я.И.Сальм, Х.Ф.Таммет // Уч.зап. Тарт.ун-та. - 1990. - Вып.880.- С.33-43.

Аппаратура, предназначенная для регистрации атмосферно-электрических и метеорологических величин, содержит шестиканальный и десятиканальный спектрометры подвижности аэроионов, источник высокостабильных напряжений, контроллер, ЭВМ "Электроника Д3-28", автономный источник питания и ряд датчиков. В настоящее время осуществлена регистрация спектра подвижности в диапазоне от $3*10^{-4}$ до 3 $см^2/(В*с)$ в 20 фракциях и основных метеорологических величин.

Илл.-3. Табл.-2. Библ.-14. Рез. русск.

УДК 551.594

ОБСЕРВАТОРИЯ АЭРОИОНОВ ТАХКУЗЕ: ПРОГРАММНОЕ ОБЕСПЕЧЕНИЕ. Х.Ф.Таммет// Уч.зап. Тарт. ун-та. - 1990.- Вып.880. - С.44-51.

Рассматривается программа измерений и процедура технической диагностики аппаратуры, использованные в обсерватории Тахкузе. Программа измерений построена по принципу разделения основных алгоритмов и информации о конкретной конфигурации аппаратуры. Описываются основные структуры и функции программ и структуры данных.

Табл.-3. Библ.-4. Рез. русск.

УДК 551.594

О ПРИРОДЕ ОТРИЦАТЕЛЬНЫХ ЛЕГКИХ АЭРОИОНОВ ОДНОСЕКУНДНОГО ВОЗРАСТА. Т.М.Партс// Уч.зап. Тарт. ун-та. – 1990. – Вып.880. – С.52-61.

Измерено более 1000 спектров подвижности односекундных легких отрицательных аэроионов в безлюдном помещении лаборатории в разных физико-химических условиях (температура, давление, влажность и состав воздуха). Делается вывод о существенной роли реакции переноса протона в газовой фазе. Влияние примесей на спектры подвижности может быть объяснено повышением концентрации более стабильных аэроионов типа $OH^-(H_2O)_n$ и $NO_3^-(HNO_3)_m(H_2O)_n$.

Илл.-2. Табл.-2. Библ.-12. Рез. русск.

УДК 551.594

О ЗАВИСИМОСТИ ЭЛЕКТРИЧЕСКИХ ХАРАКТЕРИСТИК ВОЗДУХА ОТ ЕГО ЗАГРЯЗНЕННОСТИ. Л.Ю.Виснапуу, Р.Э.Прийман // Уч.зап. Тарт. ун-та. – 1990. – Вып.880. – С.62-66.

Рассмотрены измерение спектра электрических подвижностей аэроионов при загрязнении воздуха и оценка загрязненности воздуха по этому спектру. Приведены средние данные весенне-летних измерений полярностей заряда легких и тяжелых аэроионов в г.Тарту в 1937-1988 гг. Показаны постоянное уменьшение средних плотностей заряда легких аэроионов и увеличение средних плотностей заряда тяжелых аэроионов, обусловленные ростом загрязнения атмосферного воздуха. Рассмотрена очистка воздуха от различных загрязняющих примесей растениями. Загрязненность воздуха снижается при этом в основном летучими фитоорганическими выделениями растений.

Илл.-1. Табл.-1. Библ.-2. Рез. русск.

УДК 551.594.25:53.092.7

АНАЛИЗ МЕТОДОВ ИЗМЕРЕНИЯ СПЕКТРА РАЗМЕРОВ АЭРОЗОЛЯ ЭЛЕКТРИЧЕСКИМ АНАЛИЗАТОРОМ TSI-3030. М.Г.Ноппель // Уч.зап. Тарт. ун-та. - 1990. - Вып.880. - С.67-83.

В работе численным моделированием изучается точность в предложенных в литературе двух подходов к обработке сигналов электрического анализатора TSI-3030. В качестве исходного спектра размеров использовалась одномодальная модель среднего спектра атмосферного аэрозоля. Распространенный способ вычисления спектра размеров путем масштабного преобразования канальных сигналов приведет к появлению двух ложных пиков в результатах. При матричном подходе к обработке ложные пики устраняются, точность восстановления повышается. Сигнал в приборе вызывают также частицы, размер которых больше верхней границы области измерения. В случае туманов это может привести к значительным погрешностям в получаемом спектре. Изучено влияние погрешностей настройки прибора и флуктуации значений режимных параметров на точность измерения спектра. По теоретическим и экспериментальным данным вычислена аппаратная матрица для перевода значений канальных сигналов во фракционные концентрации частиц аэрозоля. Проведено сравнение двух экземпляров прибора TSI-3030. Сравнение выявило заметное расхождение в результатах измерения.

Табл.-2. Библ.-19. Рез. русск.

УДК 551.510
551.508

ДИНАМИКА АТМОСФЕРНОГО АЭРОЗОЛЯ В ГОРОДЕ И В СЕЛЬСКОЙ МЕСТНОСТИ. М.Э.Кикас, А.А.Мирме, Э.И.Тамм // Уч.зап. Тарт.ун-та. – 1990.– Вып.880.– С.84–93.

Представлены результаты наблюдений спектров атмосферного аэрозоля в диапазоне диаметров частиц от 10 нм до 10 мкм с помощью электрического аэрозольного спектрометра ТГУ. Сравнены данные трех измерительных серий проведенных в двух сельских местностях и в городе. Статистически обработаны 5000 спектров аэрозольных частиц.

Представлена суточная динамика спектра, получены оценки стабильности аэрозольных фракций.

Илл.–5. Табл.–2. Библ.–2. Рез. русск.

УДК 621.319.7.001

К ВОПРОСУ ГЕНЕРАЦИИ И РАЗДЕЛЕНИЯ ЗАРЯДА ПРИ ИСПАРЕНИИ КАПЕЛЬ ВОДНОГО АЭРОЗОЛЯ. В.Б.Тамме // Уч.зап. Тарт. ун-та.– 1990.– Вып.880.– С.94–99.

Исследованы генерация и разделение заряда при монодисперсном распылении дистиллированной воды. При помощи счетчика аэроионов регистрировались измерения проводимости воздуха в процессе высыхания водяных капель в воздухе.

Измерялся и спектр размеров аэрозольных продуктов электростатического взрыва высыхающих в воздухе капель.

Илл.–2. Табл.–1. Библ.–6. Рез. русск.

УДК 681.322.1

УНИВЕРСАЛЬНЫЙ КОНТРОЛЛЕР ДЛЯ УПРАВЛЕНИЯ ДОЛГОВРЕМЕННЫМИ ЭКСПЕРИМЕНТАМИ. А.Э.Рейнарт // Уч. зап. Тарт.ун-та. -1990.- Вып.880. -С.100-104.

Разработан универсальный контроллер для управления долговременными экспериментами и экспериментами в полевых условиях. Контроллер позволяет осуществить сбор данных, управление датчиками и обработку данных в реальном масштабе времени.

В контроллере используется 16-битовый микропроцессор КР1810ВМ86А. Обьемы как ОЗУ, так и ПЗУ контроллера от 4 до 16 кбайт. Разработаны также 10-разрядный 32-канальный аналого-цифровой преобразователь и модуль для последовательного обмена данными.

Составление программ для контроллера производится с помощью ЭВМ "ИСКРА 1030".

Илл.-1. Библ.-1. Рез. русск.

УДК 551.594:537.56

ЭЛЕКТРОСТАТИЧЕСКОЕ РАССЕИВАНИЕ ДВУХ ГРУПП АЭРОИОНОВ РАЗНЫХ ПОДВИЖНОСТЕЙ. А.М.Лутс, Я.И.Сальм// Уч.зап. Тарт.ун-та. -1990.- Вып.880. -С.105-110.

Рассматривается однородно и униполярно ионизированный газ, в котором происходит только процесс электростатического рассеивания аэроионов (частиц аэрозоля). Рассмотрена задача о двух группах аэроионов с подвижностями k_1 и k_2. Соответствующие уравнения приведены в безразмерном виде. Для вычисления безразмерных концентраций предложены аппроксимирующие функции. Определены границы применения и погрешности аппроксимирующих функций.

Табл.-3. Библ.-4. Рез. русск.

УДК 541.141.13

К ОБРАЗОВАНИЮ ФОТООКСИДАНТОВ ПРИ ВЗАИМОДЕЙСТВИИ КОРОТКОВОЛНОВОГО УФ-ИЗЛУЧЕНИЯ И НЕКОТОРЫХ ЛЕТУЧИХ ОРГАНИЧЕСКИХ ВЕЩЕСТВ. Р.Э.Прийман, Л.Ю.Виснапуу // Уч.зап. Тарт. ун-та. - 1990. - Вып.880. - С.111-115.

Экспериментально установлено, что при облучении воздуха, содержащего летучие фитоорганические соединения, коротковолновым и бактерицидным УФ-излучением образуются повышенные концентрации озона. В работе рассматриваются процессы, протекающие в воздухе закрытых помещений при совместном применении УФ-излучения и аэрозолей фитоорганических композиций, обладающих фитонцидными свойствами. Приведены измеренные концентрации фитоорганических примесей озона и диоксида азота в камере в случае УФ-излучения при разной относительной влажности и степени ионизации воздуха. Показано, что при УФ-излучении с уменьшением влажности воздуха и увеличением плотности заряда аэроионов концентрации озона и диоксида азота повышаются. С увеличением концентрации фитоорганических примесей концентрация озона растет, а концентрация диоксида азота изменяется неоднозначно (например, в случае экстрактов мяты и хвои, пиненов растет, а при скипидаре, смеси эфирных масел падает). Повышение концентрации озона в сочетании с УФ-излучением усиливает эффективность обеззараживания воздуха.

Табл.-2. Библ.-3. Рез. русск.

УДК 621.317.723

ИЗМЕРИТЕЛЬ МАЛЫХ ПЕРЕМЕННЫХ ТОКОВ. М.Х.Ансо, Л.П.Кярнер // Уч.зап. Тарт. ун-та. - 1990. - Вып.880. - С.116-121.

Описан измеритель малых токов типа интегратор-дифференциатор, предназначенный для измерения переменного тока 10^{-12}...10^{-10}А в частотном диапазоне 3...100 кГц на фоне постоянного тока 2.10^{-10}...2.10^{-8}А в условиях открытого космоса. Дается анализ шумовых свойств данного прибора и факторов, ограничивающих его быстродействие.

Илл.-2. Рез. русск.

Ученые записки Тартуского университета.
Выпуск 880.
ИССЛЕДОВАНИЯ ПО АЭРОЗОЛЯМ И ВЫСОКОЧАСТОТНОМУ РАЗРЯДУ.
Ионизация, аэрозоли, электрометрия.
На английском языке.
Резюме на русском языке.
Тартуский университет.
ЭССР, 202400, г.Тарту, ул.Юликооли, I8.
Ответственный редактор Х. Роос.
Корректор М. Лимберг.
Подписано к печати 25.01.1990.
МВ 00419.
Формат 60x90/I6.
Бумага писчая.
Машинопись. Ротапринт.
Учетно-издательских листов 7,39. Печатных листов 8,25.
Тираж 650.
Заказ № 34.
Цена I руб. 50 коп.
Типография ТУ, ЭССР, 202400, г.Тарту, ул.Тийги, 78.